

# Chemical vapor deposition of (in)organic layers : in situ film growth studies, nano-porosity and moisture permeation barrier properties

**Citation for published version (APA):**

Aresta, G. (2012). *Chemical vapor deposition of (in)organic layers : in situ film growth studies, nano-porosity and moisture permeation barrier properties*. [Phd Thesis 1 (Research TU/e / Graduation TU/e), Applied Physics and Science Education]. Technische Universiteit Eindhoven. <https://doi.org/10.6100/IR732966>

**DOI:**

[10.6100/IR732966](https://doi.org/10.6100/IR732966)

**Document status and date:**

Published: 01/01/2012

**Document Version:**

Publisher's PDF, also known as Version of Record (includes final page, issue and volume numbers)

**Please check the document version of this publication:**

- A submitted manuscript is the version of the article upon submission and before peer-review. There can be important differences between the submitted version and the official published version of record. People interested in the research are advised to contact the author for the final version of the publication, or visit the DOI to the publisher's website.
- The final author version and the galley proof are versions of the publication after peer review.
- The final published version features the final layout of the paper including the volume, issue and page numbers.

[Link to publication](#)

**General rights**

Copyright and moral rights for the publications made accessible in the public portal are retained by the authors and/or other copyright owners and it is a condition of accessing publications that users recognise and abide by the legal requirements associated with these rights.

- Users may download and print one copy of any publication from the public portal for the purpose of private study or research.
- You may not further distribute the material or use it for any profit-making activity or commercial gain
- You may freely distribute the URL identifying the publication in the public portal.

If the publication is distributed under the terms of Article 25fa of the Dutch Copyright Act, indicated by the "Taverne" license above, please follow below link for the End User Agreement:

[www.tue.nl/taverne](http://www.tue.nl/taverne)

**Take down policy**

If you believe that this document breaches copyright please contact us at:

[openaccess@tue.nl](mailto:openaccess@tue.nl)

providing details and we will investigate your claim.

Chemical vapor deposition of (in)organic layers:  
*in situ* film growth studies, nano-porosity and  
moisture permeation barrier properties

PROEFSCHRIFT

ter verkrijging van de graad van doctor aan de  
Technische Universiteit Eindhoven, op gezag van de  
rector magnificus, prof.dr.ir. C.J. van Duijn, voor een  
commissie aangewezen door het College voor  
Promoties in het openbaar te verdedigen  
op dinsdag 12 juni 2012 om 16.00 uur

door

Gianfranco Aresta  
geboren te Bari, Italië

Dit proefschrift is goedgekeurd door de promotoren:

prof.dr.ir. M.C.M. van de Sanden

Copromotor:  
dr. M. Creatore

This research forms part of the research programme of the Dutch Polymer Institute (DPI), Technology Area Large Area Thin Film Electronics, DPI project #663”



Printed and bound by universiteitsdrukkerij Technische Universiteit Eindhoven

Cover design by Paul Verspaget from Verspaget & Bruinink.

Cover picture: courtyard of “Castel del Monte” castle, Andria, Italy

A catalogue record is available from the Eindhoven University of Technology Library

ISBN: 978-90-386-3160-8

NUR: 926

Chemical vapor deposition of (in)organic layers:

*in situ* film growth studies, nano-porosity and moisture permeation barrier properties

By Gianfranco Aresta, Eindhoven University of Technology, 2012

# Contents

Chapter 1:	
<i>Introduction</i>	
Research framework	3
Aim of the thesis	22
Research questions	26
Conclusions and Outlook	31
Chapter 2:	39
<i>Initiated-chemical vapor deposition of organosilicon layers: monomer adsorption, bulk growth and process window definition</i>	
Chapter 3:	69
<i>Evidence of the filling of nano-porosity in SiO<sub>2</sub>-like layers by an initiated-CVD monomer</i>	
Chapter 4:	87
<i>Initiated-chemical vapor deposition of organosilicon interlayers for moisture diffusion barrier systems</i>	
Chapter 5:	111
<i>Optical characterization of plasma-deposited SiO<sub>2</sub>-like layers on anisotropic polymeric substrates</i>	
Summary	135
Publications related to this work	139
Acknowledgements	141
Curriculum Vitae	145



# Chapter 1

## *Introduction*



## Research framework

### Moisture and vapor permeation barrier films technology

Polymers have appealing characteristics such as being lightweight, flexible, transparent, low cost, and compatible with roll-to-roll processing<sup>1-4</sup>, which make them the substrate of choice, with respect to other materials such as metals and ceramics, in many fields of application. Examples range from the most traditional food/drink/drug packaging<sup>5</sup> to the most recent and challenging areas of thin film inorganic and polymer solar cells and OLEDs<sup>6-11</sup>. Despite the above mentioned properties, the main bottle-neck<sup>1</sup> to polymer-based applications is their high permeability to moisture, oxygen and aromas present in the environment. This poses severe limitations to the performance, better known as shelf-life of the device<sup>2,6,8-11</sup>.

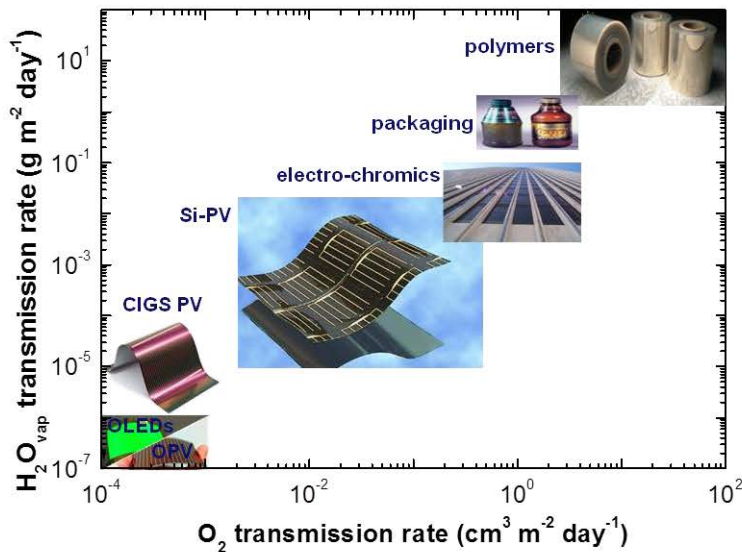


**Figure 1:** Fields of application for moisture and O<sub>2</sub> permeation barrier layers.<sup>7, 10, 13-19</sup>. Extremely low H<sub>2</sub>O and O<sub>2</sub> transmission rates are required for organic based solar cells (OPV) and for OLEDs.<sup>7, 10, 18, 19</sup>.

<sup>4</sup> Another drawback of polymeric substrates is represented by their relatively low glass transition temperature T<sub>g</sub>, which requires low temperature processing<sup>12</sup>.



A well known approach to compensate for the polymer permeability is to develop barrier layers, i.e. inorganic (metal or ceramic) thin films ( $\leq 100$  nm), which reduce the overall polymer/inorganic barrier permeability according to a barrier improvement factor (BIF)<sup>2</sup>. However, as indicated in Figure 1, the several technologies require a different level of permeation barrier and a single barrier layer deposited on a polymer substrate can generally satisfy the requirement of a WVTR value down to  $10^{-1}$  g m<sup>-2</sup> day<sup>-1</sup>, sufficient for packaging. For high-end devices, the requirements to meet are more challenging from several perspectives and presently not yet satisfied by a single layer barrier approach:

1. WVTR values down to  $10^{-6}$  g m<sup>-2</sup> day<sup>-1</sup> <sup>3</sup>;
2. flexible devices such as OLEDs and solar cells do require also a barrier solution to encapsulate the device itself and the barrier layer performance is often dependent on the substrate of choice;

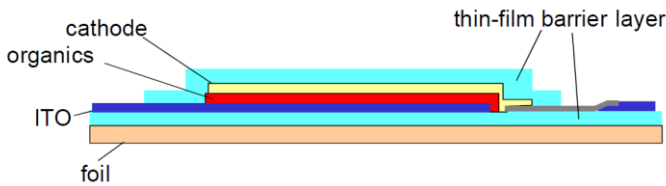


**Figure 2:** Schematic diagram of a flexible OLED device protected by a thin-film barrier layer on both sides. The thin film barrier layer on top of the cathode is usually referred to as thin-film encapsulation; the thin-film barrier layer on the polymer foil is referred to as barrier-on-foil<sup>1</sup>. The (10nm) cathode (Ba for polymer-based LEDs) is generally coated with a (100 nm) thick Al layer<sup>2</sup>. The anode is a transparent conductive oxide (Indium-Tin-Oxide: ITO)<sup>0, 21</sup>.

3. Next to the overall barrier performance, it is necessary to evaluate and control also the local performance of the barrier. Devices such as OLEDs do always suffer from imperfections in the several processing steps or from a non-completely dust-free

---

<sup>2</sup> The Barrier Improvement Factor (BIF) defines the improvement in terms of oxygen or moisture barrier property, which the polymer substrate undergoes upon deposition of a barrier layer. The oxygen permeation rate is also defined as Oxygen Transmission Rate (OTR) and generally expressed in cm<sup>3</sup> (STP) m<sup>-2</sup> day<sup>-1</sup>. The moisture permeation rate is referred to as Water Vapor Transmission Rate (WVTR) and generally reported in g m<sup>-2</sup> day<sup>-1</sup>.

<sup>3</sup> This WVTR value is required to ensure an OLED device lifetime of 10 years and it is based on the estimation of the amount of H<sub>2</sub>O<sub>vap</sub> needed to completely oxidize a 5-10 nm thick Ba reactive cathode layer typically used in polymers based LEDs<sup>20</sup>.

clean room environment leading to a morphologically defective surface. The presence of dust, pinholes, anti-block particles on polymer substrates as well as defects on the (Al/Ba) cathode surface of the OLED eventually lead to local permeation paths in the barrier layer, affecting the performance of the device.

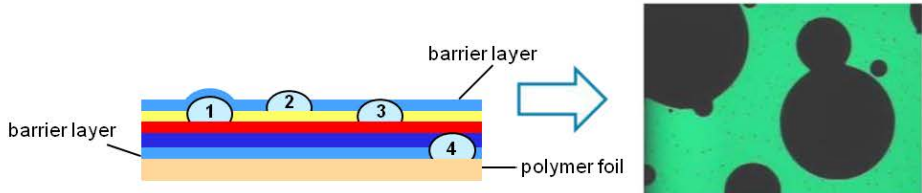


**Figure 3:** Examples of sources of defects/pinholes related to the polymeric substrate and the cathode surface status leading to the formation of “black spots” during electroluminescence measurements of an OLED device (dimensions = 2 mm x 1.5 mm). In the figure: the yellow layer is the Al covered Ba cathode; the active polymer layer is the red layer; the blue layer is the anode ITO layer. A particle/pinhole present on the cathode/active polymer interphase (1) is not harmful for the operation of the OLED as long as the barrier layer encapsulates it. The same consideration can be made for a particle/pinhole (2), which is not covered by the barrier layer but it is blocked by the thick Al layer. A particle (3) present at the cathode/active polymer interphase which is covered neither by the Al layer, nor by the barrier layer, will let water permeate through it, causing the oxidation of the cathode/active polymer interphase, leading to local areas where no electron injection from the cathode to the active layer develops: i.e. a “black spot”<sup>21, 22</sup>. The polymer substrate (polymer foil) can be contaminated by particles (4), which can protrude through the barrier layer creating “spikes” in the ITO anode. This will result in local regions with high electric field which will turn in short-circuited areas, leading also to “black spots”<sup>10</sup>.

In order to understand the limits of the single layer barrier technology, a review of the early studies on the moisture and oxygen permeation through single inorganic barrier layers is presented. This serves as basis for understanding and engineering of the present barrier technology approaches for high-end devices.

## Single barrier layer technology: approaches and permeation models

The development in barrier film technology has originally found application in the food and drink packaging industry already in the 50's. Initially, Al metalized foils were laminated to polyethylene (PE) polymers<sup>23</sup>. After, the Al metallization (by sputtering or evaporation) process has been set up in the late 50's<sup>23</sup>. Although this kind of packaging is still in use, the Al thin films have been replaced by ceramic thin films ( $\leq 100$  nm) such as  $\text{SiO}_2$ <sup>24-28</sup>,  $\text{Si}_3\text{N}_4$ <sup>29-33</sup>, and  $\text{Al}_2\text{O}_3$ <sup>34-37</sup> because of the added values given by their transparency in the visible range and microwave compatibility. Different deposition processes have been employed, such as sputtering<sup>34-38</sup>, thermal/reactive evaporation<sup>39-41</sup> and plasma-based deposition techniques<sup>24-33</sup>. Although their bulk ceramic counterparts (e.g. glass and alumina) show excellent barrier properties<sup>4</sup>, thin films exhibit a BIF generally limited to the range of  $10\text{-}10^2$ . The origin of this discrepancy has been associated to the presence of macro-defects present in the thin film (ranging from hundreds of nm up to few  $\mu\text{m}$  in size), which represent an unhindered path for the permeant molecules<sup>23</sup>. The early work of Jamienson and Windle<sup>43</sup> showed the correlation between the macro-defects (often referred to as pinholes), detected by transmission electron microscopy and optical microscopy, and the oxygen and water vapor barrier properties of thin (10 -50 nm) Al layers vacuum deposited on polyester substrates. Furthermore, they accompanied their experimental studies with a permeation model, addressing the unhindered permeation through the pinholes.

The pristine polymer surface status (high surface roughness, presence of anti-static particles, defects and slurries) represents one of the main sources of macro-defects, which causes the local development of a defective barrier layer<sup>44, 45</sup>. In an exhaustive review, Chatham<sup>44</sup> investigated the oxygen permeation rate through different single barrier layers as a function of their thickness. It is generally observed that, independently on the chosen layer chemistry and deposition method, a critical thickness can be defined, i.e. the thickness above which the barrier performance does not show any further improvement.

---

<sup>4</sup> For example the water diffusivity of glass<sup>24</sup> is  $10^{-18}\text{-}10^{-19}$   $\text{cm}^2 \text{s}^{-1}$  and the one of alumina<sup>42</sup> is of  $\sim 10^{-30}$   $\text{cm}^2 \text{s}^{-1}$ . On the contrary the water diffusivity in thin films is orders of magnitude lower, for example, the estimated water diffusivity of an  $\text{AlO}_x$  thin film is only  $1.4 \cdot 10^{-13}$   $\text{cm}^2 \text{s}^{-1}$ <sup>42</sup>.

The author made a comparison of the thickness/permeation data with a simple permeation model based on the laminate theory<sup>5</sup> and on the diffusion through the pinholes/defects present into the barrier layer (as derived from the works of Prins and Herman<sup>23</sup> and Jamienson and Windle<sup>43</sup>). From this comparison Chatham concluded that the oxygen permeation through the single barrier layer is dominated by the permeation through defects. The investigation carried out by da Silva Sobrinho<sup>33</sup> on PE-CVD deposited SiO<sub>2</sub>-like<sup>6</sup> and SiN<sub>x</sub> layers on poly(ethyleneterephthalate) summarizes the above-reported discussion (Figure 4).

---

<sup>5</sup> The transport through a solid is considered to occur through a so-called solubility-diffusion mechanism<sup>44, 46</sup>. The permeability of a molecule as O<sub>2</sub> and H<sub>2</sub>O<sub>vap</sub> in a solid is therefore given by the product of its diffusivity (cm<sup>2</sup> s<sup>-1</sup>) and solubility (cm<sup>3</sup>(or g) cm<sup>-3</sup> atm<sup>-1</sup>),  $P = D \cdot S$ . Being D and S characteristic properties of a material, the solubility-diffusion mechanism implies that the flow (or permeation) of a molecule through a material, in steady-state conditions, is inversely proportional to the material thickness<sup>44,46</sup>. In the conditions in which the upstream (O<sub>2</sub> and H<sub>2</sub>O<sub>vap</sub>) partial pressure  $p_0$  on the solid is much larger the one downstream  $p_f$  ( $p_0 \gg p_f$ ), the flow (or permeation) can be expressed as<sup>46</sup>:

$$\text{flow (permeation)} \approx P \cdot \frac{p_0}{d}$$

The ideal laminate theory states that the permeability of a molecule into a layered system (such as polymer substrate/barrier layer) is given by the following series<sup>46</sup>:

$$\frac{d_{\text{polymer/barrier}}}{P_{\text{polymer/barrier}}} = \frac{d_{\text{polymer}}}{P_{\text{polymer}}} + \frac{d_{\text{polymer}}}{P_{\text{polymer}}}$$

where  $P_{\text{polymer}}$  and  $P_{\text{barrier}}$  are the polymer substrate and barrier permeabilities,  $d_{\text{polymer}}$  and  $d_{\text{barrier}}$  are the polymer and barrier layer thicknesses,  $P_{\text{polymer/barrier}}$  and  $d_{\text{polymer/barrier}}$  are the permeability and the thickness of the polymer/barrier layer system, respectively.

<sup>6</sup> In literature, thin films deposited by gas phase methods are referred to as SiO<sub>x</sub> (also SiO<sub>2</sub>-like), SiN<sub>x</sub>, AlO<sub>x</sub>, etc. pointing to the possibility for a broad stoichiometric range.

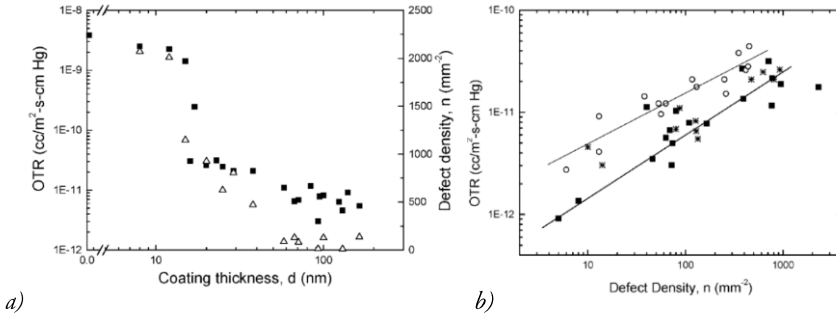


**Figure 4:** a) Defect density ( $\Delta$ ;  $\text{mm}^{-2}$ ) and oxygen transmission rate ( $\blacksquare$ ; OTR) as a function of the  $\text{SiO}_2$ -like barrier layer thickness. A critical thickness of about 12 - 15 nm is visible in the graph. b) OTR as a function of defect density for  $\text{SiO}_2$ -like ( $\circ$ ),  $\text{SiN}_x$  ( $\blacksquare$ ) layers, Al ( $\circ$ )<sup>33</sup>. The data related to the Al are taken from the work of Jamienson and Windle<sup>43</sup>. Below the critical thickness ( $d < 12\text{-}15$  nm), the higher permeability is attributed to a non-continuous barrier layer present on the substrate. A complete coverage of the substrate surface occurs by approaching the critical thickness. The independence of the total permeability above the critical thickness indicates a change in permeation from solubility-diffusion controlled to defects-driven permeation.

Moreover Tropsha and coworkers<sup>24</sup>, by applying the activate rate theory to the  $\text{O}_2$  transmission rate data set of plasma-deposited  $\text{SiO}_2$ -like layers on PET, concluded that the free activation energy for the transport through the PET/  $\text{SiO}_2$ -like system was equal to the one of the pristine polymer substrate ( $\Delta E_p = (30 \pm 3)$  KJ/mole and  $\Delta E_p = (30 \pm 4)$  KJ/mole, for the PET and PET/ $\text{SiO}_2$ -like, respectively), pointing out to the concept of an unhindered, macro-defects driven permeation through a single barrier layer<sup>7</sup>. Later on, other authors argued on this conclusion and proposed complementary permeation pathways occurring through defects of smaller size, i.e. down to the nm scale, the so-defined nano-defects or layer porosity. Evidence of this permeation is given by the studies of Erlat<sup>25</sup>, concerning the barrier properties of magnetron-PE-CVD  $\text{SiO}_2$ -like on PET. These films were macro-defects free, but,

<sup>7</sup> In their work, Tropsha and coworkers also pointed out to the fact that, in the case of  $\text{H}_2\text{O}_{\text{vap}}$ , a more complex permeation mechanism has to be taken into account as  $\text{H}_2\text{O}_{\text{vap}}$  interaction with the barrier layer deviates from the ideal gas permeation mechanism. Indeed, it was considered that the interaction of  $\text{H}_2\text{O}_{\text{vap}}$  molecules with the oxide such as adsorption/chemisorption and chemical reaction of  $\text{H}_2\text{O}_{\text{vap}}$  with the  $\text{SiO}_x$  matrix could play a role in the permeation mechanism of the latter through the barrier system<sup>24</sup>. This has been also confirmed by Henry for  $\text{AlO}_x$  layers deposited on PET substrates, who pointed out to an interaction between the  $\text{H}_2\text{O}_{\text{vap}}$  molecules and the internal surface of the  $\text{AlO}_x$  pores/defects<sup>37</sup>.

nevertheless, were characterized by an improvement of barrier performance in the same order of the one associated to barriers containing macro-defects. A careful surface morphology analysis revealed nano-pores in the range of 4 - 6 nm size covering approximately 30% of the barrier layer surface and still representing an unhindered path for oxygen and moisture through the barrier layer. Furthermore, Rossi and Nulman<sup>47</sup> in their permeation model, pointed out that the total permeation through many “small holes” is much more effective than the permeation through few pinholes with the same total area. Affinito<sup>46</sup> estimated that the density of the nano-defects (or pores) can reach a level up to 4 orders of magnitude higher than the pinhole density, which is translated into an area density of nano-defects/pores 15-20 time larger than the pinhole area density. Accordingly, the total permeation through the nano-defects will increase, proportionally to the nano-defect total area<sup>46</sup>. Roberts and coworkers<sup>48</sup> proposed a quantitative model to take into account the experimentally determined permeation data, since these were neither fitted through the ideal laminate theory, nor with the assumption that permeation occurs only through macro-defects. The model considered the diffusion through the amorphous oxide lattice (<0.3 nm), nano-defects (0.3 – 1 nm) within the lattice and macro-defects (>1 nm) as reported in Equation 1 (and depicted in Figure 5):

$$P_b = C_{md}P_p + \left( \frac{\phi_p}{P_p} + \frac{\phi_g}{P_{la} + P_{nd}} \right)^{-1} \quad (1)$$

in which  $P_b$  is the barrier layer permeability,  $P_p$ ,  $P_{la}$ ,  $P_{nd}$  are the polymer substrate, oxide lattice and oxide nano-defects permeability, respectively,  $C_{md}$  is a dimensionless constant which depends on the size and number of macro-defects in the barrier layer<sup>48</sup>, and  $\phi_p = d_p/d$   $\phi_g = d_g/d$  being the polymer and barrier layer volume fraction (with  $d_g$ : barrier layer thickness;  $d_p$ : polymer thickness and  $d_g + d_p = d$  and  $\phi_p + \phi_g = 1$ )<sup>48</sup>.

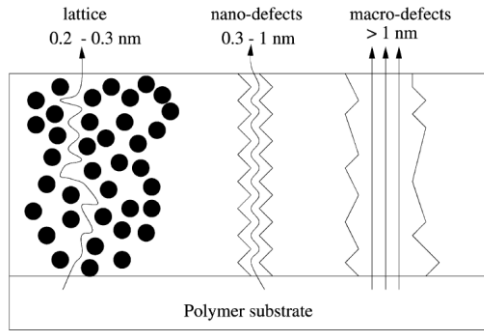


**Figure 5:** A schematic diagram showing the proposed gas/vapor transport pathways through the barrier layer. The relative contribution of each path to the final permeation depends on the permeant molecular diameter<sup>48</sup>. The size classification of the defects is related to the diameter of the H<sub>2</sub>O and O<sub>2</sub>, of 0.33 nm and 0.32 nm, respectively<sup>48</sup>.

It is therefore necessary to control both the local permeation through the pinholes and the permeation through the nano-defects of the barrier layer matrix. Both issues will be addressed in this Thesis (Chapter 4), by providing an insight into the layer intrinsic porosity and its influence on the barrier performance, and into the effect of the deposition technique/parameters on the macro-defect density.

A diagnostic tool capable to discern the permeation through macro-defects and matrix intrinsic porosity is the Calcium test<sup>10</sup>, as addressed in the Frame I at page 18. Provided the basic understanding of the limits of the single layer barrier technology, two main approaches, presently addressed in literature, are now described, both aiming towards the further improvement of the barrier performance. One approach is to control the nano-scale porosity of the barrier layer, leading to a decrease of the permeation through the nano-scale defects. A second approach is the engineering of the so-defined multilayer system, which generally allows the decoupling of macro-defects present in the inorganic barrier layers by means of an organic interlayer.

### Towards the ultimate control in nano-porosity?

Recently, atomic layer deposition (ALD) has been literally booming in the field of inorganic barrier layers for high-end flexible devices. Its potential of delivering virtually dense, defect-free ultra-thin films has generated several studies, mainly based on  $\text{Al}_2\text{O}_3$  deposition, either on polymer substrates or directly on OLED and PV devices<sup>13, 49-55</sup>. Langereis<sup>52</sup> reported a value of WVTR of  $5 \cdot 10^{-3} \text{ g m}^{-2} \text{ day}^{-1}$  (at  $T = 294 \text{ K}$  and R.H. = 60%) for a 20 nm thick  $\text{Al}_2\text{O}_3$  layer deposited by means of plasma assisted-ALD (PA-ALD) on PEN substrates at room temperature. Groner<sup>54</sup> also reported a WVTR of  $\sim 1 \cdot 10^{-3} \text{ g m}^{-2} \text{ day}^{-1}$  (at  $T = 298 \text{ K}$  and R.H. = 100%) for a 26 nm thick  $\text{Al}_2\text{O}_3$  deposited by ALD on several polymers. Also Carcia and coworkers<sup>51</sup> deposited a 25 nm thick  $\text{Al}_2\text{O}_3$  layer on PEN showing a WVTR =  $1.7 \cdot 10^{-5} \text{ g m}^{-2} \text{ day}^{-1}$  (at  $T = 311 \text{ K}$  and R.H. = 85%). However, in both cases reported by Langereis and Groner<sup>52, 54</sup>, the water vapor permeation was shown to decrease with the increase in layer thickness and reaching a plateau at 20-25 nm<sup>52, 54</sup>, suggesting that even for the virtually defect-free ALD layer the permeation mechanism is still defect-driven. However, the superior barrier properties with respect to those obtained by other conventional techniques, such as PE-CVD or sputtering, indicate a better control over the nanoporosity level.

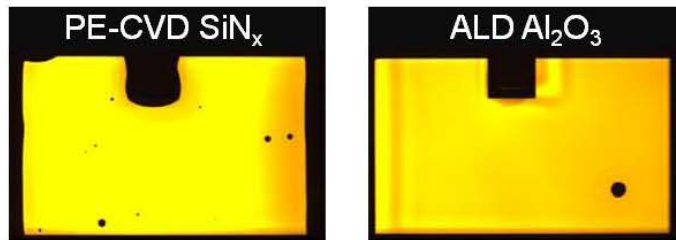


*Figure 6: Electroluminescence measurements on polymer LEDs encapsulated with a 300nm  $\text{SiN}_x$  deposited by PE-CVD (left panel) and 40nm  $\text{Al}_2\text{O}_3$  deposited by plasma-assisted ALD (right panel). The reduction of black spots in the operating OLED encapsulated by the ALD  $\text{Al}_2\text{O}_3$  layer with respect to the PE-CVD deposited  $\text{SiN}_x$  points out to better conformality and particles coverage of the ALD layer. However, the application of a single ALD layer still results in black spot development<sup>56</sup>. The  $\text{SiN}_x$  layer has a barrier performance similar to the ALD  $\text{Al}_2\text{O}_3$  layer<sup>49</sup>.*



Moreover a better conformality/encapsulation in the proximity of the defects present on the surface<sup>49, 56</sup> can be observed, as the total density of black spots decreases in the case of the application of the ALD layer (Figure 6). The better control on the film quality in the case of the ALD deposition process, is also confirmed by the excellent intrinsic water barrier properties of the Al<sub>2</sub>O<sub>3</sub> in the range of 10<sup>-6</sup> g m<sup>-2</sup> day<sup>-1</sup> (at T = 298 K and R.H. = 50%)<sup>49</sup>, reached for a thin layer (20-40nm). However, also in the case of the ALD encapsulated OLEDs, black spots formation still occurs.

Recently, also the development of high throughput ALD processes has been addressed<sup>57</sup>, based on novel approaches such as spatial-ALD leading to WVTR values below 10<sup>-5</sup> g m<sup>-2</sup> day<sup>-1</sup> at T = 323 K and R.H. = 85%, for a 50 nm thick Al<sub>2</sub>O<sub>3</sub> layer.

## Multilayer barrier film technology: approaches and role of the organic interlayer

The multilayer barrier approach is nowadays largely tested at lab and R&D scale for flexible OLED and PV devices, and appears to be the preferred choice for both the barrier-on-foil, as well as for the encapsulation. The state-of-the-art of this technology is represented by the Barix<sup>®1</sup> multilayer and similar structures which allow reaching WVTR down to  $10^{-6}$  g m<sup>-2</sup> day<sup>-1</sup> at ambient conditions of temperature and relative humidity<sup>58</sup>.

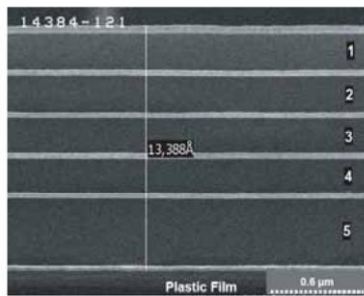


**Figure 7:** Organic/inorganic multilayer structure of the Barix<sup>®</sup> multilayer from Vitex Systems (taken from Ref. 11).

The Barix<sup>®</sup> multilayer is deposited by a hybrid approach in which the inorganic barrier is a thin layer (30 – 100 nm) of AlO<sub>x</sub> deposited by reactive sputtering while the polymeric interlayer (from 0.25 μm to several μm) is delivered by flash evaporation/condensation of the monomer followed by UV (or electron beam) induced polymerization<sup>1</sup>. Another example of organic/inorganic multilayer deposited by a hybrid approach is the one of Han *et al.*<sup>59</sup>, consisting of an electron beam-evaporated MgO inorganic layer separated by a spin coated/UV cured epoxy polymeric interlayer, reporting a value of WVTR of  $5 \cdot 10^{-5}$  g m<sup>-2</sup> day<sup>-1</sup> (at T= 303 K and R.H. = 90%) for a system composed by 6 dyads<sup>8</sup>. Vaško *et al.*<sup>61</sup> reported on electron beam evaporation deposited SiO<sub>2</sub>-like layer coupled with an (inorganic/organic) hybrid polymer ORMOCER<sup>®</sup> deposited by sol-gel technique, followed by thermal curing, with a BIF of ~ 290 for a two dyads system at the T = 296 K and R.H. = 85%<sup>61</sup>. Dameron *et al.* reported also on Al<sub>2</sub>O<sub>3</sub>/Alucone

<sup>8</sup> A dyad is composed by an organic/inorganic (or vice versa) bilayer<sup>60</sup>.

organic/inorganic multilayer deposited by ALD and Molecular Layer Deposition (MLD)<sup>62, 63</sup>. Very recently, another vacuum compatible polymer deposition technique (namely the initiated-CVD, or i-CVD)<sup>64-65</sup> has been used for the deposition of organic interlayers in combination with PE-CVD SiO<sub>2</sub>-like barriers. A 3 dyad structure has delivered a BIF of 100 with respect to the single layer<sup>66</sup>. Another example is reported by Spee *et al.* in which poly(glycidyl methacrylate) polymers have been successfully coupled with a HW-CVD deposited SiN<sub>x</sub> layer, presently under evaluation in terms of barrier performances<sup>67</sup>. Other approaches/deposition techniques have been used for the deposition of the multilayers. Schaepekens *et al.* reported on a multilayer barrier system deposited by PE-CVD with graded interphases between the organic (SiO<sub>x</sub>C<sub>y</sub>) and inorganic (SiO<sub>x</sub>N<sub>y</sub>) layers, with WVTR results < 10<sup>-5</sup> g m<sup>-2</sup> day<sup>-1</sup> at 293 K and 50% of R.H.<sup>3</sup>. Promising inorganic/organic multilayers, to be tested in terms of (moisture) barrier properties, are the PE-CVD deposited hybrid nanolaminates composed of Al<sub>2</sub>O<sub>3</sub>/silicone<sup>68</sup> and SiO<sub>2</sub>-like/silicone<sup>69</sup>. Other PE-CVD deposited organic/inorganic multilayers are reported in literature<sup>70-72</sup>.

Although several successful studies have been presented in literature, the role of the organic interlayer remains still unraveled. Among the most reported hypotheses, Burrows<sup>1</sup> attributes the improvement of the barrier properties to the smoothening effect provided by the μm-thick organic interlayer when deposited on top of the defective surface of the polymeric substrate, as shown in Figure 8, thus promoting a better growth of the subsequent inorganic barrier layer as characterized by a lower defect density.

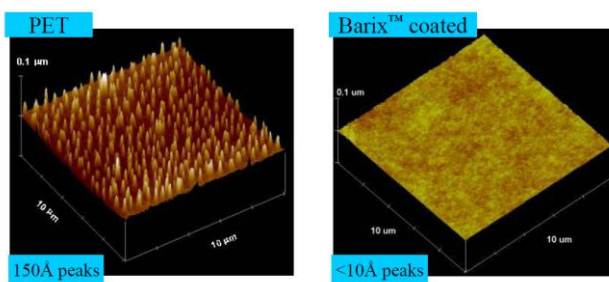


**Figure 8:** AFM images of the Barix<sup>®</sup> coated substrate, compared to those of the pristine PET substrate, show a drastic reduction of the surface roughness due to the acrylate polymer smoothening effect<sup>1</sup>.

Graff<sup>42</sup> developed a time dependent moisture permeation model through a multilayer, which highlighted that the drastic reduction in moisture permeation rate was associated to the decoupling of the macro-defects present in two adjacent inorganic barrier layers. A so-defined tortuous diffusion path of the permeant would therefore develop within the multi-layer (Figure 9).

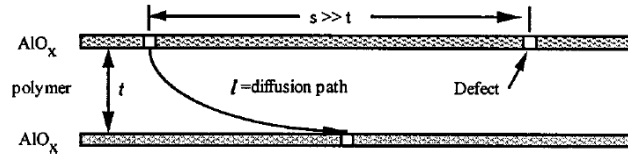


**Figure 9:** schematic representation of the decoupling of defects through a tortuous diffusion path<sup>54</sup>.

The model was based on the solubility-diffusion permeation mechanism of the permeant molecule through the organic/inorganic multilayer, which included also the lag time<sup>9</sup> as a parameter. The comparison between the steady state flux results provided by the model and the experimental data related to AlO<sub>x</sub>/acrylate multilayers<sup>1</sup> pointed out that the tortuous path induced by the organic interlayer lead to an increased lag-time rather than to a decrease of the steady-state flux of the permeant, which would take years before being reached. The diffusivity of the AlO<sub>x</sub> barrier layer was described by a macro-defect driven mechanism as reported in Equation 2:

$$D_{eff(barrier)} = D_p f_{defects} + D_{barrier} f_{barrier} \quad (2)$$

in which  $D_p$  and  $D_{barrier}$  are the acrylate interlayer and bulk AlO<sub>x</sub> diffusivity and  $f_{defects}$  and  $f_{barrier}$  are the area fraction of the defects and the bulk material<sup>42</sup>. The derived value of effective diffusivity of the AlO<sub>x</sub> layer was consistent with a defect size in the range of  $\mu\text{m}$  with defect spacing of 200  $\mu\text{m}$ , rather than high concentration of nano-defect, based on the extensive layer defects analysis and the outcomes of the

---

<sup>9</sup> The lag-time is defined as the time needed to reach the steady-state diffusion of the permeant molecule through the multilayer system.

literature. Thus the macro-defects were considered to be the main path of the permeation of moisture through the single inorganic barrier layer.

As described earlier, next to the macro-defects, which represent an unhindered path for the permeant molecule, nano-defects also contribute to the permeation. Therefore, in a parallel work, Affinito<sup>46</sup> considered the hypothesis of an additional role of the organic interlayer. Infiltration of the organic layer in its liquid phase into the nano-sized defects of the inorganic barrier layer underneath can eventually have an impact on the local transmission of the permeant molecule through the filled pores, as depicted in Figure 10.

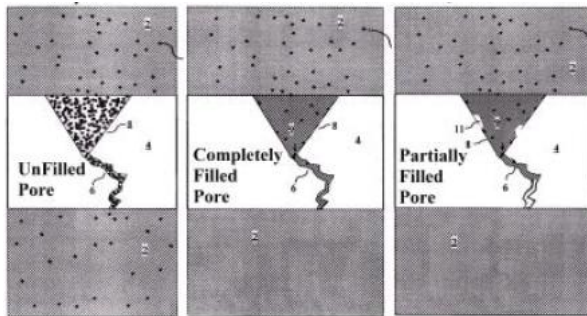


**Figure 10:** schematic representation of the nano-defects/pores filling by the polymeric layer, as described by Affinito<sup>46</sup>.

On the basis of the outcome of Roberts and coworkers<sup>48</sup>, and by considering the average molecular size of an acrylate monomer (0.4 nm), i.e. the typical chosen chemistry for the organic interlayer, Affinito classified the defects as it follows. Defects larger than the size of the monomer units are defined as macro-defects, i.e. from few nms to the largest pinholes/defects of few hundred nms and  $\mu\text{ms}$ . The nano-defects range from the size of the monomer unit to 1-2 nm, and, therefore, are still accessible for monomer infiltration and filling; the matrix defects, i.e. below the monomer size,  $< 0.2 - 0.3$  nm, are not accessible to the monomer<sup>46</sup>.

To support the hypothesis on this synergistic effect between the organic interlayer and the barrier layer, Affinito<sup>46</sup> developed a permeation model described as “tortuous solubility controlled diffusion through infiltrated defects that are within individual

porous barrier layer” (see Figure 10) based on the coverage model<sup>10</sup>, which takes also into account the tortuosity factor<sup>11</sup>, related to the nano-defects. By means of this model Affinito was able to describe the improvements of oxygen barrier properties, shown by a PET/AlO<sub>x</sub> barrier system, due to deposition of and acrylate-based polymer top coating.

Worth to note is that this synergic effect is defined and proposed in the case of organic interlayers which are applied in the liquid phase on the barrier layer underneath, under the assumption that a proper wetting of the internal surface of the nano-defects occurs.

### **Barrier performance evaluation**

The evaluation of the performance of a barrier layer system can be rather challenging when WVTR and OTR values approach those required for OLED devices, i.e.  $10^{-6}$  g m<sup>-2</sup> day<sup>-1</sup> and  $10^{-5} < 10^{-3}$  cm<sup>3</sup> m<sup>-2</sup> day<sup>-1</sup>, respectively. The traditional permeameters do have a detection limit of  $5 \cdot 10^{-4}$  g m<sup>-2</sup> day<sup>-1</sup> for H<sub>2</sub>O<sub>vap</sub>  $5 \cdot 10^{-4}$  cm<sup>3</sup> m<sup>-2</sup> day<sup>-1</sup> for O<sub>2</sub><sup>73</sup>. In the case of the OTR permeation techniques, an ultrahigh vacuum chamber outfitted with a residual gas analyzer has been used along with a calibrated aperture to obtain OTR measurements as low as  $10^{-6}$  cm<sup>3</sup> m<sup>-2</sup> day<sup>-1</sup><sup>10</sup>. Nevertheless, performing the same measurements for moisture is much more difficult and it would require long pumping times<sup>10</sup>. Moreover, the challenge to distinguish between the permeation through the macro-defects/pinholes and the nano-defects poses other constraints to the choice of the diagnostic tools to be adopted. In the case of the WVTR determination, the calcium test is described here in detail, since it has been adopted during this research work.

---

<sup>10</sup> In the coverage model, the layer matrix and each class of defects are assumed to act as independent and parallel permeation pathways, with each pathway weighted in proportion to its individual fractional coverage of the surface.

<sup>11</sup> The tortuosity factor takes into account the effect of the nano-defect (or pore) geometry and it is given by the ratio between the constriction factor<sup>46</sup> (i.e. the ratio of the nano-defect diameter and its depth) and the tortuosity  $\tau$  (given by the ratio between the actual diffusion path length and the barrier layer thickness)<sup>46</sup>.

**Frame I: Calcium test**

Calcium reacts almost instantaneously with  $H_2O$  and  $O_2$  according to the following reactions<sup>72</sup>:

- (1)  $Ca + H_2O \rightarrow CaO + H_2$
- (2)  $CaO + H_2O \rightarrow Ca(OH)_2$
- (3)  $2Ca + O_2 \rightarrow 2CaO$

This process finally leads to  $CaO$  and  $Ca(OH)_2$  which have different optical and electrical properties. By following the changes of either the optical<sup>21,51,74</sup> or electrical<sup>75</sup> properties of a thin ( $< 100$  nm) Ca layer, during its reaction with  $H_2O$  and  $O_2$  permeating through a barrier system, the evaluation of the WVTR can be achieved with a detection limit of  $3 \cdot 10^{-7} \text{ g m}^{-2} \text{ day}^{-1}$ <sup>10</sup>. Since also oxygen is present in the atmosphere, the oxidation of Ca due to water cannot be distinguished by the one caused by oxygen permeation, thus these WVTR values represent an upper limit<sup>10</sup>. However, on the basis of RBS studies of the Ca oxidation by using the  $^{18}O_2$  isotope, it has been shown that metallic Ca does not react with  $O_2$  at room temperature even in presence of  $H_2O$ <sup>76</sup> and the permeation values derived in our working conditions can therefore be attributed solely to the  $H_2O_{\text{vap}}$  permeating through the barrier. Furthermore, the Ca test allows discriminating between the water permeation through the macro-defects/pinholes and the permeation through the matrix porosity when the barrier layer is placed in direct contact or deposited directly on calcium, as shown in Figure 11.

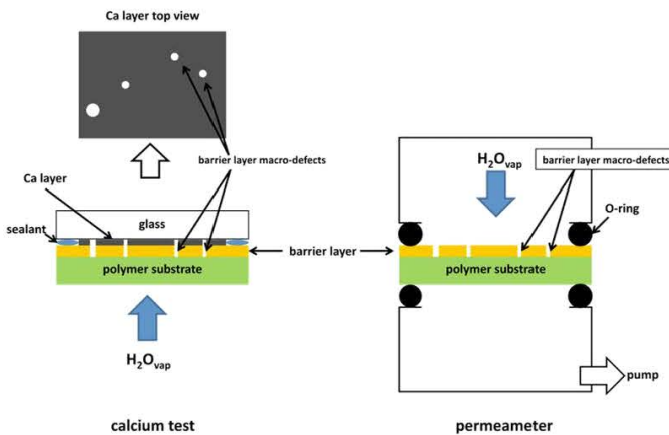


**Figure 11:** schematic representation of WVTR measurements performed by means of the calcium test (left panel) and by the traditional permeameter (right panel). As indicated in the figure, the permeation of water through the barrier layer macro-defects will lead to the fast oxidation of the Ca to  $CaO/Ca(OH)_2$  layer placed in contact with the barrier leading to the formation of white spots. The permeation through the barrier matrix is measured by excluding the white spots and measuring the homogeneous changes in transmittance with time due to the oxidation to  $CaO/Ca(OH)_2$ . In the case of the WVTR measurements performed by means of the traditional permeameter method, the total water permeation through the macro-defects and the layer matrix is measured.

In this research work the procedure of the calcium test developed by Nisato *et al.*<sup>58,74</sup> at the Philips Research Laboratories has been used for the determination of the intrinsic barrier properties. A thin (40 nm) layer of calcium is deposited by thermal evaporation on a glass plate, in a glove box environment. A structure consisting of 4 Ca samples, each one divided in 9 pads, is investigated: the Ca structure prevents that white spots generated in one pad develop across the whole calcium sample area. An example of one of these calcium samples is shown in Figure 12. On top of the calcium layer, a temporary  $\text{SiO}_2$ -like layer (intrinsic WVTR =  $10^{-2} \text{ gm}^{-2} \text{ day}^{-1}$  at  $T = 298 \text{ K}$ ; R.H. = 50%) is deposited to prevent oxidation during transport, prior to the start of the test.

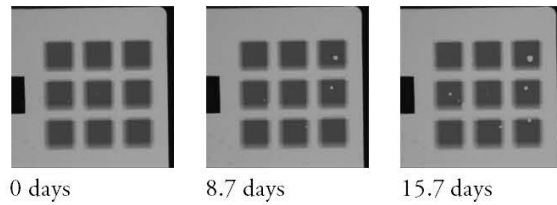


**Figure 12:** CCD camera pictures of one of the Ca samples composed of 9 calcium pads (each pad  $0.25 \text{ cm}^2$ ) at different exposure times in a climate chamber (i.e. constant temperature and relative humidity). The formation of white spots is due to the permeation of water through the pinholes extending across the barrier layer. The non transparent black reference is also visible.

Pictures of the calcium pads are acquired by a CCD camera at different time intervals (as shown in Figure 12) and the homogenous degradation of calcium is measured by following the gray tint of the calcium layer. A nontransparent black reference from the mask and a white reference from the transparent part of the glass plate have been included in every measurement to set the gray scale range and to correct for transparency changes due to the barrier film.

Through software analysis, the changes in gray tint of calcium are converted in changes in calcium layer thickness, which is related to the amount of adsorbed  $\text{H}_2\text{O}_{\text{vap}}$ <sup>58</sup>. The software also excludes the permeation occurring through the pinholes for the calculation of the intrinsic barrier properties<sup>21</sup>. A minimum decrease of calcium layer thickness of 1 nm is needed to obtain an accuracy of the 10% on the measurement.



Since the determination of the intrinsic WVTR is based on the oxidation of 1 nm of calcium, it is assumed that the oxidation of Ca to CaO is the only process to occur. The data can be provided in Ca thickness reduction with time, or converted into the amount of water needed to oxidize the whole Ca layer with the time (which decreases with the decreasing of the Ca thickness). An example is given in Figure 13.

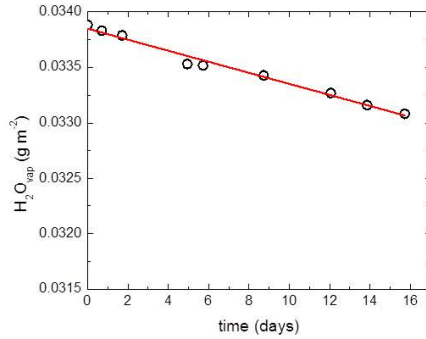


*Figure 13: Amount of water needed to completely oxidize the Ca layer as function of the time, for a barrier layer deposited on calcium at 293 K and 50 % of R.H. From the linear regression of the data shown in Figure 13, the barrier layer intrinsic WVTR value can be obtained in  $\text{g m}^{-2} \text{ day}^{-1}$ .<sup>58</sup>*

Also other techniques are reported in literature to determine the WVTR with lower detection limits than the traditional permeameter, namely the tritium based WVTR determination<sup>54, 77, 78</sup> with a detection limit of  $\sim 10^{-6} \text{ g m}^{-2} \text{ day}^{-1}$  and the permeation methods based on mass spectrometry with a detection limit of  $\sim 10^{-7} \text{ g m}^{-2} \text{ day}^{-1}$ <sup>79</sup>. However, these latter methods do not allow discerning between the permeation through the macro-defects and the one through the layer matrix.

The conclusions to be drawn from this overview in the field of moisture permeation barrier technology are:

- 1) The total water permeation through a single barrier layer occurs through different paths, which include nm-sized pores as well substrate/process induced macro-defects.
- 2) It is of paramount importance to determine and control the density of the macro-defects, as well as to control the inorganic barrier layer microstructure at the pore level.
- 3) Although empirically successful, the multilayer barrier film technology has not yet been supported by studies, which systematically address the role of the organic interlayer in affecting the multi-layer barrier performance.

## Aim of the thesis

This research work aims to unravel the role of the organic interlayer in affecting the global barrier properties of an inorganic/organic multilayer moisture diffusion barrier system. This research has been developed within a Ph.D. project funded by the Dutch Polymer Institute (DPI), within the area of Large Area Thin Films Electronics (LAFTE), and entitled “*Initiated-chemical vapor deposition of polymer interlayers for ultra-high moisture diffusion barrier systems*”. The project has been carried out in the Plasma & Materials Processing Group at the Eindhoven University of Technology in collaboration with the Holst Centre and the Philips Research Laboratories.

Within the project, a novel deposition set-up has been engineered and developed, which allows the deposition of both the organic and the inorganic barrier layers coupled with *in situ* real-time film growth studies.

Here below, the set-up is presented together with the principles of the deposition techniques and the main diagnostic tools to investigate the deposition process.

## Model of study and multilayer deposition approach

The multi-layers developed within the project are based on the siloxane chemistry, in which the inorganic layer is a PE-CVD SiO<sub>2</sub>-like layer and the organic interlayer is an organosilicon polymer synthesized by means of initiated-CVD (i-CVD). The same monomer 1,3,5-trivinyl-1,3,5-trimethyl-cyclotrisiloxane, V<sub>3</sub>D<sub>3</sub>, has been adopted for both processes.

**Frame II: Initiated-CVD**

The initiated-CVD, introduced by K.K. Gleason<sup>64, 65, 80</sup>, is a vacuum compatible free-radical-based polymerization process which allows for the deposition of polymers with the complete retention of the monomer chemistry<sup>81</sup>. The scaling up of this method to roll-to-roll processes has been also reported<sup>82</sup>.

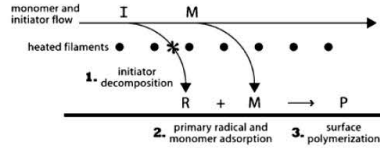


Figure 14: Schematic representation of the *i*-CVD deposition process<sup>83</sup>.

The *i*-CVD can be considered as a “mild” Hot-Wire-CVD process, in which the polymerization of monomer units (unaffected by the temperature applied to the filaments) adsorbed on the surface of a chilled substrate ( $298 < T < 333$  K)<sup>80, 81</sup> is initiated by radicals generated by the thermal ( $500 < T < 800$  K) decomposition of a volatile molecule with labile bond (e.g. a peroxide). The radicals will then react selectively with the unsaturated bond (e.g. vinyl groups) of the monomer and initiate the polymerization process. This latter then proceeds via chain growth mechanism<sup>80</sup> and it is terminated when either two growing chains or a growing chain and another initiator radical react<sup>80</sup>. It has been shown in literature<sup>84</sup> that the deposition rate is linearly dependent on the monomer surface concentration, pointing out to a polymerization process occurring at the substrate surface. The key parameter to control the monomer surface concentration is a non dimensional parameter given by the ratio of the monomer partial pressure  $P_M$  and its saturated vapor pressure at a given temperature  $P_{sat}$  ( $P_M/P_{sat}$ )<sup>84, 85</sup>. Fourier Transform Infrared spectroscopy (FT-IR) allows following the polymerization process in terms of chemistry (e.g. conversion of unsaturated to saturated chemical bonds) and degree of conversion of vinyl groups. In Figure 15, the comparison of the FT-IR spectra of the  $V_3D_3$  liquid monomer and the *i*-CVD deposited poly( $V_3D_3$ ) is reported.

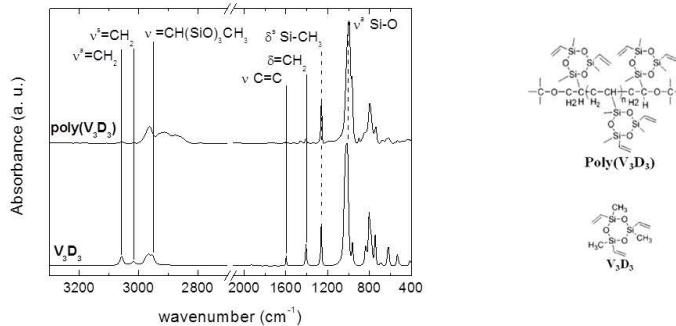
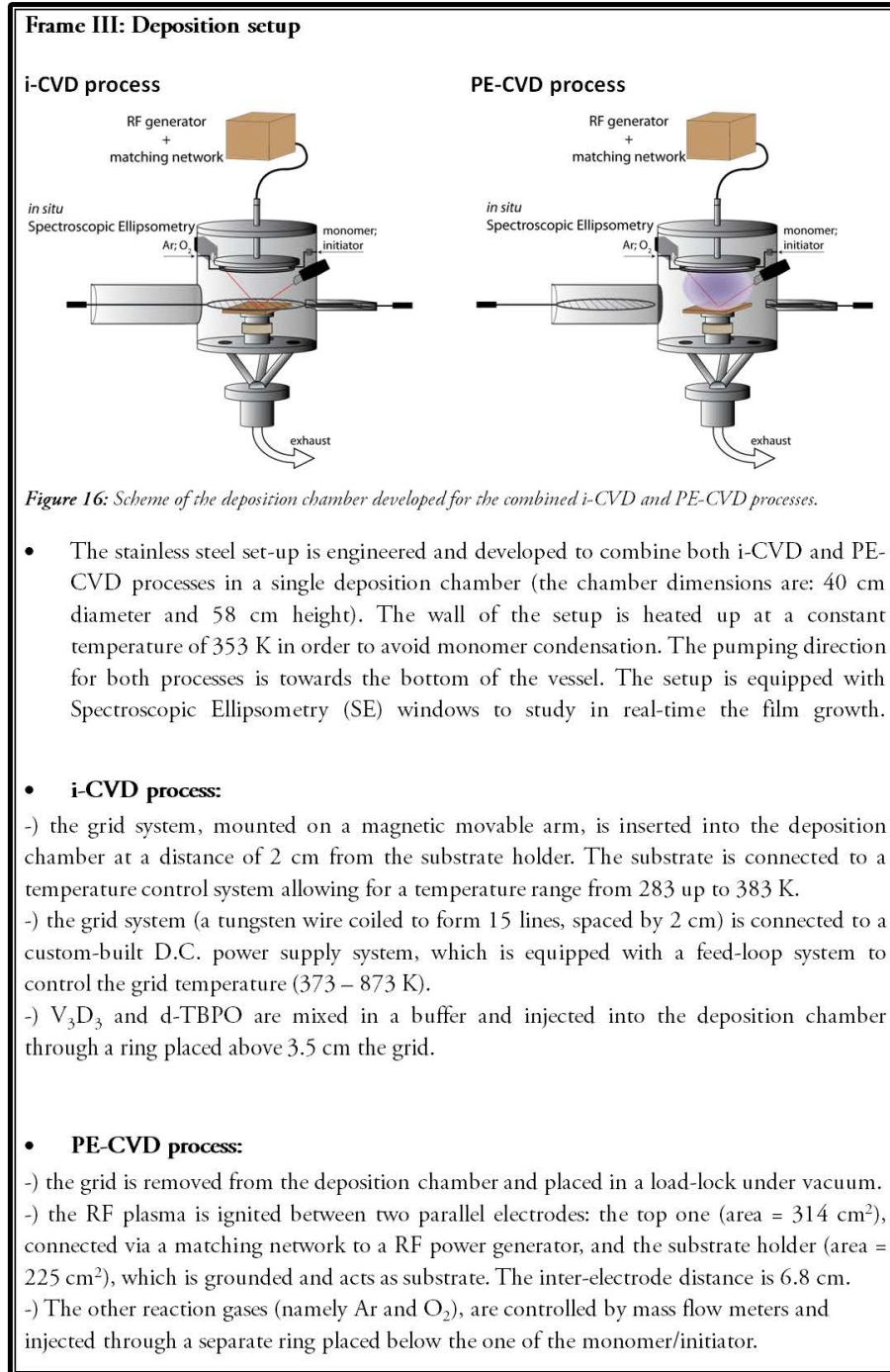


Figure 15: FT-IR comparison of the liquid  $V_3D_3$  monomer and the *i*-CVD deposited poly( $V_3D_3$ ) polymer<sup>86</sup>. The  $V_3D_3$  and poly( $V_3D_3$ ) chemical structure are also reported<sup>87</sup>.

All absorption peaks related to the vinyl groups (solid lines) are quantitatively reduced upon polymerization, while the signals related to the other monomer functional groups (namely the methyl group and the cyclotrisiloxane ring; dashed lines) are unaffected by the polymerization process<sup>86, 87</sup>.



*In situ* real-time diagnostics

The main diagnostic technique here adopted is Spectroscopic Ellipsometry (SE).

**Frame IV: Spectroscopic Ellipsometry**

Spectroscopic ellipsometry (SE) measures the change in the polarization state of a linear polarized beam upon reflection on a sample surface<sup>88</sup>. The polarization state of the incident light beam is separated into an s-component (perpendicular to the plane of incidence) and p-component (parallel to the plane of incidence) as indicated in Figure 17.

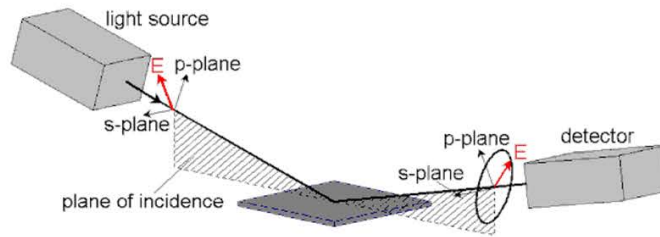


*Figure 17: Schematic representation of an incident light beam, consisting of both s- and p-polarized light, which is reflected on the sample surface. The resulting light is elliptically polarized due to changes in amplitude and phase of the s- and p-components<sup>89</sup>.*

The emitted linearly polarized light changes upon reflection in elliptically polarized light characterized by the s- and p- components. The change in polarization can be attributed to the independent change in amplitude and phase of both components. A description of the polarized light after reflection is given by the fundamental ellipsometry equation relating the Fresnel coefficients with two ellipsometric parameters,  $\Delta$  and  $\Psi$ :

$$\rho = \tan(\Psi) e^{i\Delta} = \frac{r_p}{r_s}$$

The parameters  $r_p$  and  $r_s$  represent the amplitude of respectively the p- and s-component of the polarized light after reflection. The ellipsometric parameter  $\Delta$  corresponds to the phase difference between the p- and s- polarizations while  $\tan(\Psi)$  represents the ratio of the amplitudes upon reflection. The measured ellipsometric parameters,  $\Delta$  and  $\Psi$ , determined from the reflected light, are related to the complex refractive index  $\hat{n}$  which is complex due to dielectric loss and a non-zero direct current conductivity. It is therefore defined as  $\hat{n} = n + ik$ , where  $n$  is the real part of the refractive index indicating the phase speed, and  $k$  is the imaginary part representing the light absorption in the material<sup>88</sup>.

## Research questions

As earlier introduced, this research work aims to unravel the role of the organic interlayer in affecting the global barrier properties of PECVD/i-CVD inorganic/organic multilayer moisture diffusion barrier. In details, the following research questions have been addressed, supported by the experimental approach outlined in pages 22-25:

**1) What is the growth mechanism of an organic interlayer developed by means of initiated-CVD? Can we define an i-CVD process window which allows predicting the i-CVD organic layer quality?**

This research question has been addressed in Chapter 2 where the study of the i-CVD polymer growth by means of *in situ* SE, coupled with *ex situ* diagnostics, has allowed investigating all the deposition stages, i.e. from the surface monomer adsorption to the bulk growth. Furthermore, a correlation has been made between specific process parameters (i.e. the monomer surface concentration) and the deposition of stable, highly cross-linked polymer layers (i.e. exhibiting no thickness loss upon evacuation). This has allowed defining the process parameter window, i.e.  $P_M/P_{sat}$ , followed *in situ* by SE, which controls the deposition of high quality poly( $V_3D_3$ ) layers. Figure 18 summarizes the results addressed in Chapter 2.

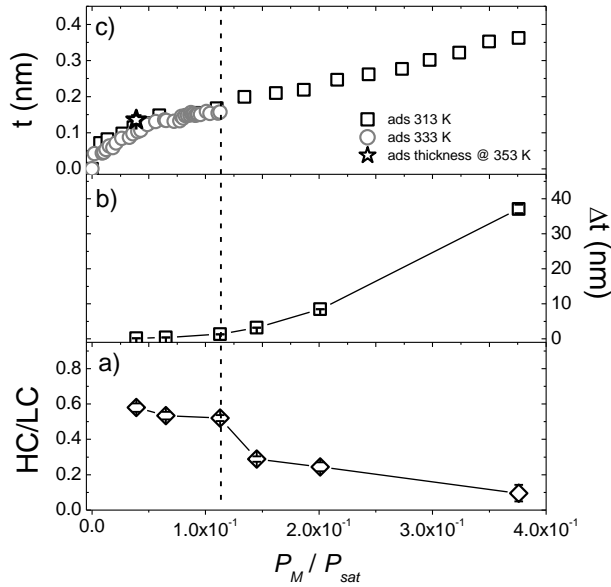


**Figure 18:** *i*-CVD process window definition: highly cross-linked poly( $V_3D_3$ ) layers exhibiting no thickness loss are deposited if the monomer adsorbed at the substrate surface is less or equal to one third of the  $V_3D_3$  monolayer thickness. a) Ratio of the low- (LC) and highly (HC) cross-linked polymer chain absorption peaks contributing to the  $(SiO)_3$  stretching peak as function of the  $P_M/P_{sat}$  parameter. b) Thickness loss as function of  $P_M/P_{sat}$ . c) Surface adsorbed monomer thickness as function of  $P_M/P_{sat}$ <sup>86</sup>.

## 2) How does an *i*-CVD organic interlayer grow on an inorganic barrier layer?

This research question has been addressed in Chapter 3, where the initial stage of the *i*-CVD growth (i.e. the monomer surface adsorption) has been investigated on a PE-CVD deposited  $SiO_2$ -like layer.

$V_3D_3$  adsorption/desorption isothermal studies have been followed by means of *in situ* SE, on  $SiO_2$ -like barrier layers characterized by different porosity level. It has been shown that the *i*-CVD monomer is able to fill/infiltrate the nano-defects in the  $SiO_2$ -like layer underneath, thus confirming the hypothesis by Affinito<sup>46</sup>.



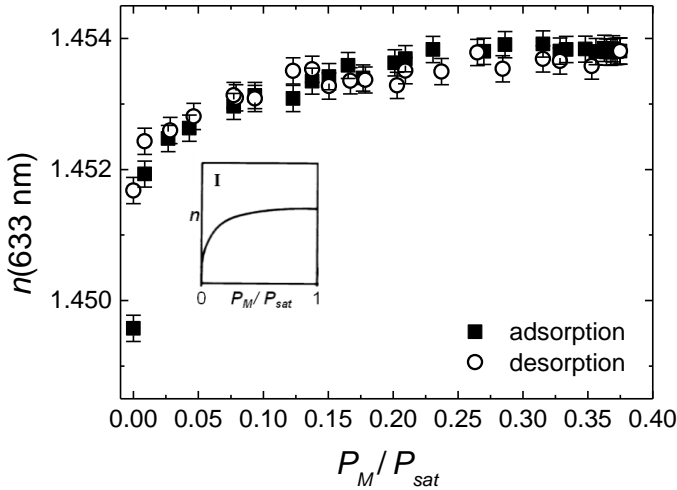


**Figure 19:**  $V_3D_3$  adsorption/desorption isotherm performed by mimicking the *i*-CVD conditions of deposition<sup>90</sup> on a dense  $SiO_2$ -like barrier layer. In the inset, a Type I isotherm<sup>91</sup> characteristic of a micro-porous layer (pores size < 2 nm) is reported for comparison.

### 3) How to discern among inorganic barrier layers exhibiting different intrinsic porosity levels?

This research question has been addressed in Chapter 4, where the principles of ellipsometric porosimetry EP<sup>91-94</sup> are introduced. EP measurements combine SE measurements with equilibrium adsorption/desorption isotherms<sup>91, 95, 96</sup>, providing information of the layer open porosity. This is performed by following the changes in the layer refractive index upon adsorption/desorption of the probing molecule in the open pores as function of the probing molecule relative pressure from 0 to saturation (i.e.  $0 < P_M / P_{sat} < 1$ ). As an example, in Figure 20,  $V_3D_3$  adsorption/desorption isotherms, performed on a porous and dense  $SiO_2$ -like layer are reported. Both isotherms are a combination of Type I (micro-porous layer, pore size < 2 nm)<sup>95, 96</sup> and Type II (non porous layer)<sup>95, 96</sup>. Due to the combination of  $V_3D_3$  adsorption into the  $SiO_2$ -like layer nano-pores and  $V_3D_3$  multilayer development on the open surface of the  $SiO_2$ -like layers, the isotherms are reported in terms of optical thickness<sup>97</sup>.

In the  $0 < P_M/P_{sat} < 0.2$  range (i.e. the  $V_3D_3$  adsorption into the layer nano-pores<sup>95,96</sup>) the dense  $SiO_2$ -like layer shows a limited optical thickness uptake. For the porous  $SiO_2$ -like layer, the optical thickness uptake is larger, pointing out to a different nano-pores density between the two layers<sup>97</sup>. A nanoporosity of 0.5 % and 0.7 % has been derived for the dense and porous  $SiO_2$ -like layer, respectively<sup>97</sup>. For  $P_M/P_{sat} > 0.2$ , the  $V_3D_3$  multilayer develops on the surface of the  $SiO_2$ -like layers. Moreover, while for the dense  $SiO_2$ -like layer the desorption curve is reversible, a hysteresis loop develops in the case of the porous  $SiO_2$ -like layer extending to the lower  $P_M/P_{sat}$  range, most certainly related to chemisorption phenomena occurring between the silanol groups present in the porous  $SiO_2$ -like layer and the oxygen of the cyclotrisiloxane ring of the  $V_3D_3$  via H bonding<sup>90</sup>.

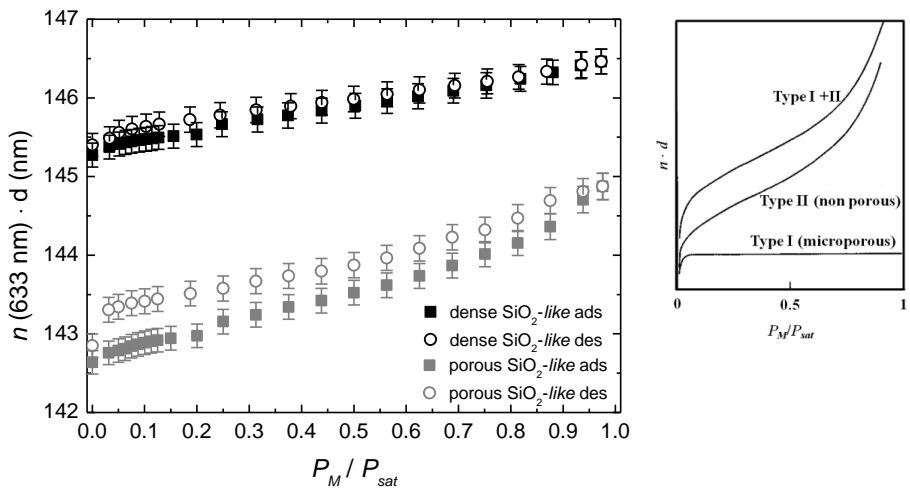


**Figure 20:**  $V_3D_3$  adsorption/desorption isotherms performed on a porous ( $n_{in situ} = 1.422$ ) and dense ( $n_{in situ} = 1.447$ )  $SiO_2$ -like layer<sup>97</sup>. Also in the Figure the types I and II isotherms and the combination of both are reported for comparison<sup>95</sup>.

#### 4) What is the role of the organic interlayer in the multilayer barrier performance?

This question has been addressed in Chapter 4 where the role of the i-CVD monomer filling/infiltration in the nano-defects present in the inorganic barrier layer is evaluated in terms of moisture permeation barrier performances. Furthermore, conclusions are drawn with respect to the *more classical* role of the organic interlayer

in terms of smoothening/decoupling of the macro-defects present in the barrier layers.

The effect of the filling/infiltration of the SiO<sub>2</sub>-like layer nano-defects has been studied as function of the intrinsic porosity of the SiO<sub>2</sub>-like layer (i.e. as function of the intrinsic WVTR values), as shown in Figure 21. It is concluded that the effect of the SiO<sub>2</sub>-like nano-defect filling by the poly(V<sub>3</sub>D<sub>3</sub>) is effective only for SiO<sub>2</sub>-like layers initially exhibiting an intrinsic WVTR value > 10<sup>-3</sup> g m<sup>-2</sup> day<sup>-1</sup>.

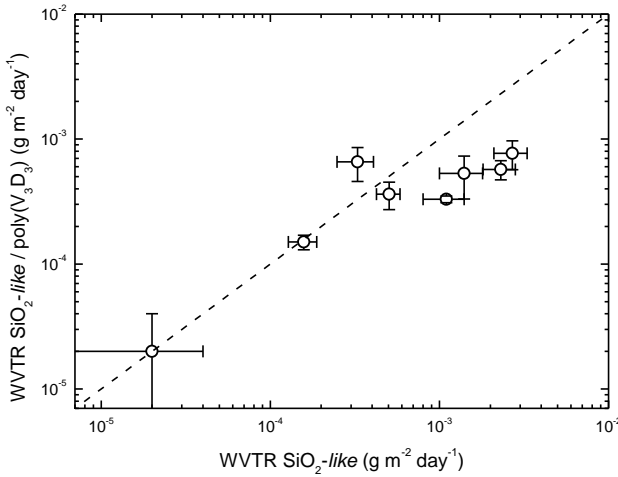


**Figure 21:** Intrinsic WVTR values of the SiO<sub>2</sub>-like/poly(V<sub>3</sub>D<sub>3</sub>) as function of the intrinsic WVTR of the SiO<sub>2</sub>-like layer: dense layers (WVTR values < 10<sup>-3</sup> g m<sup>-2</sup> day<sup>-1</sup>) do not show any improvement in terms of barrier performance upon defect filling (i.e. BIF=1). When the intrinsic barrier properties of the SiO<sub>2</sub>-like layer are progressively reduced in the range of 10<sup>-3</sup> g m<sup>-2</sup> day<sup>-1</sup>, there is an improvement in terms of barrier performance upon filling of the nano-pores (i.e. the BIF reaches values up to 4)<sup>97</sup>.

The above-mentioned results, in combination with an evaluation of the local macro-defects prior and upon deposition of the organic interlayer, and a comparison with parallel studies reported in literature<sup>66</sup>, let us to conclude that the main contribution of the i-CVD layer in improving the multilayer barrier properties is given by the smoothening/decoupling of the macro-defects.

## Conclusions and Outlook

The research carried out during this Ph.D. study has focused on the unraveling of the role of the organic interlayer on the moisture permeation barrier performance of a multi-layer system. For this purpose a vacuum set-up has been designed and engineering to carry out organic/inorganic layer deposition by means of the initiated- and plasma-enhanced CVD processes. Limiting this summary to the results in the field of barrier technology, the following conclusions can be drawn:

- The i-CVD deposited poly(V<sub>3</sub>D<sub>3</sub>) interlayer affects the global multilayer moisture permeation barrier performance in terms of smoothening and decoupling of the macro-defects present into the SiO<sub>2</sub>-like barrier layer.
- Although it has been experimentally shown that the poly(V<sub>3</sub>D<sub>3</sub>) layer is able to fill/infiltrate the nano-defects in the SiO<sub>2</sub>-like barrier underneath, this results only in a limited improvement in terms of intrinsic barrier properties.
- The improvement in terms of barrier properties due to the filling/infiltration of the SiO<sub>2</sub>-like layer nano-defects by the poly(V<sub>3</sub>D<sub>3</sub>) is observed to correlate with the residual open porosity in the barrier layer, specifically only for WVTR values of the SiO<sub>2</sub>-like layer higher than 10<sup>-3</sup> g m<sup>-2</sup> day<sup>-1</sup>, a BIF up to 4 is measured.

### Outlook:

By considering the study carried out by Graff *et al.*<sup>42</sup> on the effect of the water solubility and diffusivity of the organic interlayer in affecting the global multilayer barrier properties, it can be argued that tuning the i-CVD polymer chemistry and cross-linking may lead to a more effective improvement of the intrinsic barrier properties of the inorganic layer.

The SiO<sub>2</sub>-like layer microstructure characterization has been carried out on layers deposited on a silicon substrate. The same characterization in terms of refractive index and residual open porosity, however, should be also performed in case of

polymers as substrates, for example for barrier-on-foil applications. However, polymeric substrates often show optical anisotropy and the proper determination of the barrier layer optical constants can be achieved only by a proper optical characterization of the substrate. In order to perform the microstructure characterization of barrier layers deposited on polymers, the polymer (poly(ethylenaphtalate), PEN) anisotropy has been characterized by means of the Generalized and Spectroscopic Ellipsometry combined approach<sup>98</sup> in Chapter 5. This approach has allowed defining the optical constants of a SiO<sub>2</sub>-like barrier layer deposited on PEN, as shown in Figure 22.

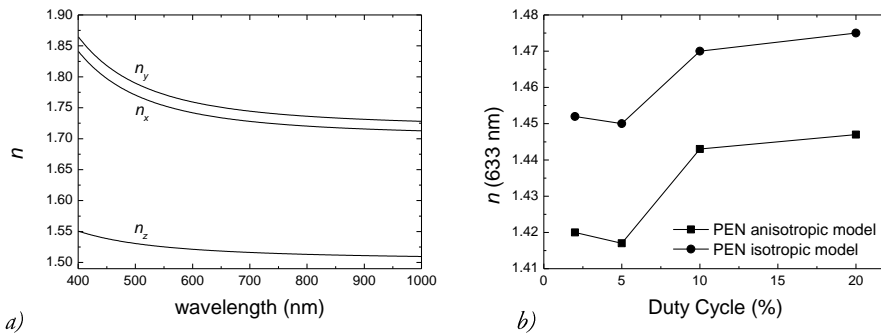


**Figure 22:** a) PEN optical dispersion along the  $x$ ,  $y$ ,  $z$  axes<sup>98</sup> b) Comparison between the values of SiO<sub>2</sub>-like layer refractive index obtained by considering an anisotropic model for the description of the PEN substrate optical properties and an isotropic model.

## References

- [1] P.E. Burrows, G.L. Graff, M.E. Gross, P.M. Martin, M.K. Shi, M. Hall, E. Mast, C. Bonham, W. Bennett, M.B. Sullivan, *Displays*, 22, 65 - 69, **2001**
- [2] M. Schaepkens, T.W. Kim, A.G. Erlat, M. Yan, K.W. Flanagan, C.M. Heller, and P.A. McConnelee, *Journal of Vacuum Science and Technology A*, 22, 1716 - 1722, **2004**
- [3] T.W. Kim, M. Yan, A.G. Erlat, P.A. McConnelee, M. Pellow, J. Deluca, T.P. Feist, R. Duggal, M. Schaepkens, *Journal of Vacuum Science and Technology A*, 23, 971 - 977, **2005**
- [4] T.N. Chen, D.S. Wu, C.C. Wu, R.H. Horng, H.F. Wei, L.Y. Jiang, H.U. Lee, Y.Y. Chang, *Vacuum*, 84, 1444 - 1447, **2010**
- [5] A. Bieder, A. Gruniger, and R. von Rohr, *Surface & Coatings Technology*, 200, 928-931, **2005**
- [6] J. Fahlreich, M. Fahland, W. Schönberger, N. Schiller, *Thin Solid Films*, 517, 3075-3080, **2009**
- [7] G. Dennler, C. Lungenschmied, H. Neugebauer, N.S. Sariciftci, M. Latrèche, G. Czeremuszkin, M.R. Wertheimer, *Thin Solid Films*, 511-512, 349 - 353, **2006**
- [8] A. Yoshida, A. Sugimoto, T. Miyadera, S. Miyaguchi, *Journal of Photopolymer Science and Technology*, 14, 327 - 332, **2001**
- [9] J.-S. Park, H. Chae, H.K. Chung, S.I. Lee, *Semiconductor Science and Technology*, 26, 034001, **2011**
- [10] J.S. Lewis and M.S. Weaver, *IEEE Journal of Selected Topics in Quantum Electronics*, 10, 45 - 57, **2004**
- [11] J. Lewis, *Materials Today*, 9, 38-45, **2006**
- [12] W.A. MacDonald, *Journal of Materials Chemistry* 14, 4 - 10, **2004**
- [13] P.F. Carcia, R.S. McLean, S. Hegedus, *Solar Energy Materials & Solar Cells*, 94, 2375 - 2378, **2010**
- [14] L.C. Olsen, M.E. Gross, G.L. Graff, S.N. Kundu, *Proceeding of SPIE*, 7048, 704806, **2008**
- [15] L.C. Olsen, S.N. Kundu, C.C. Bonham, M. Gross, *31<sup>th</sup> IEEE Photovoltaic Specialists Conference (PVSC)*, **2005**
- [16] L.C. Olsen, M.E. Gross, S.N. Kundu, *33<sup>th</sup> IEEE Photovoltaic Specialists Conference (PVSC)*, **2008**
- [17] J. Spanring, N. Depine, B. Erler, M. Feichtner, J. Gradwohl, W. Krumlacher, H. Muckenhuber, A. Reininger, F. Reisinger, A. Ruplitsch, E. Seitler, A. Skringer, A.K. Plessing, *33<sup>rd</sup> IEEE Photovoltaic Specialist Conference*, 1 - 4, 973 - 976, **2008**

- [18] P. Madakasira, K. Inoue, R. Ulbricht, S.B. Lee, M. Zhou, J.P. Ferraris, A.A. Zakhidov, *Synthetic Metals*, 155, 332 - 335, **2005**
- [19] M. Hermenau, S. Schubert, H. Klumbies, J. Fahlteich, L.M. Meskamp, K. Leo, M. Riede, *Solar Energy Materials & Solar Cells*, 97, 102 - 108, **2012**
- [20] F.J.H. van Assche, R.T. Vangheluwe, J.W.C. Maes, W.S. Mischke, M.D. Bijker, F.C. Dings, M.F.J. Evers, W.M.M. Kessels, M.C.M. van de Sanden, *Proceedings of The Society for Information Displays*, 695 - 697, **2004**
- [21] P. van de Weijer and T. van Mol, "White paper on the characterization of thin-film barrier layers for protection of organic Light-Emitting Diodes" Editor: M. Kilitziraki, **2009**
- [22] C.W.T. Bulle-Lieuwma, P. van de Weijer, *Applied Surface Science*, 252, 6597-6600, **2006**
- [23] W. Prins and J.J. Herman, *J. Phys. Chem.*, 63, 716, **1959**
- [24] Y.G. Tropsha and N.G. Harvey, *J. Phys. Chem. B*, 101, 2259-2266, **1997**
- [25] A.G. Erlat, R.J. Spontak, R.P. Clarke, T.C. Robinson, P.D. Haaland, Y. Tropsha, N.G. Harvey, E.A. Vogler, *J. Phys. Chem. B*, 103, 6047-6055, **1999**
- [26] A.G. Erlat, B.-C. Wang, R.J. Spontak, Y. Tropsha, K.D. Mar, D.B. Montgomery, and E.A. Vogler, *J. Mater. Res.*, 15, 704 - 717, **2000**
- [27] N. Inagaki, S. Tasaka, T. Nakajima, *Journal of Applied Polymer Science*, 78, 2389 - 2397, **2000**
- [28] M. Creatore, F. Palumbo, R. d'Agostino, P. Fayet, *Surface & Coatings Technology*, 142-144, 163 - 168, **2001**
- [29] M. Vogt, R. Hauptmann, *Surface & Coatings Technology*, 74 - 75, 676 - 681, **1995**
- [30] H. Lin, L. Xu,, X. Chen, X. Wang, M. Sheng, F. Stubhan, K.H. Merkel, J. Wilde, *Thin Solid Films*, 333, 71 - 76, **1998**
- [31] J.E. Klemberg-Sapieha, L. Martinu, O.M. Küttel, and M.R. Wertheimer, *36<sup>th</sup> Annual Technical Conference Society of Vacuum Coaters Proceedings*, 445-449, **1993**
- [32] A.S. da Silva Sobrinho, M. Latreche, G. Czeremuskin, J.E. Klemberg-Sapieha, and M.R. Wertheimer, *Journal of Vacuum Science and Technology A*, 16, 3190 - 3198, **1998**
- [33] A.S. da Silva Sobrinho, G. Czeremuskin, M. Latreche, and M.R. Wertheimer, *Journal of Vacuum Science and Technology A*, 18, 149-157, **2000**
- [34] C. Bichler, T. Kerbstadt, H.C. Langowski, U. Moosheimer, *Surface & Coatings Technology*, 112, 373 - 378, **1999**

- [35] B.M. Henry, A.G. Erlat, A. McGuigan, C.R.M. Grovenor, G.A.D. Briggs, Y. Tsukahara, T. Miyamoto, N. Noguchi, T. Niijima, *Thin Solid Films*, 382, 194 - 201, **2001**
- [36] B.M. Henry, A.G. Erlat, C.R.M. Grovenor, C.S. Deng, and G.A.D. Briggs, T. Miyamoto, N. Noguchi, T. Niijima, and Y. Tsukahara, *44<sup>th</sup> Annual Technical Conference Society of Vacuum Coaters Proceedings*, 469 - 475, **2001**
- [37] B.M. Henry, F. Dinelli, K.Y. Zhao, C.R.M. Grovenor, O.V. Kolosov, G.A.D. Briggs, A.P. Roberts, R.S. Kumar, R.P. Howson, *Thin Solid Films*, 355 - 356, 500 - 505, **1999**
- [38] A.G. Erlat, B.M. Henry, J.J. Ingram, D.B. Mountain, A. McGuigan, R.P. Howson, C.R.M. Grovenor, G.A.D. Briggs, Y. Tsukahara, *Thin Solid Films*, 388, 78 -86, **2001**
- [39] C. Misiano, E. Simonetti, P. Cerolini and F. Staffetti, *34<sup>th</sup> Annual Technical Conference Society of Vacuum Coaters Proceedings*, 105, **1991**
- [40] T.G. Krug, *33<sup>th</sup> Annual Technical Conference Society of Vacuum Coaters Proceedings*, 163, **1990**
- [41] G. Garcia-Ayuso, L. Vhquez, J.M. Martinez-Duart, *Surface & Coatings Technology* 80, 203 - 206, **1996**
- [42] G.L. Graff, R.E. Williford, P.E. Burrows, *Journal of Applied Physics*, 96, 1840 - 1849, **2004**
- [43] E.H.H. Jamienson, A.H. Windle, *Journal of Materials Science*, 18, 64 - 80, **1983**
- [44] H. Chatham, *Surface & Coatings Technology*, 78, 1 - 9, **1996**
- [45] J. Weiss, C. Leppin, W. Mader, and U. Salzberger, *Thin Solid Films*, 174, 155 - 158, **1989**
- [46] J. Affinito, D. Hilliard, *47<sup>th</sup> Annual Technical Conference Society of Vacuum Coaters Proceedings*, 563, **2004**
- [47] G. Rossi, M. Nulman, *J. Appl. Phys.* 74 (9), **1993**
- [48] A.P. Roberts, B.M. Henry, A.P. Sutton, C.R.M. Grovenor, G.A.D. Briggs, T. Miyamoto, M. Kano, Y. Tsukahara, M. Yanaka, *J. Membrane Sci.*, 208, 75 - 88, **2002**
- [49] W. Keuning, P. van de Weijer, H. Lifka, W.M.M. Kessels, M. Creatore, *Journal of Vacuum Science and Technology A*, 31, 01A131-1 - 01A131-6, **2012**
- [50] S. Sarkar, J. H. Culp, J.T. Whyland, M. Garvan, V. Misra, *Organic Electronics*, 11, 1896 -1900, **2010**



- [51] P.F. Carcia, R.S. McLean, M.H. Reilly, M.D. Groner, S.M. George, *Applied Physics Letter*, 89, 031915, 2006
- [52] E. Langereis, M. Creatore, S.B.S. Heil, M.C.M. van de Sanden, and W.M.M. Kessels, *Applied Physics Letters*, 89, 081915, 2006
- [53] J. Meyer, D. Schneidenbach, T. Winkler, S. Hamwi, T. Weimann, P. Hinze, S. Ammermann, H.-H. Johannes, T. Riedl, W. Kowalsky, *Applied Physics Letters*, 94, 233305, 2009
- [54] M.D. Groner, S.M. George, R.S. McLean and P.F. Carcia, *Applied Physics Letters*, 88, 051907, 2006
- [55] W.J. Potscavage, S. Yoo, B. Domercq, B. Kippelen, *Applied Physics Letters*, 90, 253511, 2007
- [56] E. Langereis, Ph.D. Thesis “Plasma-assisted atomic layer deposition: an in situ diagnostic study” Eindhoven University of Technology, 2008
- [57] P. Poodt, R. Knaapen, A. Illiberi, F. Roozeboom, A. van Asten, *Journal of Vacuum Science and Technology A*, 31, 01A142-1 - 01A142-5, 2012
- [58] G. Nisato, M. Kuilder, and P. Bouten, L. Moro, O. Philips, N. Rutherford, *Proceeding of the Society for Information Display Symposium*, 34, 550 - 553, 2003
- [59] Y.C. Han, C. Jang, K.J. Kim, K.C. Choi, K.H. Jung, B.-S. Bae, *Organic Electronics*, 12, 609 - 613, 2011
- [60] D.G. Shaw and M.G. Langlois, *37<sup>th</sup> Annual Technical Conference Society of Vacuum Coaters Proceedings*, 240-244, 1994
- [61] K. Vaško, K. Noller, M. Mikula, S. Amberg-Schwab, U. Weber, *Central European Journal of Physics*, 7, 371 - 378, 2009
- [62] A.A. Dameron, D. Seghete, B.B. Burton, S. D. Davidson, A.S. Cavanagh, J. A. Bertrand, S. M. George, *Chemistry of Materials*, 20, 3315 - 3326, 2008
- [63] S.M. George, B. Yoon and A.A. Dameron, *Accounts of Chemical Research*, 42, 498 - 508, 2009
- [64] A. Asatekin, M.C. Barr, S.H. Baxamusa, K.K.S. Lau, W. Tenhaeff, J. Xu, and K.K. Gleason, *Materials Today*, 13, 26-33, 2010
- [65] G. Ozaydin-Ince, A.M. Coclite and K.K. Gleason, *Reports on Progress in Physics*, 75, 016501, 2012
- [66] A.M. Coclite, G. Ozaydin-Ince, F. Palumbo, A. Milella, K.K. Gleason, *Plasma Processes and Polymers*, 7, 561 - 570, 2010
- [67] D.A. Spee, C.H.M van der Werf, J.K. Rath, R.E.I. Schropp, *Journal of Nanoscience and Nanotechnology*, 11, 9, 8202 - 8205, 2011

- [68] R.P. Patel, D. Chiavetta, C.A. Wolden, *Journal of Vacuum Science and Technology A*, 29, 6, 061508-1 - 061508-6, **2011**
- [69] R.P. Patel, C.A. Wolden, *Journal of Vacuum Science and Technology A*, 29, 2, 021012-1 - 021012-7, **2011**
- [70] A. Francescangeli, F. Palumbo, R. d'Agostino, C. Defranoux, *Plasma Processes and Polymers*, 6, 132 - 138, **2009**
- [71] A. Francescangeli, F. Palumbo, R. d'Agostino, *Plasma Processes and Polymers*, 5, 708 -717, **2008**
- [72] A. Patelli, S. Vezzu', L. Zottarel, E. Menin, C. Sada, A. Martucci, S. Costacurta, *Plasma Processes and Polymers*, 6, S665 - S670, **2009**
- [73] <http://www.mocon.com/>
- [74] G. Nisato, P.C. Bouten, P.J. Slickerveer, W.D. Bennet, G.L. Graaf, N. Rutherford, L. Wiese, *Proceeding Asia Display*, 1435, **2001**
- [75] S. Schubert, H. Klumbies, L. Müller-Meskamp, and K. Leo, *Review of Scientific Instruments*, 82, 094101, **2011**
- [76] S. Cros, M. Firon, S. Lenfant, P. Trouslard, L. Beck, *Nuclear Instruments and Methods in Physics Research B*, 251, 257–260, **2006**
- [77] A.A. Dameron, S.D. Davidson, B.B. Burton, P.F. Carcia, R.S. McLean, and S. George, *Journal of Physical Chemistry C*, 112, 4573 - 4580, **2008**
- [78] A.R. Coulter, R.A. Deeken and G.M. Zentner, *Journal of Membrane Science*, 65, 269 -275, **1992**
- [79] A. Ranade, N.A. D'Souza, R.M. Wallace and B.E. Gnade, *Review of Scientific Instruments*, 76, 013902, **2005**
- [80] M.E. Alf, A. Asatekin, M.C. Barr, S. H. Baxamusa, H. Chelawat, G. Ozaydin-Ince, C.D. Petruczok, R. Sreenivasan, W.E. Tenhaeff, N.J. Trujillo, S. Vaddiraju, J. Xu, K.K. Gleason, *Advanced Materials*, 22, 1993 - 2027, **2010**
- [81] T.P. Martin, K.K.S. Lau, K. Chan, Y. Mao, M. Gupta, W. S. O'Shaughnessy, K.K. Gleason, *Surface & Coatings Technology*, 201, 9400 - 9405, **2007**
- [82] H.G. Pryce Lewis, N.P. Bansal, A.J. White, E.S. Handy, *Thin Solid Films*, 517, 3551 - 3554, **2009**
- [83] K.K.S. Lau and K.K. Gleason, *Macromolecules*, 39, 3688 - 3694, **2006**
- [84] K. Chan and K.K. Gleason, *Macromolecules*, 39, 3890 - 3894, **2006**
- [85] K.K.S. Lau and K.K. Gleason, *Macromolecules*, 39, 3695 - 3703, **2006**
- [86] G. Aresta, J. Palmans, M.C.M. van de Sanden, M. Creatore, accepted for publication on *Journal of Vacuum Science and Technology A*, **2012**

- [87] W.S. O'Shaughnessy, M. Gao, and K.K. Gleason, *Langmuir*, 22, 7021 - 7026, 2006
- [88] H. Fujiwara, "*Spectroscopic Ellipsometry Principles and Applications*", John Wiley & Sons Ltd, 2007
- [89] P.H.W. Robeerst, *System Integration Project II: Diagnostics in plasma processing*, Eindhoven University of Technology, 2006
- [90] G. Aresta, J. Palmans, M.C.M. van de Sanden, M. Creatore, *Microporous and Mesoporous Materials*, 151, 434 - 439, 2012
- [91] K.S.W. Sing, D.H. Everett, R.A.W. Haul, L. Moscou, R.A. Pierotti, J. Rouquerol, T. Siemieniewska, *Pure Applied Chemistry*, 57, 603 - 619, 1985
- [92] S. Elsava, F. Iacopi, M.R. Baklanov, C.E.A. Kirschhock, K. Maens, J.A. Martens, *Journal of the American Chemical Society*, 129, 9288 - 9289, 2007
- [93] C. Licitra, R. Bouyssou, T. Chevolleau, F. Bertin, *Thin Solid Films* 518 (2010) 5140-5145
- [94] K.S.W. Sing, *Colloid. Surface, A* 241, 3-7, 2004
- [95] S. J. Gregg and K. S. W. Sing, "*Adsorption, Surface Area and porosity*", Academic Press Inc. Ltd, London, England, 1982
- [96] F. Rouquerol, J. Rouquerol, K. Sing, "*Adsorption by powders & porous solids. Principles, methodology and applications*", Academic Press, London, England, 1999
- [97] G. Aresta, E.R.J. van Beekum, J. Palmans, M.C.M. van de Sanden, M. Creatore, to be submitted
- [98] G. Aresta, P.A. Premkumar, S.A. Starostin, H. de Vries, M.C.M. van de Sanden, M. Creatore, *Plasma Processes and Polymers*, 7, 766 - 774, 2010

# Chapter 2

## *Initiated-chemical vapor deposition of organosilicon layers: monomer adsorption, bulk growth and process window definition\**

### Abstract

Organosilicon layers have been deposited from 1,3,5-trivinyl-1,3,5-trimethylcyclotrisiloxane ( $V_3D_3$ ) by means of the initiated-CVD (i-CVD) technique in a deposition setup, *ad-hoc* designed for the engineering of multi-layer moisture permeation barriers. The application of Fourier Transform-Infrared (FT-IR) spectroscopy shows that the polymerization proceeds through the scission of the vinyl bond and allows quantifying the degree of conversion of vinyl groups, which is found to be larger than 80 % for all the deposited layers. *In situ* real-time Spectroscopic Ellipsometry (SE) allows following all the i-CVD growth stages, i.e. from the initial monomer adsorption to the layer bulk growth. Finally, the combination of SE and FT-IR has allowed defining the process window for the deposition of stable and highly cross-linked poly( $V_3D_3$ ) layers by tuning a key process parameter, i.e. the surface monomer adsorption.

---

\* Accepted for publication as: G. Aresta, J. Palmans, M.C.M. van de Sanden, M. Creatore, *Journal of Vacuum Science and Technology A*, 2012

## Introduction

In the past years, Initiated Chemical Vapor Deposition (i-CVD) has proven to be a very well suited approach towards vacuum deposition of polymeric films for application in many fields where specific surface and bulk properties are desired, i.e. hydrophobicity/hydrophilicity<sup>1,2</sup>, antimicrobial<sup>3</sup>, binding of biological ligands<sup>4</sup>, biopassive dielectrics<sup>5</sup>, low-k materials<sup>6</sup> and, recently, as responsive materials<sup>7</sup> and organic interlayers in multilayer moisture and oxygen barrier systems<sup>8,9</sup>. The advantage of the i-CVD approach with respect to the widely known hot wire-CVD is the lower thermal budget required for the polymerization process to occur. The unsaturated bonds of the monomer unit are activated by the free radicals generated during the thermal dissociation of an initiator molecule (i.e. a peroxide), requiring only “mild” grid temperature conditions, typically 500 – 800 K, and, therefore, making the process compatible with the treatment of sensitive materials such as paper, polymers and membranes. The monomer structure retention, within the deposited layer, allows defining the i-CVD as an outstanding deposition tool for vacuum polymerization, compared to other well known CVD polymerization processes, such as (pulsed) PE-CVD<sup>10</sup>. Also the potential for scaling-up and compatibility with roll-to-roll solutions<sup>11</sup> have been discussed for the i-CVD process. Previous studies have shown that the deposition rate and the number-average molecular weight in the i-CVD process are linearly dependent on the monomer surface concentration<sup>12</sup>, pointing out to a polymerization process predominantly occurring at the substrate surface. The monomer surface concentration can be related to a nondimensional parameter given by the ratio of the monomer partial pressure ( $P_M$ ) and its saturated vapor pressure ( $P_{sat}$ ),  $P_M/P_{sat}$ <sup>13, 14</sup>. The  $P_M/P_{sat}$  and, hence, the monomer surface concentration, can be controlled by varying the deposition parameters such as the monomer partial pressure  $P_M$  or the substrate temperature (which will lead to changes of the monomer saturation vapor pressure  $P_{sat}$ ). The ratio  $P_M/P_{sat}$ , then, represents a key parameter for any i-CVD process to be set up<sup>13</sup>. It is therefore fundamental having *in situ* real-time diagnostics to study the overall i-CVD process and, in particular, to quantify the monomer surface adsorption and, consequently, defining the i-CVD process window for a given deposition process. Generally, the i-CVD process window can be defined as a range in which the  $P_M/P_{sat}$  parameter is large enough to sustain the polymerization process, without leading to an excess of monomer at the surface, resulting either in an incomplete polymerization or in monomer condensation. Considering these

guidelines, on the basis of studies on the relationship between the monomer surface adsorption and the deposition rate of the polymer and number-average molecular weight<sup>13,14</sup>, the recommended i-CVD process window has been defined by a  $P_M/P_{sat}$  value leading to one- up to- three monolayers of adsorbed monomer on the surface<sup>13</sup>. However, other aspects, related to the monomer reactivity and the final stability and quality of the deposited layer, may need to be taken into account when defining the i-CVD process window. On the base of our studies, it has been observed that highly cross-linked polymer structures can be obtained by reducing the presence of unreacted monomer units or short oligomers at the end of the deposition process.

The implementation of *in situ* real-time diagnostics in order to define an i-CVD process window is, therefore, fundamental. So far, in literature, quartz crystal microbalance (QCM) measurements have been used for the determination of the monomer surface concentration<sup>12-14</sup>, while the film growth development has been followed by means of laser interferometry<sup>15-18</sup>. During QCM measurements, the mass adsorption on the quartz crystal, generally gold coated, results in a frequency shift which can be directly related to the mass of the adsorbed monomer<sup>12-14</sup>. As only physisorption is considered to control the monomer/surface interaction<sup>12-14</sup>, at each value of  $P_M/P_{sat}$ , the amount of adsorbed monomer is taken as the average of the measured monomer surface concentration during the adsorption and desorption of the monomer from the surface of the QCM<sup>12-14</sup>.

Laser reflection interferometry measures the periodic interference of light waves reflected from the growing film surface and the film/substrate interface. However, in order to continuously monitor the film growth, a calibration needs to be performed by comparing the interferometry results with data collected using an independent method. This means that only the layer thickness can be monitored in real-time, as an assumption on the growing layer optical constants has to be made.

Nowadays, *in situ* Spectroscopic Ellipsometry (SE) is widely acknowledged as analytical tool providing real-time monitoring on film growth processes<sup>19-26</sup>, since it is a non destructive, versatile technique easily implemented in a deposition setup. With respect to the above mentioned techniques, SE allows the real-time, direct determination of both layer thickness and optical constants<sup>27</sup> of the growing layer. Since the thickness sensitivity with SE reaches the atomic level, this technique is also suitable for the determination of the thickness of the adsorbed monomer at the surface in the i-CVD process. For example, Karpovich and Blanchard<sup>28</sup> studied the adsorption of different vapors on a gold coated QCM crystal by means of SE and

QCM showing a linear relationship between the SE measured adsorbed vapor layer thickness and the QCM measured adsorbed vapors layer volume<sup>28</sup>. When applied to the i-CVD process, therefore, *in situ* SE represents an “all in one” diagnostic tool providing information on the whole process, i.e. starting from the monomer adsorption stage to the polymerization process and polymer bulk growth.

This paper reports on the real time study of the i-CVD process of poly(V<sub>3</sub>D<sub>3</sub>) layers by means of *in situ* SE measurements. Poly(V<sub>3</sub>D<sub>3</sub>) polymers have been synthesized by means of 1,3,5-trivinyl-1,3,5-trimethylcyclotrisiloxane (V<sub>3</sub>D<sub>3</sub>) as monomer and di-tert-butyl peroxide (d-TBPO) as initiator. Poly(V<sub>3</sub>D<sub>3</sub>) have proven their potential as biopassivating material being highly cross-linked, showing good adhesion to silicon substrates and being insoluble both in polar and apolar solvents<sup>5, 29</sup>. In our case poly(V<sub>3</sub>D<sub>3</sub>) layers were deposited as organic interlayers for an organosilicon-based organic/inorganic multilayer moisture and oxygen barrier system, where highly cross-linked organic interlayers are desirable<sup>8, 9</sup>.

The use of *in situ* SE, as a tool to study the polymer growth mechanism during all its stages, is reported for the first time, according to the authors' knowledge. The monomer surface adsorption has been studied by means of adsorption/desorption isotherms followed by *in situ* SE measurements on the same substrates used for the deposition of the polymeric layer (i.e. Si/SiO<sub>2</sub> substrate). Differently from the studies already reported in literature<sup>12-14</sup>, the desorption isotherm has also been taken into account as it allows highlighting a possible chemisorption process, between monomer and substrate. Furthermore, the polymer growth has been followed as function of the deposition time. The use of the *in situ* and *ex situ* SE coupled to other diagnostic tools (namely FT-IR) has allowed for the definition of the i-CVD process window for the monomer here under investigation, by limiting the monomer surface adsorption to 1/3 of the monomer monolayer thickness, for the deposition of stable, highly cross-linked polymers.

The paper is organized as follow: the experimental part reports on the deposition chamber, the deposition procedure and analytical techniques used to characterize the polymers chemistry, structure and degree of conversion of vinyl groups. Also in this part the description of the methodology used for the *in situ* study of the poly(V<sub>3</sub>D<sub>3</sub>) layer with SE is provided together with the description of the V<sub>3</sub>D<sub>3</sub> monomer adsorption /desorption (ads/des) measurement procedure. The results and discussion part is divided in two sections: in the first one the results on the poly(V<sub>3</sub>D<sub>3</sub>) characterization is provided; in the second part the *in situ* SE study of the

poly(V<sub>3</sub>D<sub>3</sub>) film growth in all its stages is discussed together with the studies on the polymer stability and the definition of the i-CVD process window.

## Experimental

### Deposition chamber

The deposition chamber is a custom-built cylindrical vacuum reactor shown in Figure 1.

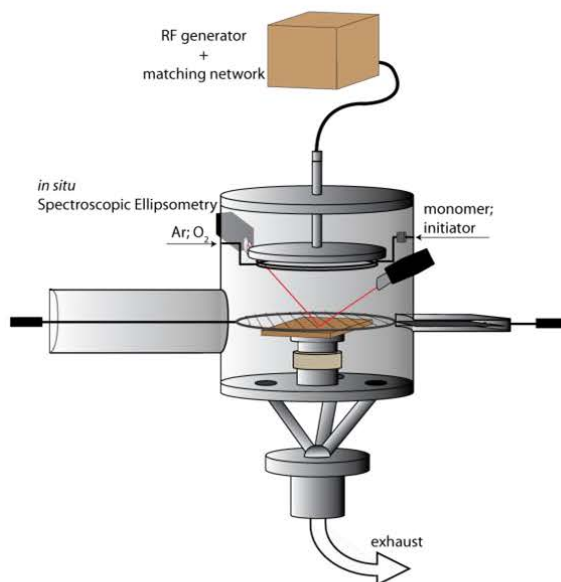


*Figure 1: Schematic of the i-CVD/PE-CVD deposition setup.*

This setup allows performing both i-CVD and PE-CVD processes, in order to develop organic and inorganic layers, respectively. The chamber measures 40 cm in diameter and 58 cm in height. The walls of the setup are heated up at a constant temperature of 353 K to avoid monomer condensation and minimize monomer adsorption. Monomer and initiator are mixed in a buffer and injected into the deposition chamber through a ring placed above the grid. The vessel is pumped through the bottom by means of a rotary vane pump (Adixen) in combination with a



turbomolecular pump (Pfeiffer). The pressure is monitored by three pressure gauges for different ranges: a Penning (Pfeiffer) pressure gauge to cover the range from  $10^{-7}$  mbar up to atmospheric pressure which is used to measure the base pressure of the setup and two capacitive (Pfeiffer) pressure gauges to monitor the pressure during the process ( $10^{-3}$  mbar – 10 mbar) and the pressurization of the system (1 mbar – atmospheric pressure). During the deposition process the pressure is controlled through a butterfly valve (VAT).

The grid consists of a single tungsten wire ( $\varnothing = 0.2$  mm) coiled to form 15 lines, 2 cm spaced one from each other, resistively heated by a DC current. A feed-loop system to read and auto adjust the grid temperature to the set value is embedded into a custom-built power supply system. The grid is mounted on a magnetic movable arm through which is removed from the deposition chamber and placed in a separate vacuum chamber, in order to avoid deposition on the wire during the PE-CVD process. The 225 cm<sup>2</sup> copper made substrate holder is connected to a temperature control system, composed by resistive heating elements (Eurotherm) and three Peltier cooling elements, which allow for the temperature control from 383 K to below room temperature. The substrate holder is connected to a moving system in order to vary the grid-substrate distance. During this work, this latter was fixed to 2 cm. The substrate holder is grounded and acts as electrode during the PE-CVD process when the plasma is ignited by applying a radiofrequency to the RF electrode (area = 314 cm<sup>2</sup>, Figure 1) placed at a distance of 6.8 cm from the grounded electrode. The setup, which has a quartz window for visual inspection, is equipped with SE windows mounted in sliding flanges in order to study the deposition process at any substrate height.

The monomer (1,3,5-trivinyl-1,3,5-trimethylcyclotrisiloxane:  $V_3D_3 > 95\%$ , Gelest) and the initiator (di-tert-butyl peroxide: d-TBPO 98%, Aldrich) are used without any further purification. Monomer and initiator are vaporized in stainless steel bubblers set at the temperature of 373 K and 298 K, respectively, and the flow rates are controlled by two vapor source controllers (VSC 1150 C, MKS). The monomer and initiator lines to the vessel are heated up at a constant temperature of 393 K and 308 K, respectively, to avoid vapor condensation. 4 inch c-Si wafers are used as substrates for the deposition of the poly( $V_3D_3$ ) layers without any cleaning procedure prior to the deposition.

During a typical i-CVD deposition, monomer and initiator are injected into the deposition chamber, then the pressure is set to the deposition value and the

deposition is started by setting the grid temperature. The deposition process is concluded by switching off the initiator and monomer flow rates and the grid power, then the chamber is gradually evacuated to the base pressure. Finally the system is brought to atmospheric pressure by pressurizing it with a controlled flow of N<sub>2</sub> gas. The deposition conditions of the i-CVD layers are listed in Table I.

**Table I**  
Conditions of deposition of the poly(V<sub>3</sub>D<sub>3</sub>) layers.

sample	V <sub>3</sub> D <sub>3</sub> (sccm)	d-TBPO (sccm)	T <sub>wire</sub> (K)	T <sub>sub</sub> (K)	P (mbar)	$P_{V_3D_3}/P_{totV_3D_3}$	T <sub>wall</sub> (K)
1	10	2	473	313	0.7	0.374	353
2				323		0.201	
3				328		0.150	
4				333		0.113	
5				343		0.065	
6				353		0.040	

### Layer Characterization

The chemical characterization of the poly(V<sub>3</sub>D<sub>3</sub>) layers is performed by means of Fourier Transform Infrared (FT-IR) spectroscopy with a Bruker Tensor 27 spectrophotometer. The FT-IR spectra are acquired in transmission mode in the range of 400 cm<sup>-1</sup> - 4000 cm<sup>-1</sup> with a resolution of 4 cm<sup>-1</sup> and number of scans varying from 256 to 2000 (depending on the film thickness) in order to reduce the signal to noise ratio. Before the spectra acquisition the spectrometer is purged for 15 min with N<sub>2</sub> to minimize the effect of H<sub>2</sub>O and CO<sub>2</sub> absorption. The monomer spectrum is acquired with the same spectrometer by placing a drop of the liquid monomer between two IR transparent KBr windows. The deconvolution of the CH<sub>x</sub> (3150 / 2800 cm<sup>-1</sup>), and the Si-O-Si (1150 / 900 cm<sup>-1</sup>) – related absorption bands is performed by OriginLab software. Lorentzian functions are applied for the deconvolution of the liquid monomer absorption band, since collision broadening contributes mainly to the vibrational modes, while a Gaussian functions are used for the deconvolution of the polymer absorption bands, as, in this case, the Doppler broadening, due to molecules thermal motion, dominates<sup>30, 31</sup>. To determine the degree of conversion of vinyl groups, the =CH<sub>2</sub> asymmetric stretching at 3057 cm<sup>-1</sup>, together with the Si-CH<sub>3</sub> bending signal at 1260 cm<sup>-1</sup> (as reference) are used, since the latter is present in both polymer and monomer and remains unaffected during

the polymerization process. Without the reference signal no quantitative comparison (monomer vs. polymer) can be made. The degree of conversion of vinyl groups is calculated by means of Equation 1:

$$\text{degree of conversion of vinyl groups (\%)} = 100 \cdot \left( 1 - \frac{\text{Area}(\nu^a = \text{CH}_2)_{\text{polymer}} / \text{Area}(\delta^s \text{Si} - \text{CH}_3)_{\text{polymer}}}{\text{Area}(\nu^a = \text{CH}_2)_{\text{monomer}} / \text{Area}(\delta^s \text{Si} - \text{CH}_3)_{\text{monomer}}} \right) \quad (1)$$

where  $\text{Area}(\nu^a = \text{CH}_2)$  and  $\text{Area}(\delta^s \text{Si} - \text{CH}_3)$  are the deconvoluted peak areas associated to the  $\text{CH}_2$  asymmetric stretching mode of the vinyl group (at  $3057 \text{ cm}^{-1}$ ) and the area of the symmetric bending absorption band ( $1260 \text{ cm}^{-1}$ ) in the polymer and monomer, respectively.

All the reported FT-IR spectra are baseline corrected and normalized with respect to the layer thickness.

### Film growth and monomer ads/des isotherms studies

The thickness and the optical properties of the poly( $\text{V}_3\text{D}_3$ ) layers are determined by means of *in situ* and *ex situ* Spectroscopic Ellipsometry (SE). The layer growth and monomer ads/des isotherms are studied by means of *in situ* SE. *Ex situ* measurements are acquired either at a single ( $70^\circ$ ) or at three angles of incidence ( $65^\circ$ ,  $70^\circ$ ,  $75^\circ$ ), in a wavelength range of 190 - 1000 nm by means of a J.A. Woollam Co. M-2000 D ellipsometer. *In situ* SE measurements are acquired at an angle of incidence of  $71.5^\circ$  with a wavelength range of 245 - 1000 nm by using a J.A. Woollam Co. M-2000 F ellipsometer. The optical model used for the film growth studies consists of: 1) silicon substrate; 2)  $\text{SiO}_2$  native oxide layer (1.5 – 2 nm); 3) poly( $\text{V}_3\text{D}_3$ ) layer modeled with the Cauchy dispersion formula and Urbach tail as reported in Equation 2:

$$n(\lambda) = A + \frac{B}{\lambda^2} + \frac{C}{\lambda^4} \quad ; \quad k(\lambda) = \alpha \cdot e^{\beta \left( \frac{12400}{\lambda} - \frac{1}{\gamma} \right)} \quad (2)$$

where  $A$ ,  $B$ ,  $C$  are the Cauchy fit parameters together with  $\alpha$  (extinction amplitude) and  $\beta$  (the exponent factor) of the Urbach function. The value of the band edge ( $\gamma$ ) is fixed to 400 nm. The use of the Urbach function is motivated by the fact that the poly( $\text{V}_3\text{D}_3$ ) layers contain carbon and hence show an absorption tail at lower

wavelengths. For the *in situ* SE data the silicon substrate temperature is fitted prior to the deposition process and the ads/des studies, and kept constant to the fitted value. The fitted values of the silicon substrate temperature have been found to be in excellent agreement (within  $\pm 2$  K) with the substrate holder temperature for all analyzed samples. The  $V_3D_3$  monomer ads/des measurements are performed in the deposition setup directly on c-Si substrates by monitoring the adsorbed monomer thickness by means of *in situ* SE measurements. The used optical model is composed of: 1) silicon substrate; 2)  $SiO_2$  native oxide layer (1.5 – 2 nm); 3)  $V_3D_3$  monomer layer, modeled with the Cauchy dispersion, being the thickness the only fit parameter and the monomer refractive index fixed to the constant value of 1.422 at 589.3 nm<sup>32</sup>, as reported in literature. The choice of studying the surface monomer adsorption by monitoring the changes in thickness is motivated, as it will be shown in the Results and Discussion part, by the fact that the silicon substrate is a non porous substrate. The refractive index has been kept fixed to the values found in literature during the measurements, as for the investigated thickness ranges ( $< 10$  Å) there is complete correlation between thickness and refractive index.

Two sets of ads/des isotherms are performed, namely equilibrium ads/des measurements and ads/des measurements by mimicking the deposition conditions. In both cases monomer and initiator<sup>1</sup> are injected into the deposition chamber with the same ratio as used during the deposition (see Table I) with the setup at the base pressure of  $10^{-6}$  mbar and the pressure is increased up to the value of 0.7 mbar. In the case of the equilibrium isotherms, the pressure is increased by 0.02 mbar steps, at each step the adsorbed monomer thickness is acquired after the pressure has stabilized. The desorption measurement is carried out in a similar fashion. In the case of the ads/des isotherms performed by mimicking the deposition conditions, the pressure is continuously increased from the base value to the set value of 0.7 mbar and the adsorbed monomer thickness is monitored in real time; a similar approach is

---

<sup>1</sup> The initiator (d-TBPO) is also present in this step, but  $P_{sat(d-TBPO)} = 118.8$  mbar against  $P_{sat(V_3D_3)} = 1.56$  mbar at 313 K. This corresponds to a value of  $P_{(d-TBPO)} / P_{sat(d-TBPO)} = 10^{-3}$  and  $P_{(V_3D_3)} / P_{sat(V_3D_3)} = 0.374$ , for a substrate temperature of 313 K and a final pressure of 0.7 mbar. Under the same conditions, ads/des isotherms, in which the monomer has been replaced by He as buffer gas, have been also measured to quantify any initiator surface adsorption. This resulted in no initiator adsorption. Moreover, a comparison of the ads/des isotherms in which the system  $V_3D_3$ /d-TBPO has been replaced by the system  $V_3D_3$ /He has been performed resulting in the same ads/des isotherm shape and final  $V_3D_3$  thickness uptake.

followed during the desorption step. In the case of the equilibrium ads/des isotherms the substrate temperature is of 313 K which allows to tune the  $P_M/P_{sat}$  parameter in the range of 0 – 0.374. In the case of the ads/des isotherms carried out by mimicking the deposition conditions the same study has been performed also at a substrate temperature of 313 K, 333 K and 353 K. The values of the monomer saturation vapor pressure ( $P_{sat}$ ) have been derived by means of the Clausius-Clapeyron relation considering the value of saturation vapor pressure at 298 K, i.e.  $P_{sat} = 0.571$  mbar<sup>33</sup> and the monomer boiling point (462 K at atmospheric pressure 1013 mbar). For all the SE measurements, the data analysis is performed by using J.A. Woollam Complete EASE™ software version 4.27 and the mean squared error between the experimental data and the model is minimized by adjusting the fit parameters using the Levenberg-Marquardt algorithm.

### **Other diagnostic tools**

The layer morphology is studied by means of Atomic Force Microscopy (AFM) and Scanning Electron Microscopy (SEM) measurements. AFM measurements are performed with a Solver Pro Scanning Probe Microscope (NT-MDT) in semi-contact mode using tips (NSG-10) with a radius of curvature of 10 nm with a scan area of 4  $\mu\text{m}^2$ . The measurement and analysis are performed with NOVA software (NT-MDT) in order to describe the surface morphology of the sample. SEM measurements are performed with a JEOL 7500FA microscope with electron energy of 5 KV.

## Results and Discussion

### A. Poly( $V_3D_3$ ) layer characterization

In Figure 2 the comparison between the FT-IR absorption spectra of the deposited poly( $V_3D_3$ ) layer and the liquid phase monomer is reported. A list of the absorption modes for both monomer and polymer spectra is reported in Table II.

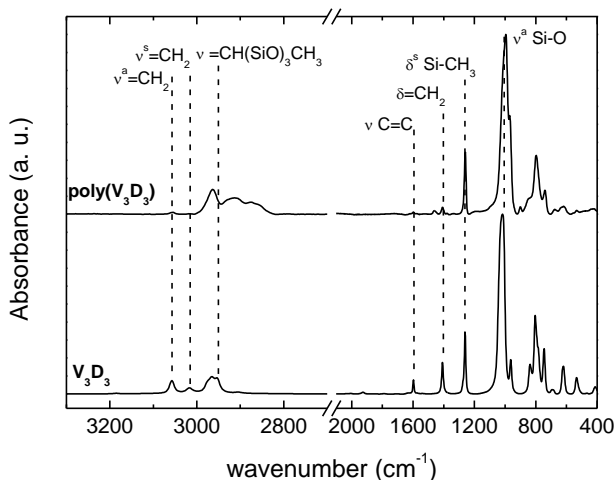


**Figure 2:**  $V_3D_3$  monomer and poly( $V_3D_3$ ) FT-IR spectra comparison.

The spectra comparison shows that the polymerization occurred via the cleavage of the vinyl groups present in the monomer, as it can be observed by the quantitative decrease of the vinyl-related signals such as the  $=\text{CH}_2$  asymmetric deformation (at  $1408 \text{ cm}^{-1}$ ), the  $\text{C}=\text{C}$  stretching (at  $1597 \text{ cm}^{-1}$ ) and, in the  $\text{CH}_x$  region ( $=\text{CH}_2$  asymmetric and symmetric stretching at  $3057 \text{ cm}^{-1}$  and  $3018 \text{ cm}^{-1}$ ), the  $=\text{CH}$  asymmetric and symmetric stretching at  $2976 \text{ cm}^{-1}$  and  $2935 \text{ cm}^{-1}$ ) in the polymer spectrum with respect to the monomer spectrum. The absorption at  $1408 \text{ cm}^{-1}$ , still present in the polymer spectrum, is also attributed to the deformation of the methylene group bonded to silicon<sup>5</sup>. As the polymerization process occurs through the activation of the vinyl groups, the features associated to the generated polyethylene chains, such as the asymmetric and symmetric stretching modes of the methylene groups at  $2910 \text{ cm}^{-1}$  and  $2861 \text{ cm}^{-1}$  and the asymmetric bending mode of the methylene groups at  $1460 \text{ cm}^{-1}$ , appear in the polymer spectrum. The retention

of the other monomer functional groups (i.e. the methyl group bonded to silicon and the tricyclo-siloxane ring) is witnessed by the Si-CH<sub>3</sub> symmetric bending signal at 1260 cm<sup>-1</sup> and the Si-O-Si asymmetric stretching signal at 995 cm<sup>-1</sup>, which do not undergo any changes upon polymerization. A shift of the peak associated to the cyclotrisiloxane ring from 1016 cm<sup>-1</sup> in the monomer to 995 cm<sup>-1</sup> in the polymer occurs. In literature a similar observation has been reported for the polymerization of the V<sub>4</sub>D<sub>4</sub> showing a shift of the cyclotretasiloxane band from 1075 cm<sup>-1</sup> (monomer) to 1065 cm<sup>-1</sup> (polymer)<sup>6</sup>. The ring opening can be excluded since this would imply a broadening of the absorption band and the appearance of a shoulder at 1080 cm<sup>-1</sup><sup>5, 17</sup>, related to linear Si-O-Si chains, which is not present in the polymer spectrum in Figure 2. The cyclotrisiloxane functionalities are known to absorb at 1010-1020 cm<sup>-1</sup>, but this absorption band can be shifted well below 1000 cm<sup>-1</sup> due to strain in the ring structure<sup>36</sup> upon polymer chain formation. To further investigate this point, the deconvolution of the Si-O-Si asymmetric stretch band (900 cm<sup>-1</sup> - 1150 cm<sup>-1</sup>) related to the (SiO)<sub>3</sub> ring has been performed for the layer deposited at different temperatures and the results are shown in Figure 3:

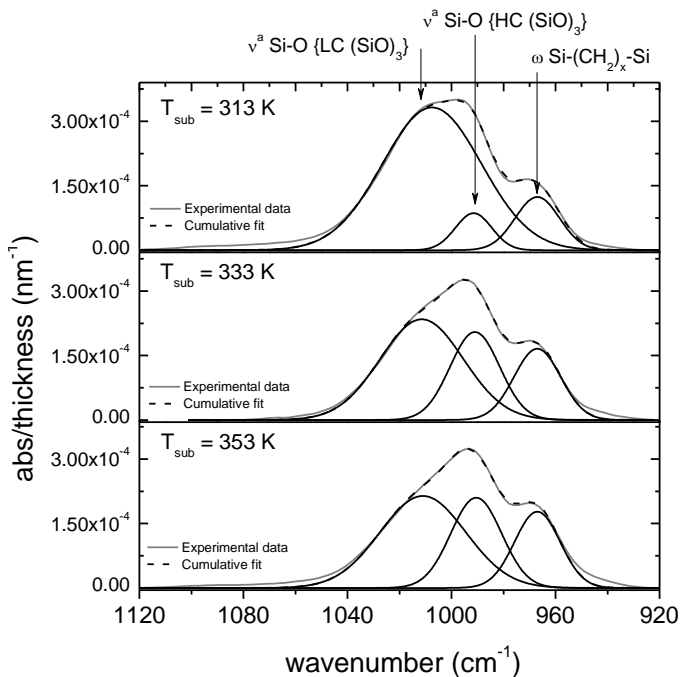


**Figure 3:** FT-IR absorption spectra normalized by the layer thickness in the Si-O-Si asymmetric stretching region together with the band deconvolution of the poly(V<sub>3</sub>D<sub>3</sub>) deposited at a substrate temperature of 313 K, 333 K, and 353 K. The assignments  $\nu^a$  Si-O{LC(SiO)<sub>3</sub>} and  $\nu^a$  Si-O{HC(SiO)<sub>3</sub>} are related to (SiO)<sub>3</sub> ring bonded to long (highly cross-linked: HC) and short (low cross-linked: LC) polymeric chains.

the band centered at 1002 cm<sup>-1</sup> is associated to the Si-O-Si asymmetric stretching of the cyclotrisiloxane bonded to short polymeric chains (low tension into the ring structure<sup>36</sup>); the one at 995 cm<sup>-1</sup> is associated to the same vibration, where the ring is bonded to long polymeric chains (higher degree of cross-linking and tension on the ring structure<sup>36</sup>); the third peak can be more likely assigned to the wagging of the methylene bridge (Si-(CH<sub>2</sub>)<sub>x</sub>-Si)<sup>8</sup>. A temperature increase induces an increase in the absorption band associated to the highly cross-linked, long polymeric chains. The effect of the substrate temperature on the deposited layer will be further addressed in the next section.

As reported in the experimental section, the degree of conversion of vinyl groups can be inferred from the area of the signal related to the =CH<sub>2</sub> asymmetric stretching at 3057 cm<sup>-1</sup>, obtained from the deconvolution of the CH<sub>x</sub> (3150 - 2800 cm<sup>-1</sup>) as



reported in Figure 4, and the area of the absorption band centered at 1260  $\text{cm}^{-1}$  associated to the Si-CH<sub>3</sub> bending.

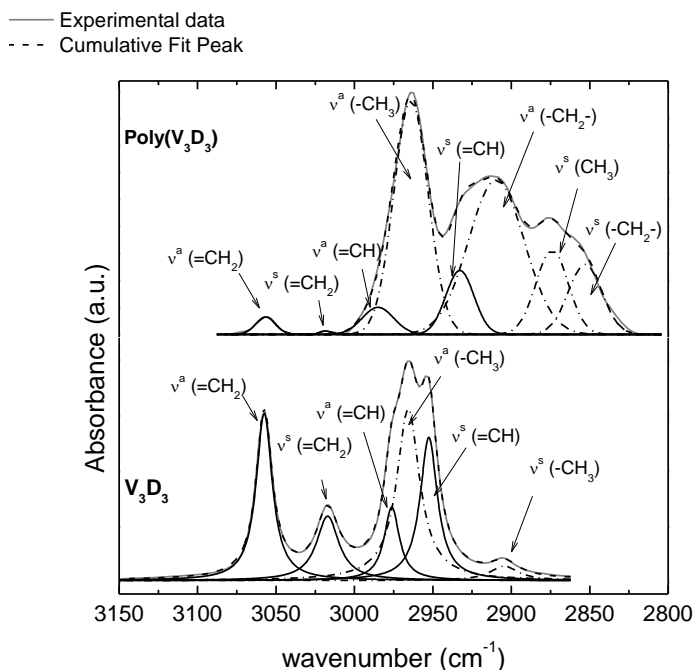


**Figure 4:** Comparison of the V<sub>3</sub>D<sub>3</sub> monomer and poly(V<sub>3</sub>D<sub>3</sub>) polymer FT-IR absorption bands in the CH<sub>x</sub> stretching region together with the bands deconvolution.

According to Equation 1, a degree of conversion of vinyl groups<sup>2</sup> of (82 ± 3) % (S.D.) and (87 ± 1) % (S.D.) has been calculated for the layers deposited at 313 K and 333 K, respectively. For higher temperatures the =CH<sub>2</sub> signal was further reduced within the noise level and thus a degree of conversion of vinyl groups larger than 87 % can be assumed for a substrate temperature higher than 333 K.

<sup>2</sup> The error in the given value of the degree of conversion of vinyl groups is the standard deviation of the results obtained by calculating the degree of conversion of vinyl groups by using at least 4 polymer spectra for each temperature.

**Table II**  
Monomer and polymer FT-IR modes assignments<sup>§</sup>.

polymer (cm <sup>-1</sup> )	monomer (cm <sup>-1</sup> )	Chemical bond	Vibration mode
3057	3057	CH <sub>2</sub> in vinyl	v <sup>a</sup> [5, 34]
3018	3017	CH <sub>2</sub> in vinyl	v <sup>s</sup> [5, 34]
2974	2976	CH in vinyl	v <sup>a</sup> [8]
2962	2966	CH <sub>3</sub> in C sp <sup>3</sup>	v <sup>a</sup> [5, 34]
2935	2953	CH in vinyl	v <sup>s</sup> [8]
2910	-	CH <sub>2</sub> in C sp <sup>3</sup>	v <sup>a</sup> [8, 34, 35]
2878	2905	CH <sub>3</sub> in C sp <sup>3</sup>	v <sup>s</sup> [8, 35]
2861	-	CH <sub>2</sub> in C sp <sup>3</sup>	v <sup>s</sup> [34]
-	1926	CH <sub>2</sub> in vinyl	Overtone of 963 cm <sup>-1</sup> signal [36]
1597	1597	C=C in vinyl	v [8, 34, 37]
1460	-	CH <sub>2</sub> in C sp <sup>3</sup>	δ <sup>a</sup> [34]
1408	1408	CH <sub>2</sub> in Si-(CH <sub>2</sub> ) <sub>x</sub> -Si and in vinyl	δ [8]
1260	1261	Si-CH <sub>3</sub>	δ <sup>s</sup> [5, 34]
		Si-O-Si in (SiO) <sub>3</sub>	
1002		(SiO) <sub>3</sub> short polym. chains	
	1016		v <sup>a</sup> [36]
		(SiO) <sub>3</sub> long polym. chains	
995			
970	-	Si-(CH <sub>2</sub> ) <sub>x</sub> -Si	ω [8]
-	963	CH <sub>2</sub> in vinyl	ω [8, 34, 36]
798	804	Si-CH <sub>3</sub>	ρ [36, 37]
617	621	Si-CH=CH <sub>2</sub>	δ [8, 34, 36,37]

<sup>§</sup> v, δ, ρ, ω denote stretching, bending, rocking, and wagging vibration modes, respectively, a and s asymmetric and symmetric vibrations, respectively.

## B. Film growth study and process window definition

Figure 5 reports all the i-CVD process steps as followed by means of *in situ* SE.

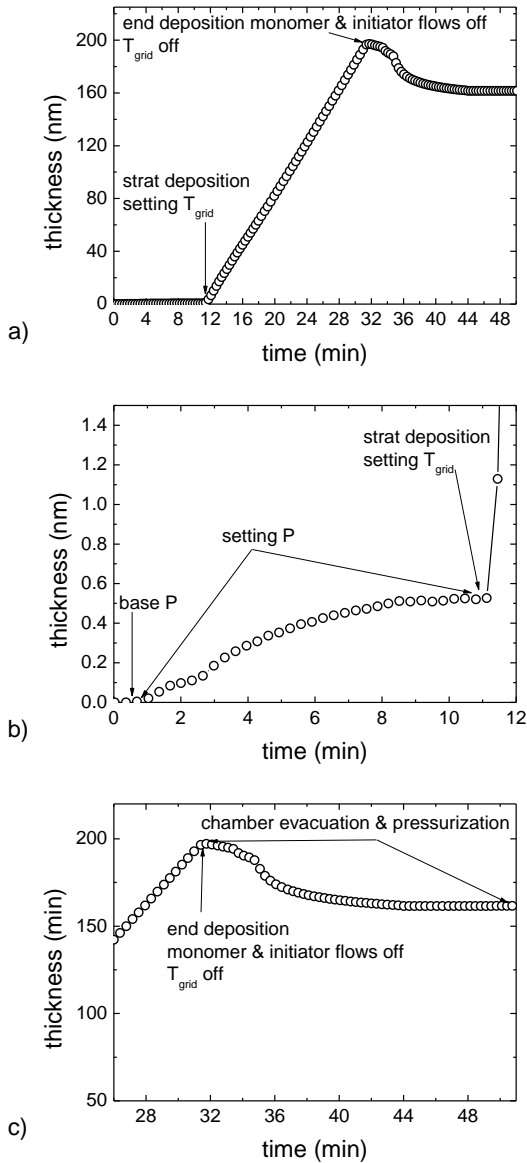


**Figure 5:** a) Thickness profiles as determined by means of *in situ* SE measurements of the i-CVD process. b)  $V_3D_3$  monomer initial thickness uptake during the setting of the deposition conditions. c) Thickness losses due to unreacted monomer/short oligomers removal upon chamber evacuation and pressurization.

Beside the linear polymer growth process, (see Figure 5a), two other characteristic steps can be highlighted: the initial thickness uptake which is related to the monomer surface adsorption during the setting of the deposition conditions (see Figure 5b) and, under certain experimental conditions (Table I, sample 1), a thickness reduction of the deposited layer, occurring upon chamber evacuation and pressurization, as highlighted in Figure 5c. In the reminder of this section, the phenomenon of the thickness losses and the monomer surface adsorption will be further addressed with the purpose of the defining the i-CVD process window.

### 1. $V_3D_3$ monomer ads/des isotherms studies

Figure 6a shows the equilibrium ads/des isotherms on silicon ( $Si/SiO_2$  native oxide ~ 1.5 nm) substrate at a temperature of 313 K in the  $P_M/P_{sat}$  range of 0 - 0.374.

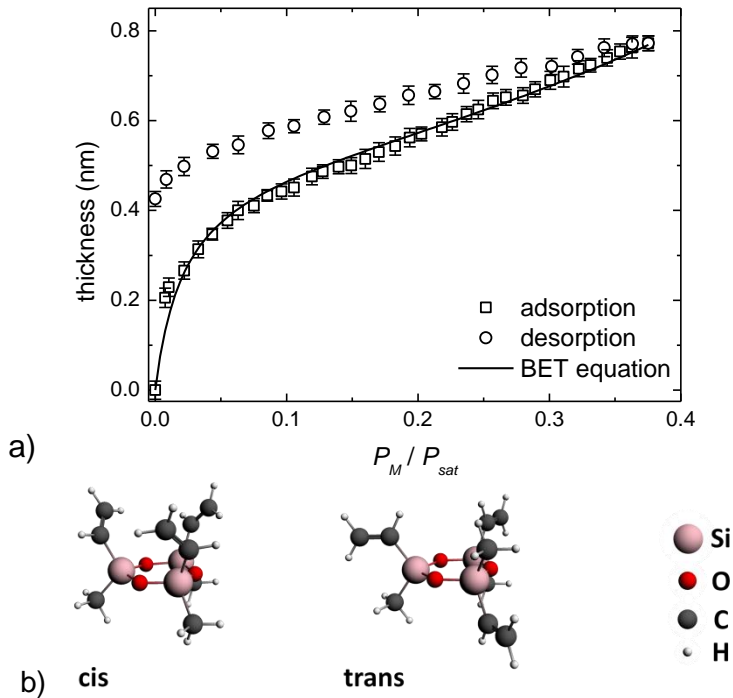


**Figure 6:** a)  $V_3D_3$  equilibrium ads/des isotherm on silicon substrate as determined by means of in situ SE measurements together with the adsorption branch fit with the B.E.T. equation. b)  $V_3D_3$  molecular structure in the cis and trans configuration.

The  $P_M/P_{sat}$  upper limit coincides with the values corresponding to the experimental conditions which led to a thickness loss (see Figure 5c). Although the  $P_M/P_{sat}$  range is not extended to 1, the shape of the isotherms clearly resembles the one of a Type II isotherm, which, according to the IUPAC classification of the ads/des isotherm<sup>38</sup>, corresponds to a non-porous substrate, as expected to occur on a silicon wafer. From the adsorption curve, the inflection point, indicative of monolayer adsorption<sup>39</sup>, is observed after a first initial increase for low  $P_M/P_{sat}$  ( $< 0.1$ ). After that monolayer thickness has been reached, the adsorbed monomer thickness further increases, pointing out to a multilayer adsorption development. Since for the i-CVD processes the monomer adsorption is reported to be governed by a physisorption mechanism<sup>13, 14</sup>, the desorption is expected to be reversible. However, a hysteresis behavior develops, which points out to chemisorption processes in the presence of the native  $\text{SiO}_2$  layer, and the  $(\text{SiO})_3$  siloxane ring of the monomer. The adsorbed monomer monolayer thickness,  $t_0$ , can be obtained by fitting the adsorption isotherm with the Brunauer-Emmet-Teller (BET)<sup>39</sup> equation reported in Equation 3,

$$t_{ad\ mon} = \frac{t_0 \cdot c \cdot k \cdot \left( \frac{P_M}{P_{sat}} \right)}{\left( 1 - k \cdot \frac{P_M}{P_{sat}} \right) \cdot \left( 1 + (c-1) \cdot k \cdot \frac{P_M}{P_{sat}} \right)} \quad (3)$$

which relates the thickness of surface adsorbed monomer to the  $P_M/P_{sat}$  ratio, via the BET constant  $c$  and a correction factor  $k$  which takes into account that even at  $P_M/P_{sat} = 1$  a finite number of multilayer is adsorbed. Since the restricted  $P_M/P_{sat}$  range in our work,  $k$  has been fixed to 1. A value of  $t_0 = 0.497 \text{ nm} \pm 0.004 \text{ nm}$  ( $R^2 = 0.989$ ;  $c = 47 \pm 3$ )<sup>40</sup> has been obtained, close to the  $\text{V}_3\text{D}_3$  molecular radius of 0.404 nm as estimated from the monomer van der Waals volume calculated as the sum of atomic and bond contributions<sup>41</sup>. Since this estimation does not take into account any geometry of the molecule (it assumes a sphere, and therefore overestimates the dimension) and the fact that the monolayer thickness is comparable with the molecular radius, it is hypothesized that the preferred direction of adsorption for the molecule is probably horizontal, with the cyclotrisiloxane ring parallel to the substrate. This is confirmed by the chemical structures of the  $\text{V}_3\text{D}_3$  molecule, which exists in a mixture of *cis* and *trans* configurations<sup>42, 43</sup>, as reported in Figure 6b in which, in both configurations, the cyclotrisiloxane ring shows a planar structure with

only a slight distortion of the Si-O-Si bonds in the case of the *trans* configuration. The equilibrium conditions, considered in the previous experiment, are slightly different from the real deposition conditions. Therefore, additional ads/des isotherms have been performed by mimicking the deposition conditions (i.e. continuous pressure increase, in the same way as the thickness uptake shown in Figure 5b). Figure 7 shows the ads/des isotherms acquired at 313 K; the adsorption isotherm is still of Type II, but the amount of adsorption is reduced since the equilibrium is not reached at every pressure step. Also the hysteresis behavior is limited.

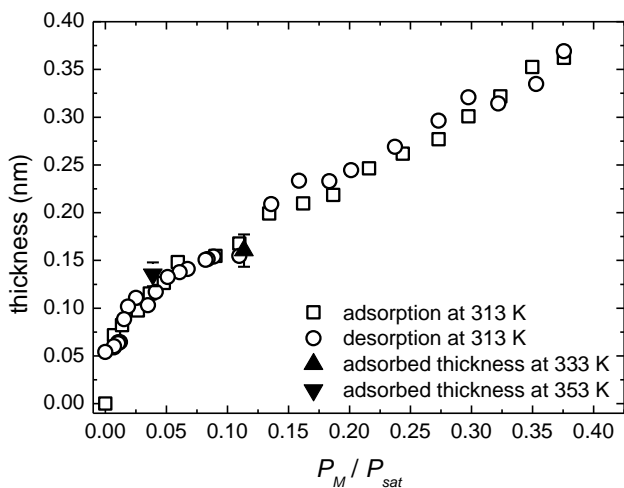


**Figure 7:**  $V_3D_3$  ads/des isotherm carried out by mimicking the deposition conditions on silicon substrate at a substrate temperature of 313K together with the values of the adsorbed monomer thickness at substrate temperature of 333 K and 353 K.

Nevertheless, also in this case the thickness of the surface adsorbed monomer is well beyond the inflection point or the so-defined monolayer thickness although this is lower than the one found under equilibrium conditions. The values of the adsorbed monomer thickness at the same final pressure of 0.7 mbar obtained from the ads/des isotherms studies performed at a substrate temperature of 333 K and 353 K are also reported in Figure 7 and they coincide, within the experimental error, with the data points of the adsorption isotherm obtained at 313 K.

## 2. Thickness loss characterization

As shown in Figure 5c, under specific deposition conditions (Table I, sample 1), the deposited layer undergoes a thickness loss ( $\Delta t$ ) upon chamber evacuation.  $\Delta t$  is defined as the difference between the film thickness as result of the deposition process (as-deposited), and the *ex situ* film thickness as measured with SE after chamber evacuation and exposure of the film to the environment. This phenomenon can be related to the presence, within the layer, of unreacted monomer units or short oligomers at the end of the deposition process which are removed from the deposited layer during the chamber evacuation<sup>3</sup>. Parallel studies on the same system  $V_3D_3/d$ -TBPO<sup>29</sup> and on  $V_3D_3/HVDSO/d$ -TBPO system<sup>17</sup> report on the existence of a pressure dependent substrate temperature threshold below which unreacted monomer or short oligomer units may be trapped into the growing layer and pumped away during the chamber evacuation and leaving, in this case, micrometric size disk-shaped holes into the layers surface<sup>29</sup> or even holes of visible size<sup>17</sup> pointing out, therefore, to a bulk related phenomenon. However, under our experimental conditions, those defects were not detected on the surface of the deposited layers even for the highest thickness loss recorded by *in situ* SE, as pointed out by the SEM image in Figure 8, showing a smooth and homogeneous surface. Furthermore, neither thickness losses are monitored, nor *in situ* real time studies are carried out to further investigate this observation, therefore, a detailed study of this phenomenon has been carried out and reported here below.

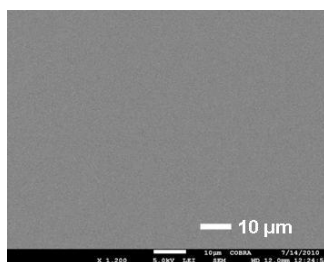


**Figure 8:** S.E.M. image of a poly( $V_3D_3$ ) layer showing a  $\Delta t = 65$  nm.

<sup>3</sup> The monomer condensation is less likely to occur since under our experimental conditions, the monomer partial pressure is still lower than its saturation pressure ( $P_{V_3D_3} = 0.583$  mbar  $<$   $P_{sat V_3D_3} = 1.56$  mbar at 313 K).

The proof that the thickness reduction is a bulk related phenomenon derives from the absolute values of the  $\Delta t$  (i.e. the thickness loss) increasing linearly as function of the deposition time, as shown in Figure 9.

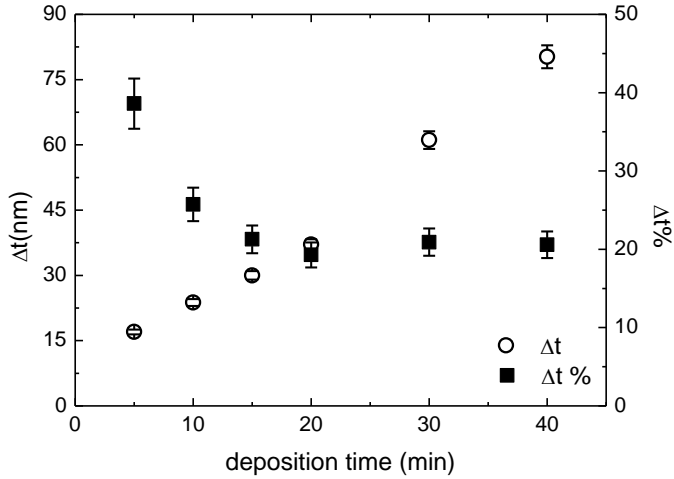


**Figure 9:** Trend of the absolute ( $\Delta t$ ) and relative ( $\Delta t\%$ ) thickness losses as function of the deposition time.

This rules out a surface related phenomenon, as in the latter case, the  $\Delta t$  values would result independent from the deposition time/layer thickness. Furthermore, the relative  $\Delta t$  (defined as the ratio between the  $\Delta t$  and the as deposited layer thickness) reaches a plateau for long deposition time as reported in Figure 9: this suggests that, under the hypothesis that the thickness reduction is attributed to unreacted monomer, this latter participates to the polymerization process also in the bulk of the growing layer. Within 20 minutes of deposition, the equilibrium between reacted and unreacted monomer is reached in the polymerization process. To support the hypothesis of the propagation of the polymerization in the layer bulk, a comparison between a continuous and a step-by-step deposition (i.e. the i-CVD layers are deposited in 5-min steps and the chamber is evacuated between two steps) is reported in Figure 10.



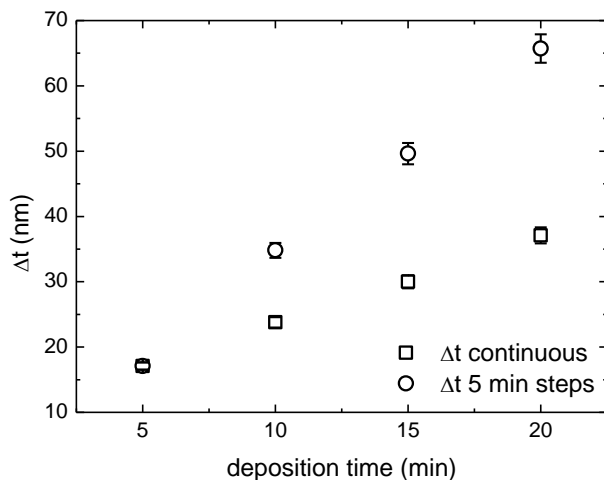


**Figure 10:** Comparison of the absolute thickness losses ( $\Delta t$ ) as function of the deposition time for  $\text{poly}(\text{V}_3\text{D}_3)$  layer deposited by continuous deposition process and by 5 min step deposition.

The layers which have been obtained from alternating deposition and evacuation steps are characterized by larger thickness losses. On the contrary, when the deposition is a continuous process, the overall thickness loss is smaller. This allows concluding that the polymerization process occurs not only at the surface of the growing layer but also in the bulk by diffusion of the non reacted monomer and reaction with polymer chains at the unsaturated sites.

### 3. Process window definition

The i-CVD process window can be defined by studying the effect of process key parameters through which the monomer adsorption can be controlled and also the monomer reactivity can be enhanced. Among all deposition parameters, the substrate temperature fits these requirements. By keeping the rest of the deposition parameters constant, (i.e. wire temperature, monomer to initiator ratio and pressure) increasing the substrate temperature would lead to a reduction of the surface monomer adsorption and to an increase of the monomer reactivity. This is confirmed by the decrease of the thickness losses with the increasing of the substrate temperature as shown in Figure 11, which also reports the trend of the surface adsorbed monomer thickness determined by means of *in situ* SE ads/des measurements done by mimicking the deposition conditions at a substrate temperature of 313 K, 333 K and 353 K.

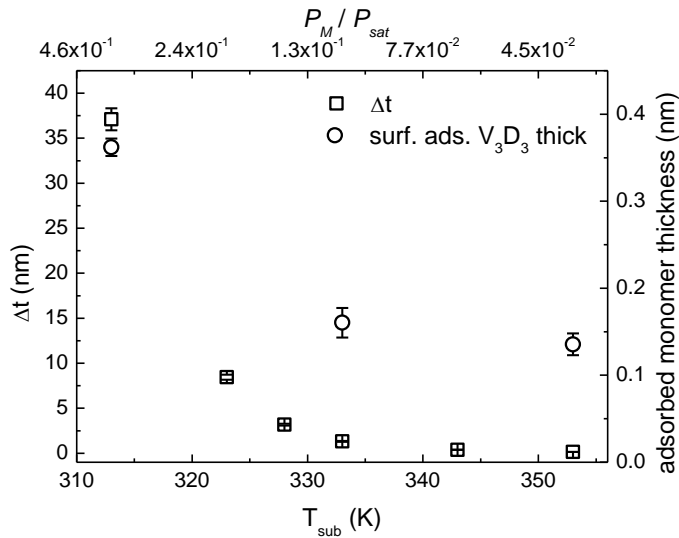
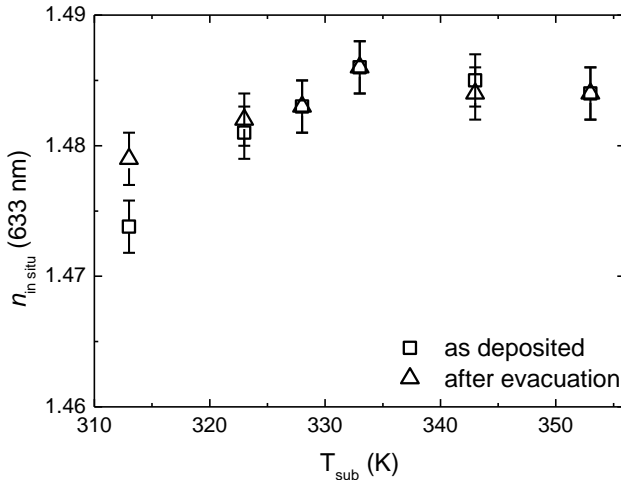


Figure 11: Trend of the absolute thickness losses as function of the substrate temperature together with the surface adsorbed monomer thickness.

Clearly, a correlation between the reduction of the surface monomer adsorption thickness and the thickness losses is evident. As the temperature increases, the monomer surface concentration is reduced, furthermore its reactivity is enhanced,

promoting the polymerization process and reducing the thickness losses. Yet, it is necessary to understand how the substrate temperature, by reducing the thickness losses, affects the layer quality.

In Figure 12 the layer refractive index values, measured for both the as-deposited and *in vacuum* condition is presented.



**Figure 12:** Poly(V<sub>3</sub>D<sub>3</sub>) as deposited and after evacuation values of refractive index as function of the substrate temperature.

A difference in refractive index values for the layer which showed high thickness loss ( $T_{\text{sub}} = 313 \text{ K}$ ) is highlighted. In particular the refractive index is increasing from the as deposited layer to the layer after evacuation. This can be related to layer densification upon evacuation, due to the matrix collapse accompanying the layer thickness reduction. The overall increase of both values of the refractive index may suggest a layer restructuring with the substrate temperature. As a matter of fact, in the previous section it has already been shown that an increase in temperature is responsible for an increase of the polymer matrix cross-linking through the increase of the signal related to the  $(\text{SiO})_3$  ring bonded to long highly cross-linked polymer chains (Figure 3) and for an increase in the degree of conversion of vinyl groups. An improvement in the polymer morphology is also observed by comparing the r.m.s. surface roughness of the layers deposited at different substrate temperatures,

corresponding to high and low  $\Delta t$  (e.g. and 313 K and 333 K), which decreases from  $0.94 \text{ nm} \pm 0.02 \text{ nm}$  to  $0.51 \text{ nm} \pm 0.02 \text{ nm}$ .

The previous results can be summarized by the i-CVD process window definition for the polymerization of the poly( $V_3D_3$ ) layers as reported in Figure 13.

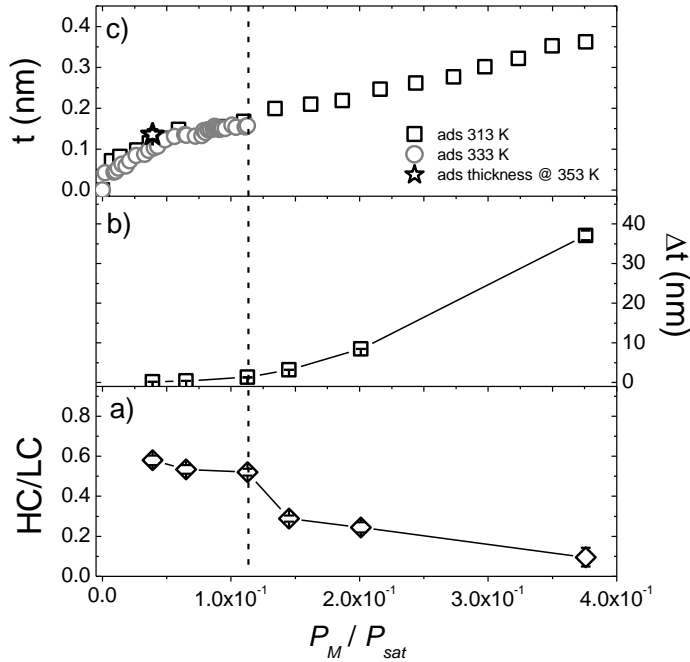


**Figure 13:** i-CVD process window: highly crosslinked poly( $V_3D_3$ ) with no thickness losses are obtained if the surface adsorbed monomer is within one third of the monomer monolayer. a) Area ratio of the  $(SiO)_3$  peaks bonded to long (highly cross-linked: HC) and short (with low cross-linking: LC) polymeric chains as function  $P_M/P_{sat}$  (varied through the substrate temperature). b) Absolute thickness losses trend as function of  $P_M/P_{sat}$ . c) Surface adsorbed monomer thickness as function of  $P_M/P_{sat}$ .

By tuning the  $P_M/P_{sat}$  parameter with the substrate temperature a well cross-linked polymer structure exhibiting no thickness loss upon evacuation can be achieved by setting the monomer adsorption on the substrate, which should be limited to a thickness corresponding to the inflection point in the isotherm. This translates in an adsorbed monomer thickness restricted to one third of the monolayer thickness.

## Summary and Conclusions

The implementation of the i-CVD process in a novel deposition setup has been successfully accomplished by the deposition of poly(V<sub>3</sub>D<sub>3</sub>) layer by using 1,3,5-trivinyl-1,3,5-trimethylcyclotrisiloxane (V<sub>3</sub>D<sub>3</sub>) and di-tert-butyl-peroxide (d-TBPO) as initiator. The comparison of the FT-IR spectra of monomer and polymer showed that the polymerization process occurred only through the cleavage of the vinyl groups present in the monomer and the retention of the other monomer functional groups, namely, the cyclotrisiloxane ring and the methyl groups attached to the silicon atoms of the cycle. A degree of conversion of vinyl groups above 80 % has been found for all the poly(V<sub>3</sub>D<sub>3</sub>) layers. The film growth has been studied *in situ* by means of Spectroscopic Ellipsometry as real-time diagnostics to follow all stages of the i-CVD process from the initial monomer adsorption to the linear film growth and to the thickness losses due to the presence of unreacted monomer units at the end of the deposition process. Furthermore, *in situ* SE measurements allowed characterizing the thickness losses as bulk-related phenomenon and brought new information on the polymerization process which propagate not only at the surface of the growing layer but also in the bulk. Finally, together with other complementary analysis (FT-IR), *in situ* SE measurements made possible to define the process window for the deposition of stable ( $\Delta t \rightarrow 0$  nm) and highly cross-linked poly(V<sub>3</sub>D<sub>3</sub>) layers which can be obtained by tuning the surface monomer adsorption below one third of the monolayer thickness. The poly(V<sub>3</sub>D<sub>3</sub>) layers showing limited thickness losses and high degree of cross-linking (i.e.  $T_{\text{sub}} = 333$  K) are presently tested as organic interlayer for inorganic/organic multilayer moisture diffusion barrier systems.

## **Acknowledgments**

The authors would like to thank J.J.A. Zeebregts, M. J. F. van de Sande, J.J.L. M. Meulendijks, H.M.M. de Jong, and W. Keuning for their skillful technical assistance. A. Kemper and W. Kemper are acknowledged for the project and engineering of the grid power supply and temperature control system. P. Liljeroth (Aalto University School of Science, Espoo, Finland) is acknowledged for the determination of the  $V_3D_3$  monomer molecular structure. T. van Mol, J.J. Michels, S. Unnikrishnan, F.J.H. van Assche (Holst Centre, High Tech Campus, Eindhoven, The Netherlands), and P. van de Weijer (Philips Research, High Tech Campus, Eindhoven, The Netherlands), are acknowledged for the fruitful discussion on the data. This work forms part of the research programme of the *Dutch Polymer Institute* (DPI), project number 663 of the Large Area Thin Film Electronics (LATFE).

## References

- [1] M. Gupta, V. Kapur, N.M. Pinkerton, and K.K. Gleason, *Chemistry of Materials*, 20, 1646–1651, 2008
- [2] M. Ma, Y. Mao, M. Gupta, K.K. Gleason, and G.C. Rutledge, *Macromolecules*, 38, 9742–9748, 2005
- [3] T.P. Martin, S.E. Kooi, S.H. Chang, K.L. Sedransk, K.K. Gleason, *Biomaterials*, 28, 909–915, 2007
- [4] G. Chen, M. Gupta, K. Chan, K.K. Gleason, *Macromolecular Rapid Communications*, 28, 2205–2209, 2007
- [5] W.S. O’Shaughnessy, M. Gao, and K.K. Gleason, *Langmuir*, 22, 7021–7026, 2006
- [6] N.J. Trujillo, Q. Wu, and K.K. Gleason, *Advanced Functional Materials*, 20, 607–616, 2010
- [7] N.J. Kramer, E. Sachtelen, G. Ozaydin-Ince, R. van de Sanden, and K.K. Gleason, *Macromolecules*, 43, 8344–8347, 2010
- [8] A.M. Coclite, G. Ozaydin-Ince, R. d’Agostino, and K.K. Gleason, *Macromolecules*, 42, 8138–8145, 2009
- [9] A.M. Coclite, G. Ozaydin-Ince, F. Palumbo, A. Milella, K.K. Gleason, *Plasma Processes and Polymers*, 7, 561–570, 2010
- [10] T.P. Martin, K.K.S. Lau, K. Chan, Y. Mao, M. Gupta, W.S. O’Shaughnessy, K.K. Gleason, *Surface & Coating Technology*, 201, 9400–9405, 2007
- [11] H.G. Pryce Lewis, N.P. Bansal, A.J. White, E.S. Handy, *Thin Solid Films*, 517, 3551–3554, 2009
- [12] K. Chan and K.K. Gleason, *Macromolecules*, 39, 3890–3894, 2006
- [13] K.K.S. Lau and K.K. Gleason, *Macromolecules*, 39, 10, pp 3688–3694, 2006
- [14] K.K.S. Lau and K.K. Gleason, *Macromolecules*, 39, 10, pp 3695–3703, 2006
- [15] B. Cruden, K. Chu, K. Gleason, and H. Sawin, *Journal of the Electrochemical Society*, 146, 12, 4590–4596, 1999
- [16] R.K. Bose and K.K.S. Lau, *Biomacromolecules*, 11, 2116–2122, 2010
- [17] A.K.H. Achyuta, A.J. White, H.G. Pryce Lewis, and S.K. Murthy, *Macromolecules*, 42, 1970–1978, 2009
- [18] G. Ozaydin-Ince and K.K. Gleason, *Journal of Vacuum Science & Technology A*, 27 (5), 1135–1143, 2009
- [19] M. Ebert, K.A. Bell, S.D. Yoo, K. Flock, D.E. Aspnes, *Thin Solid Films*, 364, 22–27, 2000

- [20] I. Volintiru, M. Creatore, and M.C.M. van de Sanden, *Journal of Applied Physics*, 103, 033704, **2008**
- [21] E. Langereis, S.B.S. Heil, H.C.M. Knoop, W. Keuning, M.C.M. van de Sanden and W.M.M. Kessels, *Journal of Physics D: Applied Physics*, 42, 073001, **2009**
- [22] Y. Zheng, H. Mizuta, Y. Tsuchiya, M. Endo, D. Sato, and S. Oda, *of Applied Physics*, 97, 023527, **2005**
- [23] P. Patsalas, S. Logothetidis, *Surface & Coating Technology*, 180 –181, 421–424, **2004**
- [24] S. Logothetidis, A. Laskarakis, A. Gika, P. Patsalas, *Surface & Coating Technology*, 151 –152, 204–208, **2002**
- [25] M. Creatore, S.M. Rieter, Y. Barrell, M.C.M. van de Sanden, R. Vernhes, L. Martinu, *Thin Solid Films*, 516, 8547–8553, **2008**
- [26] M. Creatore, M. Kilic, K. O'Brien, R. Groenen, M.C.M. van de Sanden, *Thin Solid Films*, 427, 137–141, **2003**
- [27] H. Fujiwara, “*Spectroscopic Ellipsometry Principles and Applications*”, John Wiley & Sons Ltd, **2007**
- [28] D.S. Karpovich and G.J. Blanchard, *Langmuir*, 13, 4031-4037, **1997**
- [29] W.S. O’Shaughnessy, S.K. Murthy, D. J. Edell, and K.K. Gleason, *Biomacromolecules*, 8, 2564-2570, **2007**
- [30] W.F. Maddams, *Applied Spectroscopy*, 34, 3, 245-267, **1980**
- [31] K.S. Seshadri and R. Norman Jones, *Spectrochimica Acta*, 19, 1013-1085, **1963**
- [32] H. Ahmed, C.F. Poole, G.E. Kozerski, *Journal of Chromatography A*, 1169 179–192, **2007**
- [33] [www.scifinder.cas.org](http://www.scifinder.cas.org)
- [34] C. Rau, W. Kulisch, *Thin Solid Films*, 249, 28- 37, **1994**
- [35] A. Grill and D.A. Neumayer, *Journal of Applied Physics*, Vol 94, N. 10, **2003**
- [36] A. Lee Smith, “*Analysis of Silicones*”, John Wiley & Sons, Inc. **1974**
- [37] S.K. Murthy, B. D. Olsen, K.K. Gleason, *Journal of Applied Polymer Science*, Vol. 91, 2176–2185, **2004**
- [38] K.S.W. Sing, D.H. Everett, R.A.W. Haul, L. Moscou, R.A. Pierotti, J. Rouquerol, T. Siemieniewska, *Pure Applied Chemistry*, 57, 4, pp. 603-619, **1985**
- [39] S.J. Gregg and K.S.W. Sing, “*Adsorption, Surface Area and porosity*”, Academic Press Inc. Ltd, **1982**
- [40] The isotherm shape found in this work differs from the ones reported in literature for similar studies<sup>13, 14</sup>. Although a comparison between the different



isotherms is difficult to be made, as their shape (and hence the BET curve) depends on the adsorbing molecule chemistry, the substrate chemistry/porosity and, hence, the substrate/adsorbing molecule interaction<sup>39, 44</sup>, some conclusions can still be drawn. The shape of the BET equation is function of the BET constant  $c$ <sup>39</sup> and, for a non-porous substrate (as Si/SiO<sub>2</sub> and gold substrates), it shifts from a Type II to a Type III isotherm, characteristic of weak monomer/substrate interactions, for  $c < 2$ . In the case reported in literature, a value of  $c = 1.950$  and  $c = 2.536$  for ethyl acrylate<sup>13</sup> and butyl acrylate<sup>14</sup>, respectively, on gold coated quartz crystal are reported in comparison with the fitted valued of  $c = 47 \pm 3$  found in this work for the V<sub>3</sub>D<sub>3</sub> on Si/SiO<sub>2</sub> substrate, pointing out that differences in the substrate/adsorbing molecule interaction are playing a role. As a matter of fact a value of  $c = 12$  (Type II isotherm) has been also reported in literature for the adsorption study of glycidyl methacrylate monomer on Si/SiO<sub>2</sub> substrate<sup>45</sup>.

[41] Y.H. Zhao, M.H. Abraham, A.M. Zissimos, *Journal of Organic Chemistry*, 68, 7368-7373, 2003

[42] Y. Itami, B. Marciniec, M. Kubicki, *Organometallics*, 22, 3717-3722, 2003

[43] G. Cai, W.P. Weber, *Polymer*, 43, 1753-1759, 2002

[44] F. Rouquerol, J. Rouquerol, K. Sing, "Adsorption by powders & porous solids. Principles, methodology and applications", Academic Press Inc. Ltd, 1999

[45] R. Bakker, "Hot-wire chemical vapour deposition at low substrate temperatures for optoelectronics applications" Ph.D. Thesis, Utrecht University, 2010

## Chapter 3

### *Evidence of the filling of nano-porosity in SiO<sub>2</sub>-like layers by an initiated-CVD monomer\**

#### Abstract

Although very promising results in terms of moisture and oxygen barrier properties have been achieved by alternating organic and inorganic layers composing a multilayer structure, the impact of the organic interlayer on the global barrier performance is still unravelled. Three main hypotheses have been reported in literature so far, although consistently applied to the case of a liquid-phase polymerization process of the organic layer: smoothening of the polymeric substrate surface by the organic layer; decoupling, by means of a tortuous path, of the defects present in two adjacent inorganic barrier layers; filling of the nano-defects present in the barrier layer during the (liquid phase) polymerization of the organic layer. Within this framework, this contribution reports on the adsorption/desorption study of an initiated-CVD (i-CVD) monomer (trimethyl-trivinyl-cyclotrisiloxane), V<sub>3</sub>D<sub>3</sub>, performed on plasma deposited SiO<sub>2</sub>-like layers by means of *in situ* Spectroscopic Ellipsometry measurements. The SiO<sub>2</sub>-like layers are used as moisture permeation barriers followed by an organic interlayer deposited by means of the i-CVD technique. The experimental evidence for the V<sub>3</sub>D<sub>3</sub> molecule infiltration and filling in the open micro/meso porosity present in the inorganic layer underneath, confirms the hypothesis on the filling of nano-defects in the barrier layer upon organic layer deposition and shows that the defect filling occurs also in the case of a CVD-based approach.

---

\* Published as: G. Aresta, J. Palmans, M.C.M. van de Sanden, M. Creatore, *Microporous and Mesoporous Materials*, 151, 434 - 439, 2012

## Introduction

The path from rugged (metal foil and glass lid) to bendable (wearable) and foldable flexible devices is highly challenged by the low work function cathode (Ba in the case of poly-LEDs) oxidation. The oxidation is caused by the water permeation through the pinholes of the thick Al layer covering the 10 nm-thick Ba layer. As metal oxidation occurs at the cathode/polymer interface, local areas where no electron injection from the cathode to the polymer develop, leading to the formation of black spots in the device under operation<sup>1, 2</sup>. Thus, the application of organic light emitting diodes (OLEDs) in the field of (flexible) electronics (e.g. displays) and lighting is hampered by the challenges related to the device encapsulation against water vapor permeation. Estimated<sup>1, 3</sup> water vapor transmission rates (WVTR) as low as  $10^{-6}$  g m<sup>-2</sup> day<sup>-1</sup> are required for the barrier systems in order to ensure ten years device lifetime. It is common knowledge that the barrier properties of a single inorganic layer (generally,  $\leq 100$  nm thick Al<sub>2</sub>O<sub>3</sub>, Si<sub>3</sub>N<sub>4</sub> or SiO<sub>2</sub>) are ultimately controlled by the substrate/process- induced macro-defects (e.g. pinholes and particles ranging from few hundreds of nm up to  $\mu\text{m}$ s) within the layer<sup>4</sup> leading to WVTR values orders of magnitude higher than the required  $10^{-6}$  g m<sup>-2</sup> day<sup>-1</sup>. The state-of-the art solution towards ultra-high barrier layer is an alternated,  $\mu\text{m}$ - thick organic/ inorganic multi-layer, which already showed moisture permeation levels as low as  $< 10^{-5}$  g m<sup>-2</sup> day<sup>-1</sup><sup>5</sup>. Multilayer systems are generally deposited by a hybrid approach: sputtering or PE-CVD of the inorganic barrier layer, in combination with flash evaporation/condensation of the organic precursor, usually acrylate-based, followed by curing/polymerization<sup>5</sup>. Alternatively, also full PE-CVD based approaches have been reported in literature<sup>6-9</sup>. The impact of the organic interlayer on the multilayer barrier performances is still under debate. The ( $\mu\text{m}$ - thick) organic polymer layer is expected to induce a so-defined “prophylactic mechanism” as introduced by Affinito *et al.*<sup>10</sup>, later better known as planarizing effect, i.e. surface smoothing of the layer underneath, which allows for a better development of the subsequent inorganic barrier layer<sup>5, 11</sup>. Furthermore, Graff *et al.*<sup>12</sup> proposed a numerical simulation, which allows to conclude that the better performance of a multilayer is associated to the tortuous path which the permeant molecule must follow through the organic interlayer before approaching a pinhole/defect in the subsequent barrier layer. In an exhaustive overview of the literature in the field of O<sub>2</sub> and moisture permeation barrier layers, Affinito *et al.*<sup>10</sup> pointed out the unsatisfactory prediction of the enhancement of barrier performances based on the

tortuous path mechanism, because relying on the assumption that the permeation is only macro-defect controlled, whereas the matrix of the inorganic barrier layer may offer also a permeation path to O<sub>2</sub> and water vapor molecules. As a matter of fact, next to the presence of macro-defects, which essentially represent an unhindered path for the permeant molecule<sup>13, 14</sup>, permeation through defects of nano-scale size (comparable to or larger than the size of the permeant molecule, i.e. 0.33 nm for H<sub>2</sub>O and 0.32 nm for O<sub>2</sub>) should also be taken into account. These latter are estimated to represent an area density approximately 15-20 times larger than the density of the macro-defects, therefore witnessing 15-20 times more permeation than the macro-defects<sup>10</sup>. The permeation through nano-defects has been also confirmed by Roberts *et al.*<sup>15</sup>, who modeled the permeation data of a single barrier layer/polymer substrate, which neither did fit the laminate model nor the macro-defects model, especially in the case of O<sub>2</sub> and H<sub>2</sub>O permeation. Affinito *et al.*<sup>10</sup>, therefore, proposed an additional role of the organic interlayer, which takes into account the infiltration of the organic layer in its liquid phase into the nano-sized defects of the inorganic barrier layer underneath, and eventually having an impact on the local transmission of the permeant molecule through the filled pores. On the basis of the findings of Roberts *et al.*<sup>15</sup>, and by considering the average molecular size of an acrylate monomer (0.4 nm), i.e. the typical chosen chemistry for the organic interlayer, Affinito classified the defects as it follows, and developed a theoretical and mathematical model to support the hypothesis on this synergistic effect between the organic interlayer and the barrier layer. Defects larger than the size of the monomer units are defined as macro-defects, i.e. from few nms to the largest pinholes/defects of few hundred nms and μms. The nano-defects range from the size of the monomer unit to 1-2 nm, and, therefore, are still accessible for monomer infiltration and filling; the matrix defects, i.e. below the monomer size, < 0.2 – 0.3 nm, are not accessible for filling. Worth to note is that this synergistic effect is defined and proposed in the case of organic interlayers which are applied in liquid phase on the barrier layer underneath and assuming that a proper wetting of the internal surface of the nano-defects occurs.

Up to now, to the authors' knowledge, no experimental evidence for the infiltration and filling of the nano-defects in the inorganic barrier layer has been reported, nor has the above-mentioned synergistic effect been extended to the case of organic interlayers developed under "dry-chemistry" conditions (i.e. PE-CVD or the recently reported initiated-CVD<sup>16</sup>). In particular, in this contribution we focus our studies on

organosilicon-based interlayers deposited by means of initiated CVD (i-CVD), coupled to PE-CVD deposited SiO<sub>2</sub>-like barrier layers. The appeal of the i-CVD, introduced by Gleason *et al.*<sup>17, 18</sup>, is related to its vacuum compatibility, good conformality and retention of the monomer chemistry. During the i-CVD process a free-radical polymerization process is initiated by volatile radicals generated by thermal decomposition (on a heated grid: T= 423 – 773K) of an initiator molecule (e.g., a peroxide) reacting with monomer molecules (stable in the temperature range of the grid) adsorbed on the surface of a cooled substrate (T= 298 – 353 K)<sup>19</sup>. Similarly to the conventional polymerization routes, the i-CVD process propagates via chain growth reaction by radical transfer to the monomer units and it is terminated by the reaction of two growing chains or by the reaction of a growing chain with an initiator radical<sup>20, 21</sup>. Recently, the successful implementation of an i-CVD deposited organosilicon-based interlayer coupled with PE-CVD deposited SiO<sub>2</sub>-like barrier layer has been reported by Coclite *et al.*<sup>16</sup> In this case, the engineering of an hexa-layer structure has delivered a barrier improvement factor of 100 with respect to the single layer and this has been attributed to the smoothening effect by the i-CVD deposited polymer interlayer and defects decoupling effect, as described by Graff<sup>12,16</sup>.

In this paper, we address the i-CVD process by providing experimental proof for nano-defect filling of the inorganic barrier underneath. The monomer unit infiltration and filling steps of the nano-defects will be highlighted by means of isothermal adsorption/ desorption studies followed by *in situ* spectroscopic ellipsometry (SE) which will additionally provide information on the size range of the defects. In literature, studies have been already reported, where SE is coupled to adsorption/ desorption isotherms<sup>22</sup>, with the purpose of quantifying the fraction of open porosity, i.e. accessible to the ambient. In these studies, the uptake of the probe molecule within the open porosity of the layer is followed *in situ* by monitoring the changes in refractive index which the layer undergoes: the technique is, therefore, known as ellipsometric porosimetry (EP)<sup>22-24</sup>. The advantage of the EP approach with respect to the more classical volumetric and gravimetric methods<sup>25-27</sup> is the high sensitivity to small adsorbant molecule uptakes, as in the case of the thin films ( $\leq 100$  nm) here under examination. So far, EP measurements have been only reported to evaluate the integrity of thin low-*k* dielectric films<sup>28, 29</sup> and of TiO<sub>2</sub> layers used as gas sensors and as catalysts<sup>30</sup>, and, according to the authors' knowledge, no such study has ever been performed in the field of moisture permeation barrier layers.

In the present contribution, we make use of the EP technique to prove the hypothesis on the infiltration and filling of the nano-defects present in the SiO<sub>2</sub>-like layers, by means of the i-CVD monomer. For this purpose, the experimental conditions for the adsorption studies have been intentionally chosen to mimic the initial steps of the i-CVD polymerization process.

The paper is organized as follow. In the Experimental section, the description of the deposition chamber and of the deposition process of the SiO<sub>2</sub>-like layer is provided, together with the layer chemical and optical characterization and the experimental procedure related to the EP measurements. In the Results and Discussion part, the chemical and optical characterization of the SiO<sub>2</sub>-like layers is provided and the adsorption/desorption studies are discussed by correlating our results with those by Affinito<sup>10</sup>.

## Experimental

Both depositions and isothermal studies are performed, without breaking the vacuum, in a custom-built setup which allows for thin film deposition by means of both PE-CVD and i-CVD approaches. The chamber walls are set at a constant temperature of 353 K to avoid monomer condensation and minimize monomer adsorption. The substrate holder (which acts also as grounded electrode) is connected to a temperature- control system based on a resistive heating unit (Eurotherm) and three Peltier cooling elements. The substrate temperature is monitored by an embedded thermocouple. The pressure is controlled by three gauges: a Penning (Pfeiffer) gauge, monitoring the setup base pressure (10<sup>-7</sup> mbar up to atmospheric pressure) and two capacitive (Pfeiffer) gauges for process monitoring (10<sup>-3</sup> mbar – 10 mbar) and the pressurization of the system (1 mbar – atmospheric pressure). During the deposition process and the adsorption/desorption isothermal studies the pressure is controlled through a (VAT) butterfly valve. The same monomer is adopted for the PE-CVD SiO<sub>2</sub>-like process, the i-CVD polymer layer deposition and the isothermal studies: 1,3,5-trivinyl-1,3,5-trimethylcyclotrisiloxane (V<sub>3</sub>D<sub>3</sub>).

In the case of the i-CVD deposition and isothermal studies, the monomer is mixed with the initiator, di-tert-butyl peroxide, d-TBPO<sup>1</sup>. V<sub>3</sub>D<sub>3</sub>, (> 95%; Gelest) and d-TBPO (98%; Aldrich) are evaporated in stainless steel bubblers (kept at a constant temperature of 373 K and 298 K, respectively) and their flow rates measured through Vapor Source Controllers (VSC 1150C, MKS Instruments). Two lines, kept at 393 K and 308 K, to avoid the V<sub>3</sub>D<sub>3</sub> and d-TBPO vapors condensation, connect the vapor source controllers to the deposition chamber. V<sub>3</sub>D<sub>3</sub> and d-TBPO vapors, after pre-mixing in a buffer chamber, are injected into the deposition chamber through a ring. Ar and O<sub>2</sub> flow rates, controlled by mass flow controllers (MFC 1179B, MKS), are injected through a separate ring placed below the one of the monomer/initiator line. For both processes, the pumps operate at the bottom of the deposition chamber. SiO<sub>2</sub>-like layers are deposited by means of an RF-plasma ignited between two parallel electrodes: the top one connected via a matching network to a RF power generator and the grounded bottom electrode. The conditions of deposition of the SiO<sub>2</sub>-like layers on c-Si samples are listed in Table I.

**Table I**

*Experimental conditions for the deposition of the SiO<sub>2</sub>-like layers.*

V <sub>3</sub> D <sub>3</sub> (sccm)	0.7
Ar (sccm)	70
O <sub>2</sub> (sccm)	35
P (W)	150; 250
P (mbar)	0.3
T <sub>sub</sub> (K)	373

The adsorption/desorption studies as well as the film growth processes are followed by means of *in situ* spectroscopic ellipsometry, at an angle of incidence of 71.5°, wavelength range of 245 - 1000 nm, 1.6 nm resolution, by using a J.A. Woollam Co. M-2000 F ellipsometer. The SiO<sub>2</sub>-like layer refractive index values have been

<sup>1</sup> As mentioned, the initiator (d-TBPO) is also present during the adsorption/desorption studies, but its surface adsorption is considered negligible with respect to the V<sub>3</sub>D<sub>3</sub> adsorption because of the difference in saturation pressure, i.e.  $P_{sat}(d-TBPO) = 118.8$  mbar vs.  $P_{sat}(V_3D_3) = 1.56$  mbar at the substrate temperature of 313 K.

determined also by means of *ex situ* SE measurements at an angle of incidence of 75° in order to investigate any ageing effect upon film exposure to the ambient air. The optical model consists of: silicon substrate, SiO<sub>2</sub> native oxide layer (2 nm), SiO<sub>2</sub>-like layer modeled with the Cauchy dispersion formula as reported in Equation 1, since this layer is optically transparent in the investigated wavelength range:

$$n(\lambda) = A + \frac{B}{\lambda^2} ; \quad k(\lambda) = 0 \quad (1)$$

where  $A$ ,  $B$ , are the Cauchy fitting parameters. The silicon substrate temperature is a fitting parameter under vacuum condition, prior to the deposition process and kept constant to the fitted value (373 K ± 2 K) during the film deposition and fixed to 313 K during the adsorption/desorption studies. The same Cauchy layer is applied for the study of V<sub>3</sub>D<sub>3</sub> adsorption/desorption isotherm since the monomer ( $n = 1.422$  at  $\lambda = 589$  nm and  $T = 293$  K)<sup>31</sup> is transparent in the investigated wavelength range. The SiO<sub>2</sub>-like layer thickness has been kept constant to the value obtained at the end of the deposition process, under the hypothesis, which will be addressed later on, that the layer does not swell upon V<sub>3</sub>D<sub>3</sub> adsorption, i.e. it is relatively dense. The V<sub>3</sub>D<sub>3</sub> adsorption/desorption measurements are performed with the setup arranged in the i-CVD configuration (grid placed inside the deposition chamber on top of the substrate holder without being switched on) and by reproducing the setting of a typical i-CVD process, as reported in Table II.

**Table II**

*Experimental conditions for the isothermal adsorption/desorption studies.*

V <sub>3</sub> D <sub>3</sub> (sccm)	10
d-TBPO (sccm)	2
T <sub>sub</sub> (K)	313
T <sub>grid</sub> (K)	-
P (mbar)	10 <sup>-6</sup> - 0.7
$P_M/P_{sat}$	0 - 0.374

V<sub>3</sub>D<sub>3</sub> and d-TBPO are injected into the deposition chamber at the base pressure of 10<sup>-6</sup> mbar, and the pressure into the chamber is gradually increased to the set value



of 0.7 mbar. This value corresponds to the pressure used to deposit the i-CVD poly(V<sub>3</sub>D<sub>3</sub>) layers investigated in our group, which will be the subject of a next paper, allowing for the deposition of a i-CVD layer with a degree of vinyl group conversion > 80 %. The substrate temperature is kept at 313 K, which allows, within the pressure range investigated, to control the parameter  $P_M/P_{sat}$  between 0 to 0.374, where  $P_M$  is the monomer partial pressure and  $P_{sat}$  is the monomer saturation pressure at 313 K ( $P_{sat} = 1.56$  mbar), as determined by the Clausius-Clapeyron relation<sup>16</sup>. The i-CVD monomer adsorption studies are performed by mimicking the deposition conditions of the i-CVD layer on top of the SiO<sub>2</sub>-like layers during the adsorption path (i.e. the pressure is gradually increased till the set value), while, during the desorption path the pressure is gradually decreased till the base pressure is reached. The data have been acquired as it follows. The first step consists in measuring the as-deposited SiO<sub>2</sub>-like refractive index value under vacuum conditions ( $n_0$ ) at the substrate temperature of 313 K. Then, V<sub>3</sub>D<sub>3</sub> and d-TBPO are injected into the chamber, time is given to the system to stabilize at a pressure of 10<sup>-2</sup> mbar and the refractive index of the layer upon adsorption of V<sub>3</sub>D<sub>3</sub> is determined. Then, the pressure is increased from 10<sup>-2</sup> mbar to the set values (0.7 mbar) and the change in refractive index values is monitored. The increase in pressure is also recorded to determine the  $P_M/P_{sat}$  parameter. At the pressure of 0.7 mbar, time is given to the system to stabilize and the value of the refractive index ( $n_{fill}$ ) is acquired as averaged value. The same procedure has been adopted for the desorption curve. In order to evaluate the uncertainty accompanying the refractive index values, the standard deviation of the averaged values of the  $n_0$  and  $n_{fill}$  (where  $n_{fill}$  corresponds to  $P_M/P_{sat} = 0.374$ ) is taken, being equal to  $\pm 2 \cdot 10^{-4}$ . The data analysis is performed by using the J.A. Woollam Complete EASE™ software version 4.27 and the mean squared error between the experimental data and the model is minimized by adjusting the fit parameters using the Levenberg-Marquardt algorithm.

Further layer analysis includes Fourier Transform Infrared (FT-IR) measurements carried out with a Bruker Tensor 27 spectrophotometer. FT-IR spectra are acquired in the range of 400 cm<sup>-1</sup> - 4000 cm<sup>-1</sup> with a resolution of 4 cm<sup>-1</sup> and 256 scans. Before the spectra acquisition the spectrometer has been purged for 15 min with N<sub>2</sub> to minimize the effect of H<sub>2</sub>O and CO<sub>2</sub> absorption.

The SiO<sub>2</sub>-like layer atomic concentrations (see Table III) and density are evaluated by means of Rutherford backscattering (RBS) and Elastic Recoil Detection (ERD) techniques. For both methods a 2 MeV He<sup>+</sup> beam was applied. The RBS spectra

were acquired under channeling conditions to reduce the contribution of the c-Si substrate to the spectrum. The beam was perpendicular on the sample surface and a scattering angle of 170° was used. The ERD spectra were obtained under 15° glancing incidence. Detection took place under a forward angle of 30° with the incoming beam direction.

## Results and Discussion

Figure 1 reports the FT-IR absorption spectra, normalized by the layer thickness, of the SiO<sub>2</sub>-like layers deposited at two power settings. While the SiO<sub>2</sub>-like layer deposited at 250 W exhibits a negligible signal at 3670 cm<sup>-1</sup> associated to the Si-OH stretching of the isolated silanol groups pointing out a residual porosity (Figure 1a), the Si-OH- related absorption is higher in the case of the SiO<sub>2</sub>-like layer deposited at 150 W, suggesting a higher degree of porosity (Figure 1b). The latter is also confirmed by the higher intensity of the high wavenumber shoulder (1150 cm<sup>-1</sup>) of the Si-O-Si asymmetric stretching signal, associated to short siloxane chains and, therefore, to matrix disorder and porosity.

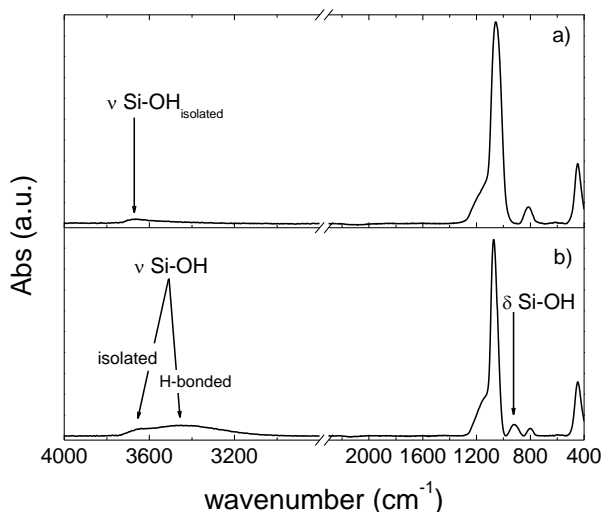


**Figure 1:** High (a) and low (b) plasma power deposited SiO<sub>2</sub>-like layer absorption FT-IR spectra, normalized by the layer thickness.  $\nu$  and  $\delta$  refer to the stretching and bending vibrational mode respectively.

Moreover, a shift of the Si-O-Si asymmetric stretching signal from 1072 cm<sup>-1</sup> to 1056 cm<sup>-1</sup> for the layer deposited at 250 W with respect to the one deposited at 150 W is observed. This, according to the literature<sup>32</sup>, points out to higher bond (SiOSi) strain and, hence, higher matrix density. The difference in residual porosity between the two SiO<sub>2</sub>-like layers is supported by the comparison in terms of the as deposited, *in vacuum*, and *ex situ* refractive index values. Whereas the layer deposited at 250 W shows a water uptake ( $n_{H_2O} = 1.33$ ) in the open porosity which leads only to a limited increase in refractive index (i.e. from 1.451 to 1.465), the film deposited at 150 W exhibits a larger water uptake corresponding to an increase in refractive index from 1.413 to 1.453<sup>33, 34</sup>. Furthermore, RBS/ERD measurements point to an increase in density from (2.0 ± 0.1) g cm<sup>-3</sup> for the porous layer to (2.2 ± 0.1) g cm<sup>-3</sup> for the dense film. In order to evaluate the residual porosity in the SiO<sub>2</sub>-like layers, the concentration of the silanolic groups present in the layer has been calculated from the absorption band<sup>35</sup> of the Si-OH stretching signal by using the O-H proportionality constant of 0.44 · 10<sup>20</sup> cm<sup>-2</sup><sup>36</sup>.

**Table III**

*SiO<sub>2</sub>-like layer atomic concentrations as determined by RBS/ERD measurements as function of the RF Power. The layer thickness is also included.*

RF Power (W)	10 <sup>15</sup> at cm <sup>-2</sup>					SiO <sub>2</sub> -like layer thick (nm)
	Si	O	C	H	tot	
150	200	420	0	64.2	685	104.9 ± 0.1
250	212	449	0	33.9	695	100.6 ± 0.1

An O-H concentration of 3 · 10<sup>21</sup> cm<sup>-3</sup> and 6 · 10<sup>21</sup> cm<sup>-3</sup> has been found for the dense and porous SiO<sub>2</sub>-like layer respectively. These results are in very good agreement with the H concentration determined by RBS/ERD measurements. This comparison holds if we assume that all the hydrogen is present as OH group in the SiO<sub>2</sub>-like layer, since no Si-H stretching band is observed in the FTIR spectra. An estimation of the residual porosity can be, therefore, made from the ratio between the silanol concentration and the SiO<sub>2</sub>-like density (in terms of at cm<sup>-3</sup>): the porous and dense SiO<sub>2</sub>-like layers are characterized by a porosity of 9 and 5%, respectively.

Figure 2 shows the adsorption/ desorption isotherms acquired at a substrate temperature of 313 K for the dense SiO<sub>2</sub>-like layer. Although the explored  $P_M/P_{sat}$  range is not extended to 1, the isotherm shape clearly resembles Type I, associated to a micro-porous layer<sup>23</sup>. Considering the pores size classification given by IUPAC<sup>2</sup>, this isotherm shape corresponds to a pore size lower than 2 nm, also defined as micro-porosity<sup>23</sup>.

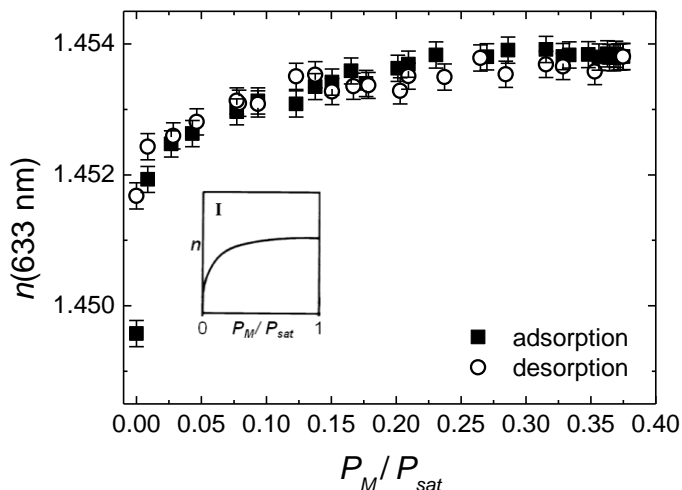


**Figure 2:** V<sub>3</sub>D<sub>3</sub> adsorption/desorption isotherm acquired on a dense SiO<sub>2</sub>-like layer. The inset shows the adsorption/desorption isotherm of Type I<sup>23</sup>, related to micro-porous layers.

The monomer adsorption at low  $P_M/P_{sat}$  shows a steep initial increase indicating the abrupt filling of the identified micro-pores at very low partial pressures ( $P_M/P_{sat} < 0.05$ ), which is a primary micro-pore filling (i.e. a single monolayer adsorption) occurring in pores twice the molecular diameter of the probing molecule<sup>25, 26, 37</sup>. Considering the size of the probing molecule V<sub>3</sub>D<sub>3</sub> (estimated molecular diameter ~ 0.5 nm)<sup>3</sup> this means that the minimum pore diameter that can be probed/filled by

<sup>2</sup> According to the IUPAC pore size classification, a micro-pore has a diameter of < 2 nm, corresponding to a type I isotherm (see inset of Figure 2); a meso-pore ranges from 2 nm to 50 nm, corresponding to a type IV isotherm (see inset of Figure 3); a macro-pore corresponds to a size > 50 nm, associated to a type II isotherm<sup>23</sup>.

<sup>3</sup> The V<sub>3</sub>D<sub>3</sub> molecular size has been estimated by determining the thickness of a V<sub>3</sub>D<sub>3</sub> monolayer from the fitting of the equilibrium V<sub>3</sub>D<sub>3</sub> adsorption isotherm, carried out on a Si/SiO<sub>2</sub> substrate, via the Brunauer, Emmet and Teller (BET) equation<sup>25, 26</sup>.

the V<sub>3</sub>D<sub>3</sub> molecules is 1 nm. After this initial phase, the monomer adsorption further develops through the so-called secondary micro-pore filling until it reaches a constant level of adsorption, implying the completion of the micro-pore filling. The desorption curve is reversible, i.e. no hysteresis is shown, pointing out the lack of meso-porosity in the layer. However, at very low relative pressure ( $0 < P_M/P_{sat} < 0.025$ ), the value of the refractive index corresponding to vacuum conditions is not reached. This can indicate an irreversible uptake of the V<sub>3</sub>D<sub>3</sub> molecule in pores of about the same size of the molecular probe, or chemisorption phenomena of the V<sub>3</sub>D<sub>3</sub> on the surface of the micro-pore<sup>23</sup>. This latter is a plausible explanation if we take into account the possibility for H-bonding between the siloxane ring of the V<sub>3</sub>D<sub>3</sub> molecule and the Si-OH groups present in the inorganic layer. Such activated surface of the pore walls would facilitate the wetting, infiltration and filling of the open nano-defects, as suggested by Affinito<sup>10</sup>.

The monomer adsorption/desorption isotherms performed on the porous SiO<sub>2</sub>-like layer are shown in Figure 3.

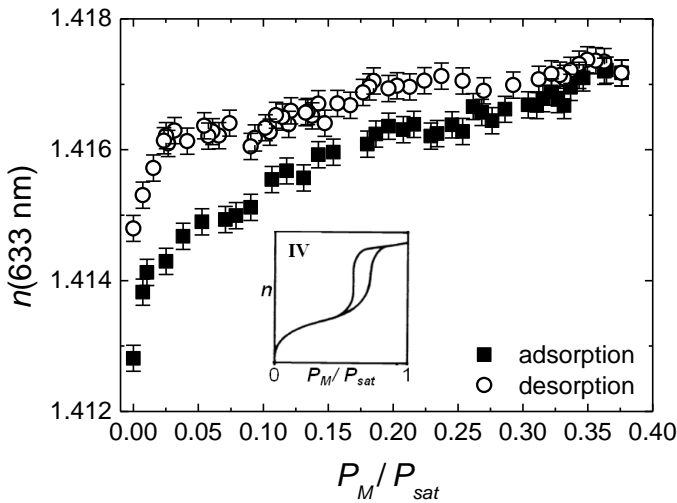


**Figure 3:** V<sub>3</sub>D<sub>3</sub> adsorption/desorption isotherm acquired on a porous SiO<sub>2</sub>-like layer. The inset shows the adsorption/desorption isotherm of Type IV<sup>23</sup>, related to meso-porous layers.

Differently from the case of the dense SiO<sub>2</sub>-like layer, the adsorption branch shows a smaller initial uptake, compared to the previous case, in the same  $P_M/P_{sat}$  range ( $0 < P_M/P_{sat} < 0.05$ ) and, after an inflection point at  $P_M/P_{sat} = 0.05$ , it linearly increases

without leveling off, till the maximum of the  $P_M/P_{sat}$  range here investigated. Moreover, the desorption branch clearly shows a hysteresis loop starting from  $P_M/P_{sat} = 0.25$  which becomes more pronounced up to a  $P_M/P_{sat}$  equal to 0.1. Also in this case, the desorption branch does not reach the  $n_0$  value. The lack of a steep initial uptake at  $P_M/P_{sat} < 0.05$  and the continuous linear increase of the refractive index with the whole range of  $P_M/P_{sat}$  point out that the V<sub>3</sub>D<sub>3</sub> monomer adsorption occurs in pores larger than in the case of the SiO<sub>2</sub>-like layer in Figure 2, most certainly exhibiting a transition from micro- to meso-porosity, i.e. above 2 nm of diameter. This is also confirmed by the presence of the hysteresis loop during the desorption path extending through the whole  $P_M/P_{sat}$  here investigated. In conclusion, the adsorption/desorption isotherm shape is closer to a Type IV isotherm (see inset Figure 3)<sup>23</sup>. Strictly speaking, the presence of a hysteresis behavior occurs at higher relative pressure ( $P_M/P_{sat}$ ) than the one reported in Figure 3 and it is associated to meso-porosity, as a consequence of capillary condensation phenomena<sup>25, 26</sup>. In the specific case of the layer here under investigation, the transition from micro- to meso-porosity is accompanied by the development of hysteresis limited to low  $P_M/P_{sat}$  values, because of the relatively small meso-pore size ( $\leq 2$  nm). Also in this case the non reversibility (i.e. the layer refractive index does not reach the  $n_0$  value at  $P_M/P_{sat} = 0$ ) of the desorption curve can be regarded as due to either trapping in smaller micro-pores (pore size  $< 1$  nm) or chemisorption of the V<sub>3</sub>D<sub>3</sub> molecules on the surface of the micro-meso pores, which is expected to be higher since the Si-OH groups content is higher in this porous SiO<sub>2</sub>-like layer as confirmed by the FT-IR and the RBS/ERD analysis. Despite the difference in the isotherm shape between the dense and the porous SiO<sub>2</sub>-like layers and the above- mentioned comparison in terms of density and silanol concentration, the total change in refractive index in the two layers, from  $P_M/P_{sat} = 0$  to  $P_M/P_{sat} = 0.374$ , is comparable ( $\Delta n = (40 \pm 4) \cdot 10^{-4}$  for the dense SiO<sub>2</sub>-like layer and  $\Delta n = (44 \pm 4) \cdot 10^{-4}$  for the porous one). This suggests that not all the meso-porosity in the porous SiO<sub>2</sub>-like layer is probed and that a broader range of  $P_M/P_{sat}$  should be investigated (i.e.  $P_M/P_{sat}$  up to 1, when monomer condensation occurs) to correctly determine the open porosity in the layer and compare the values with those earlier determined from the RBS/ERD analysis. However, this analysis is beyond the purpose of this paper.

From the analysis of the adsorption/ desorption isotherms reported in Figures 2 and 3 it is clear that the V<sub>3</sub>D<sub>3</sub> can effectively fill the nano-pores present during the initial step of the i-CVD process and hence polymerize into the pores, once that the

polymerization process is started by the initiator radicals. These results, although coupled to a CVD- based polymerization process, confirm the hypothesis by Affinito on the possibility of filling the nano-pores/defects of a barrier layer by the organic layer deposition precursor molecule. Furthermore, the evidence of the interaction between the V<sub>3</sub>D<sub>3</sub> molecule and the SiO<sub>2</sub>-like pores via the H-bonding with the silanol groups present on the pore walls, suggests that the chemically activated internal surface of the pores may be the key towards the good adhesive properties of the i-CVD layer<sup>38, 39</sup>.

## Conclusions

In this work, i-CVD monomer isothermal adsorption/desorption studies by means of *in situ* SE measurements, have been performed on plasma deposited SiO<sub>2</sub>-like layers acting as barrier layers in an i-CVD/PE-CVD moisture diffusion barrier stack. The i-CVD precursor, V<sub>3</sub>D<sub>3</sub>, is also used for the deposition of the i-CVD organic interlayer. These measurements point out the infiltration/filling of the deposition precursor molecule into the nano-scale defects (micro/meso-pores) of the SiO<sub>2</sub>-like barrier layer underneath. As a corollary, i-CVD monomer adsorption/desorption measurements provide also information on the SiO<sub>2</sub>-like layer microstructure. The ability of the i-CVD monomer to fill the pores is directly related to the i-CVD process itself, which is a vacuum compatible, free-radical polymerization process behaving in a similar manner to a liquid polymerization process. These results, obtained in the case of a CVD process, confirm the hypothesis by Affinito on the filling of the nano-defects in the barrier layer upon deposition of an organic layer. The presented study is considered relevant for the understanding and control of ultra-high barrier layer systems and their engineering, since nano- and meso-pores represent a relevant path of permeation.

### **Acknowledgements**

The authors would like to thank J. J. A. Zeebregts, M. J. F. van de Sande, J. J. L. M. Meulendijks, H. M. M. de Jong, and W. Keuning for their skillful technical assistance. T. van Mol, J. J. Michels, S. Unnikrishnan, F. J. H. van Assche (Holst Centre, High Tech Campus, Eindhoven, The Netherlands), and P. van de Weijer (Philips Research, High Tech Campus, Eindhoven, The Netherlands), are acknowledged for the fruitful discussion of the data. W. M. Arnold Bik (Acc. Tec. B.V.) is acknowledged for the RBS/ERD measurements. This work forms part of the research programme of the *Dutch Polymer Institute (DPI)*, project number 663 of the Large Area Thin Film Electronics (LATFE).



## References

- [1] J.S. Lewis and M.S. Weaver, *IEEE Journal of Selected Topics in Quantum Electronics*, Vol. 10, No 1, 45-57, 2004
- [2] C.W.T. Bulle-Lieuwma, P. van de Weijer, *Applied Surface Science*, 252, 6597–6600, 2006
- [3] F.J.H. van Assche, R.T. Vangheluwe, J.W.C. Maes, W.S. Mischke, M. D. Bijker, F.C. Dings, M.F.J. Evers, W.M.M. Kessels, M.C.M. van de Sanden, *Proceedings Society for Information Display*, 695 – 697, 2004
- [4] A. S. da Silva Sobrinho, M. Latreche, G. Czeremuszkin, J. E. Klemberg-Sapieha, and M. R. Wertheimer, *Journal of Vacuum Science and Technology A*, 16, (6), 3190-3198, 1998
- [5] P.E. Burrows, G.L. Graff, M.E. Gross, P.M. Martin, M.K. Shi, M. Hall, E. Mast, C. Bonham, W. Bennet, M.B. Sullivan, *Displays*, 22, 65-69, 2001
- [6] T.W. Kim, M. Yan, A.G. Erlat, P.A. McConnelee, M. Pellow, J. Deluca, T. P. Feist, A.R. Duggal, M. Schaepkens, *Journal of Vacuum Science and Technology A*, 23, (4), 2005
- [7] A. Francescangeli, F. Palumbo, R. d'Agostino, *Plasma Processes and Polymers*, 5, 708–717, 2008
- [8] G. Dennler, C. Lungenschmied, H. Neugebauer, N. S. Sariciftci, M. Latreche, G. Czeremuszkin, M. R. Wertheimer, *Thin Solid Films*, 511 – 512, 349 – 353, 2006
- [9] J. Fahlteich, M. Fahland, W. Schönberger, N. Schiller, *Thin Solid Films*, 517, 3075–3080, 2009
- [10] J. Affinito, D. Hilliard, *47<sup>th</sup> Society of Vacuum Coaters Annual Technical Conference Proceedings*, 563-593, 2004
- [11] M. Schaepkens, T.W. Kim, A.G. Erlat, M. Yan, K. W. Flanagan, C.M. Heller, P.A. McConnelee, *Journal of Vacuum Science and Technology A*, 22, 1716 -1722, 2004
- [12] G.L. Graff, R. E. Williford, P. E. Burrows, *Journal of Applied Physics*, Vol. 96, No. 4, 1840-1849, 2004
- [13] Y.G. Tropsha and N.G. Harvey, *Journal of Physical Chemistry B*, 101, 2259-2266, 1997
- [14] A.G. Erlat, B.C. Wang, R.J. Spontak, Y. Tropsha, K.D. Mar, D.B. Montgomery, and E.A. Vogler, *Journal of Materials Research*, Vol. 15, No. 3, 704 – 717, 2000

- [15] A.P. Roberts, B.M. Henry, A.P. Sutton, C.R.M. Grovenor, G.A.D. Briggs, T. Miyamoto, M. Kano, Y. Tsukahara, M. Yanaka, *Journal of Membrane Science*, 208, 75–88, 2002
- [16] A.M. Coclite, G. Ozaydin-Ince, F. Palumbo, A. Milella, K.K. Gleason, *Plasma Processes and Polymers*, 7, 561–570, 2010
- [17] M.E. Alf, A. Asatekin, M.C. Barr, S.H. Baxamusa, H. Chelawat, G. Ozaydin-Ince, C. D. Petruczok, S. Sreenivasan, W.E. Tenhaeff, N.J. Trujillo, S. Vaddiraju, J. Xu, and K.K. Gleason, *Advanced Materials*, 22, 1993–2027, 2010
- [18] A. Asatekin, M.C. Barr, S.H. Baxamusa, K.K.S. Lau, W. Tenhaeff, J. Xu, and K.K. Gleason, *Materials Today*, Vol. 13, N. 5, 26-33, 2010
- [19] T.P. Martin, K.K.S. Lau, K. Chan, Y. Mao, M. Gupta, W.S. O'Shaughnessy, K.K. Gleason, *Surface & Coatings Technology*, 201, 9400–9405, 2007
- [20] K.K.S. Lau and K.K. Gleason, *Macromolecules*, 39, 3695-3703, 2006
- [21] K.K.S. Lau and K.K. Gleason, *Macromolecules*, 39, 3688-3694, 2006
- [22] C. Licitra, R. Bouyssou, T. Chevolleau, F. Bertin, *Thin Solid Films*, 518, 5140-5145, 2010
- [23] K.S.W. Sing, D.H. Everett, R.A.W. Haul, L. Moscou, R. A. Pierotti, J. Rouquerol, T. Siemieniewska, *Pure and Applied Chemistry*, Vol. 57 No. 4, 603 – 619, 1985
- [24] K.S.W. Sing, *Colloids and Surface A*, 241, 3–7, 2004
- [25] S.J. Gregg and K.S.W. Sing, “*Adsorption, Surface Area and porosity*”, (Academic Press Inc. Ltd, London, England), 1982
- [26] F. Rouquerol, J. Rouquerol, K. Sing, “*Adsorption by powders & porous solids. Principles, methodology and applications*”, (Academic Press, London, England), 1999
- [27] R. Denoyel, P. Llewellyn, I. Beurroies, J. Rouquerol, F. Rouquerol, L. Luciani, *Particle & Particle Systems Characterization*, 21, 128 – 137, 2004
- [28] S. Elsave, F. Iacopi, M.R. Baklanov, C.E.A. Kirschhock, K. Maens, J.A. Martens, *Journal of the American Chemical Society*, 129, 9288 – 9289, 2007
- [29] W. Puyrenier, V. Rouessac, L. Broussous, D. Rebiscoul, A. Ayrat, *Microporous and Mesoporous Materials*, 106, 40–48, 2007
- [30] O. Dubreuil, J. Dewalque, G. Chene, F. Mathis, G. Spronck, D. Strivay, R. Cloots, C. Henrist, *Microporous and Mesoporous Materials*, 145, 1–8, 2011
- [31] N. Atapattu, C.F. Poole, *Journal of Chromatography A*, 1216, 7882–7888, 2009
- [32] R.A.B. Devine, *Journal of Vacuum Science and Technology A*, 6, 3154-3156, 1988

- [33] A. Brunet-Bruneau, D. souche, S. Fisson, V.N. Van, G. Vuye, F. Abeles, and J. Rivory, *Journal of Vacuum Science and Technology A*, 16, 2281-2286, 1998
- [34] M. Creatore, M. Kilic, K. O'Brien, R. Groenen, and M.C.M. van de Sanden, *Thin Solid Films*, 427, 137- 141, 2003
- [35] L.N. He, D. M. Wang, S. Hasegawa, *Journal of Non-Crystalline Solids*, 261, 67-69, 2000
- [36] A. Ermaoloeff, T. Sindzingre, S. Marthon, P. Martin, F. Pierre and L. Peccoud, *Applied Surface Science*, 64, 175-183, 1993
- [37] M. Kruk, M. Jaroniec, and K.P. Gadkaree, *Langmuir*, 15, 1442-1448, 1999
- [38] W.S. O'Shaughnessy, D.J. Edell, K.K. Gleason, *Thin Solid Films*, 516, 684-686, 2008
- [39] A.M. Coclite, G. Ozaydin-Ince, R. d'Agostino, and K.K. Gleason, *Macromolecules*, 42, 8138-8145, 2009

## Chapter 4

### *Initiated-chemical vapor deposition of organosilicon interlayers for moisture diffusion barrier systems\**

#### Abstract

Although very promising results in terms of moisture and oxygen permeation barrier properties have been achieved by organic/ inorganic multilayers, the impact of the organic interlayer on the global barrier performance is still under discussion. It is generally considered that the organic interlayer acts as smoothening layer allowing the decoupling between macro-defects either present on the polymer substrate and/or in the inorganic barrier layer. It is also hypothesized that the organic interlayer infiltrates into the nano-pores present in the barrier layer, therefore affecting the barrier itself at microstructure level. In the present work we discuss the moisture permeation barrier performance of multilayers deposited by means of initiated- and plasma enhanced- CVD methods. Calcium test measurements allowed discriminating between the water permeation through the macro-defects/pinholes and the permeation through the matrix porosity. It has been found that the improvement in terms of barrier properties, due to the filling/infiltration of the SiO<sub>2</sub>-like layer nano-pores by the organic interlayer, correlates with the residual open porosity in the barrier layer. Specifically, only for WVTR values of the SiO<sub>2</sub>-like layer larger than 10<sup>-3</sup> g m<sup>-2</sup> day<sup>-1</sup>, a barrier improvement factor up to 4 is reported, upon deposition of the organic interlayer. The combination of these results with the defect density study performed on the multilayer, and a comparison with parallel studies reported in literature, led to the conclusion that the main contribution of the i-CVD layer in improving the multilayer barrier properties is given by the smoothening/defects decoupling of the macro-defects.

---

\* G. Aresta, E.R.J. van Beekum, J. Palmans, M.C.M. van de Sanden, M. Creatore, to be submitted

## Introduction

The state-of-the art in the field of ultra-high moisture diffusion barriers is represented by a multilayer in which an inorganic ( $\text{Al}_2\text{O}_3$ ,  $\text{Si}_3\text{N}_4$  or  $\text{SiO}_2$ ) thin film (<100 nm) barrier is coupled with an organic (generally an acrylate- or organosilicon- based polymer) interlayer. This approach has led to water vapor transmission rates (WVTR) lower than  $10^{-5} \text{ g m}^{-2} \text{ day}^{-1}$ <sup>1, 2</sup>, therefore suitable for the encapsulation of high-end devices such as flexible OLEDs, which require WVTR values of  $10^{-6} \text{ g m}^{-2} \text{ day}^{-1}$  in order to reach a ten year lifetime<sup>3, 4</sup>. The multilayer barrier systems are generally deposited by a hybrid approach: sputtering or PE-CVD of the inorganic barrier layer, in combination with flash evaporation/condensation of the organic precursor, usually acrylate-based, followed by curing/polymerization<sup>1, 5-8</sup>, but also novel deposition approaches like ALD (for the barrier layer) in combination with MLD (for the organic interlayer)<sup>9-11</sup> and fully PE-CVD developed multilayers have been reported in literature<sup>12-15</sup>. Recently, Coclite *et al.*<sup>16</sup> reported on the deposition of multilayers based on organosilicon chemistry, in which the inorganic barrier layer is deposited by means of PE-CVD and the organic interlayer is deposited by means of initiated-CVD (i-CVD)<sup>17-19</sup>. The appeal of the i-CVD lays in its compatibility with vacuum systems and the full retention of the monomer chemistry, as in the case of liquid phase polymerization processes<sup>20, 21</sup>. Furthermore, the polymerization rate of the i-CVD process is fully controlled by the monomer surface adsorption<sup>20, 21</sup>.

The necessity for a multilayer barrier technology derives from the limit associated with single inorganic layers, i.e. their permeation barrier level being controlled by the presence of defects. These defects range in diameter from nms (equal or larger than the  $\text{H}_2\text{O}$  molecular size of  $0.33 \text{ nm}^{22}$ ), up to substrate/process- induced macro-defects (e.g. pinholes and particles reaching a size up to  $\mu\text{ms}$ )<sup>23</sup>. The successful application of a multilayer is generally attributed to the smoothening effect by means of the ( $\mu\text{m}$ - thick) organic polymer layer, which allow for a better development of the subsequent inorganic barrier<sup>1, 24, 25</sup>. Graff *et al.*<sup>26</sup>, who carried out numerical simulation studies, reported on the development of a tortuous path which the permeant molecule must follow through the organic interlayer before approaching a pinhole/defect in the subsequent barrier. Worth to mention is that this simulation has been carried out assuming that the moisture permeation occurs only through the

macro-defects present in the barrier layer which is considered elsewhere as impermeable (i.e. no permeation occur through nano-pores). However, Affinito *et al.*<sup>24</sup> highlighted that, although the macro-defects represent an unhindered path for the permeant molecule<sup>27, 28</sup>, the estimated area density of the nano-pores can be approximately 15-20 times larger than the one of the macro-defects resulting in a 15-20 times higher permeation flux than the latter<sup>24</sup>. Therefore, Affinito *et al.*<sup>24</sup> proposed an additional role of the organic interlayer, i.e. the infiltration of the liquid phase organic layer into the nano-sized pores of the inorganic barrier layer underneath, eventually affecting the local transmission of the permeant molecule through the filled pores. Recently<sup>29</sup>, we reported on the experimental evidence for the infiltration of the inorganic ( $\text{SiO}_2$ -like) barrier layer nano-pores (from 1 nm to larger than 2 nm) by means of an i-CVD monomer during the initial step of the polymerization process. These studies confirmed, therefore, the hypothesis of Affinito *et al.*<sup>24</sup> to be also valid for a CVD-based process, and not only limited to liquid phase polymerization.

The present work focuses on PECVD/i-CVD multilayers and addresses the contribution of the above-mentioned filling/infiltration of the nano-porosity to their moisture permeation barrier performance. Furthermore, a comparison is carried out with a fully PECVD- developed multilayer system. In order to discern between the effect of the filling/infiltration (affecting the porosity of the  $\text{SiO}_2$ -like matrix) and the better known decoupling/smoothening effect (associated to the layer macro-defects), intrinsic WVTR measurements (i.e. by excluding the permeation through the macro-defects/pinholes) have been also carried out, by means of the calcium test<sup>30</sup>. The filling/infiltration effect has been further addressed by studying the open porosity of the  $\text{SiO}_2$ -like layer by means of ellipsometric porosimetry (EP) measurements<sup>31-34</sup>. Adsorption/desorption isotherms<sup>33, 35, 36</sup> can be carried out providing information of the layer microstructure and estimation of the pore size. This is performed by following, by means of spectroscopic ellipsometry measurements, the changes in layer refractive index upon adsorption/desorption of the probing molecule in the open pores as function of the probing molecule relative pressure from 0 to saturation (i.e.  $0 < P_M/P_{sat} < 1$ ), at constant temperature.

The paper is organized as follow: in the experimental part a description of the deposition chamber is provided, together with the diagnostic techniques, i.e. IR

spectroscopy, *in situ* spectroscopic ellipsometry, EP measurements and the calcium test. The section on Results and Discussion addresses the comparison in terms of chemistry and barrier properties of the i-CVD/PECVD and fully PECVD developed multilayers. Then, the effect of the nanoporosity filling by means of the organic interlayer is addressed in the case of SiO<sub>2</sub>-like barrier layers exhibiting a different level of porosity. Finally conclusions are drawn and also discussed with respect to the experimental data set presented by Coclite *et al.*<sup>16</sup>.

## Experimental

All depositions are performed, without breaking the vacuum, in a custom-built setup which allows for thin film deposition by means of both PE-CVD and i-CVD approaches described in details elsewhere<sup>29, 37</sup>. During the i-CVD process the grid system, which is mounted on a magnetic movable arm, is inserted into the deposition chamber at a distance of 2 cm from the substrate holder. Its temperature can be controlled between 383 K and room temperature. The monomer (1,3,5-trivinyl-1,3,5-trimethylcyclotrisiloxane: V<sub>3</sub>D<sub>3</sub>, purity > 95%, Gelest) and the initiator (di-tert-butyl peroxide: d-TBPO, purity 98%, Aldrich) are mixed in a buffer and injected into the deposition chamber through a ring placed above the grid. The grid<sup>37</sup> is connected to a custom-built D.C. power supply system, which is equipped with a feed-loop system. During the PE-CVD process the grid is transferred from the deposition chamber to a load-lock chamber. SiO<sub>2</sub>-like and the SiO<sub>x</sub>C<sub>y</sub>H<sub>z</sub> layers are deposited by means of parallel plate RF-plasma<sup>29, 37</sup>. For both processes, the pumping direction is towards the bottom of the chamber. Before starting each deposition process, the chamber is completely evacuated to the base pressure of 10<sup>-6</sup> mbar and the setup is arranged for either the i-CVD or the PE-CVD process. Table I reports the conditions of deposition for all processes. In the case of the poly(V<sub>3</sub>D<sub>3</sub>) layer, the conditions have been chosen according to previous studies aimed to the deposition of stable, smooth layer with a high conversion (i.e. > 85%) of vinyl groups<sup>37</sup>. The setup is equipped with spectroscopic ellipsometry (SE) windows to study the film growth during each process.

**Table I**  
Multilayer conditions of deposition.

	i-CVD / poly(V <sub>3</sub> D <sub>3</sub> )	PE-CVD / SiO <sub>x</sub> C <sub>y</sub> H <sub>z</sub>	PE-CVD / SiO <sub>2</sub> -like
V <sub>3</sub> D <sub>3</sub> (sccm)	10	0.7	0.7
d-TBPO (sccm)	2	-	-
Ar (sccm)	-	100	70
O <sub>2</sub> (sccm)	-	-	35
P (mbar)	0.7	0.45	0.3
P (W)	-	50	250
T <sub>wire</sub> (K)	673	-	-
T <sub>sub</sub> (K)	333	373	373

### Film growth study and single layer characterization

The film growth processes is followed by means of *in situ* SE, at an angle of incidence of 71.5°, wavelength range of 245 - 1000 nm, 1.6 nm resolution, by using a J.A. Woollam Co. M-2000 F ellipsometer. The data analysis is performed by using the J.A. Woollam Complete EASE™ software version 4.27 and the mean squared error between the experimental data and the model is minimized by adjusting the fit parameters using the Levenberg-Marquardt algorithm. The optical model for the film growth study consists of a Si substrate; native SiO<sub>2</sub> (~ 2nm); Cauchy and Cauchy coupled with the Urbach adsorption tail functions for the SiO<sub>2</sub>-like and the SiO<sub>x</sub>C<sub>y</sub>H<sub>z</sub> and poly(V<sub>3</sub>D<sub>3</sub>) layers, respectively according to Equations 1-2:

$$n(\lambda) = A + \frac{B}{\lambda^2} \quad ; \quad k(\lambda) = 0 \quad (1)$$

$$n(\lambda) = A + \frac{B}{\lambda^2} + \frac{C}{\lambda^4}; \quad k(\lambda) = \alpha \cdot e^{\beta \left( 12400 \left( \frac{1}{\lambda} - \frac{1}{r} \right) \right)} \quad (2)$$

in which  $A$ ,  $B$  and  $C$  are the Cauchy fitting parameters and  $\alpha$  (extinction amplitude) and  $\beta$  (the exponent factor) the ones of the Urbach function used to fit the adsorption tail due to the carbon presence in both the poly(V<sub>3</sub>D<sub>3</sub>) and the SiO<sub>x</sub>C<sub>y</sub>H<sub>z</sub> layer. The substrate temperature is also a fit parameter which has been fitted prior to



the deposition process and then kept constant. The layer chemistry is investigated by means of Fourier Transform Infrared (FT-IR) measurements carried out with a Bruker Tensor 27 spectrophotometer. FT-IR spectra are acquired in the range of  $400\text{ cm}^{-1}$  -  $4000\text{ cm}^{-1}$  with a resolution of  $4\text{ cm}^{-1}$  and 256 scans. Before the spectra acquisition the spectrometer is purged for 15 min with  $\text{N}_2$  to minimize the effect of  $\text{H}_2\text{O}$  and  $\text{CO}_2$  absorption. All the spectra have been baseline corrected and normalized by the layer thickness.

### Ellipsometric Porosimetry measurements

The open porosity of the  $\text{SiO}_2$ -like layer has been studied by means of EP measurements by using  $\text{V}_3\text{D}_3$  as probing molecule and He as buffer gas under the conditions described in Table II.

**Table II**

Conditions used during the  $\text{V}_3\text{D}_3$  EP measurements on  $\text{SiO}_2$ -like layers.

$\text{V}_3\text{D}_3$ (sccm)	5
He (sccm)	2
$T_{\text{sub}}$ (K)	298
P (mbar)	$10^{-6}$ - 0.78
$T_{\text{walls}}$ (K)	353

After loading the  $\text{SiO}_2$ -like sample, the chamber is evacuated in order to remove adsorbed water ( $n = 1.33$ ) due to the layer exposure to ambient. For each sample an overnight evacuation was performed and the value of the  $\text{SiO}_2$ -like layer refractive index after evacuation is taken as the starting value of the adsorption/desorption measurements (i.e.  $n_0$ ). After the layer degassing, monomer and He are injected into the chamber at the base pressure of  $10^{-6}$  mbar and the pressure is then increased by equilibrium steps from  $2.5 \cdot 10^{-2}$  mbar to 0.78 mbar during the adsorption path. An equivalent procedure is followed for the desorption path. At the substrate temperature of 298 K, this allows to scan the entire  $P_M/P_{\text{sat}}$  range from 0 to  $\sim 1$ , being the monomer vapor pressure equal to 0.571 mbar at this temperature<sup>38</sup>. The monomer adsorption and desorption on the  $\text{SiO}_2$ -like layers is monitored continuously by means of *in situ* SE measurements. As shown later, all the studied

layers are characterized by nano-porosity followed by monomer multilayer adsorption. Therefore, in order to present both effects, the adsorption/desorption isotherms have been reported in terms of optical thickness as follow:

In the  $0 < P_M/P_{sat} < 0.2$  range the optical thickness is given by Equation 3:

$$n \cdot d = n_{SiO_2-like(fill)} \cdot d_{SiO_2-like} \quad (3)$$

where  $n_{SiO_2-like(fill)}$  is the  $SiO_2$ -like refractive index due to the nano-pore filling and  $d_{SiO_2-like}$  is the constant  $SiO_2$ -like layer thickness;

for  $P_M/P_{sat} > 0.2$ , i.e. under multilayer adsorption, the optical thickness is given by Equation 4:

$$n \cdot d = n_{SiO_2-like(P_M/P_{sat}=0.2)} \cdot d_{SiO_2-like} + n_{V_3D_3} \cdot d_{V_3D_3} \quad (4)$$

where  $n_{V_3D_3}$  is monomer refractive index (1.422 at 589 nm<sup>39</sup>) and  $d_{V_3D_3}$  is the monomer multilayer thickness. The same procedure has been adopted during the desorption path. The optical model for the fit of the SE data, for  $0 < P_M/P_{sat} < 0.2$ , is the same as in equation 1, being the monomer transparent in the investigated wavelength range. For  $P_M/P_{sat} > 0.2$  the  $V_3D_3$  multilayer uptake has been fitted by adding a Cauchy layer on top of the  $SiO_2$ -like layer with fixed refractive index of the  $V_3D_3$  and being the thickness the only fit parameter.

### Water Vapor Transmission Rate measurements

Water Vapor Transmission Rate (WVTR) measurements are carried out by means of the calcium (Ca) test according to the procedure described by Nisato *et al.*<sup>2, 30</sup> at a constant temperature of 298 K and 50 % of relative humidity (R.H.). The determination of the WVTR value is related to the changes in optical transmittance of a 40 nm thick Ca layer due to oxidation to CaO after reaction with  $H_2O_{vap}$ . A minimum decrease of calcium layer thickness of 1 nm is needed to obtain an accuracy of the 10% on the measurement. The measurement setup for the Ca test (developed by the Philips Research laboratories) consists of a Philips CL5000M light source with a diffuser for uniform back lighting and a sample holder with mask. A

12 bit Adimex MX12p camera was used to obtain a gray scale image of the sample. The amount of oxidation is determined from the gray tint. A nontransparent black reference from the mask and a white reference from the transparent part of the glass plate have been included in every measurement to set the gray scale range and to correct for transparency changes due to the barrier film. Several configurations can be adopted for the Ca test according to the different substrates on which the barrier systems are deposited. Ca can be deposited on glass substrates followed by the deposition of the barrier system or directly on the barrier system if the latter has been deposited on polymer substrate. In the first case a temporary PE-CVD  $\text{SiO}_x$  (intrinsic WVTR of  $10^{-2} \text{ g m}^{-2} \text{ day}^{-1}$ ) barrier layer is deposited on Ca to avoid moisture permeation during transportation. In the second configuration glass is replaced by a PE-CVD deposited  $\text{a-SiN}_x\text{:H}$ <sup>40</sup> barrier layer with excellent ( $10^{-6} \text{ g m}^{-2} \text{ day}^{-1}$ ) intrinsic barrier properties<sup>40</sup>. The sample size is of  $100 \text{ cm}^2$ . Ca has been deposited by thermal evaporation on the glass plates or barrier systems in a structure consisting of 4 samples, each divided in 9 squares of  $0.25 \text{ cm}^2$ , to avoid that the water vapor permeating through one defect would affect the whole area of the samples. The determination of the barrier properties of the multilayers on PEN substrate has been performed by using the following configuration: glass/PEN/barrier/Ca/a-SiN<sub>x</sub>:H. The glass/PEN substrates have been made by laminating  $125 \mu\text{m}$  thick PEN (DuPont) foils on  $100 \text{ cm}^2$  glass plates. Prior to the Ca test the PEN/barrier/Ca/a-SiN<sub>x</sub>:H systems have been delaminated from the glass. The determination of the extrinsic WVTR values has been performed by taking a weighted average of the transmission through the barrier system matrix and pinholes. No effect of potential side-leakage is taken into account. As a matter of fact, in our measurement configuration, a water molecule diffusing laterally, through the barrier, to the Ca samples should make a path in the cm range, while the vertical path, through the PEN/barrier, is in the order of  $\mu\text{m}$  and the latter represents the dominant path, also considering the short measurement time (4 - 7 days). The comparison in terms of intrinsic WVTR values between the single  $\text{SiO}_2$ -like barrier layer and the  $\text{SiO}_2$ -like/poly( $\text{V}_3\text{D}_3$ ) system has been carried out on glass/Ca/ $\text{SiO}_x$  (40 nm thick) substrates. The use of the temporary  $\text{SiO}_x$  layer has no effect on the determination of the intrinsic WVTR values since the  $\text{SiO}_x$  layer has a barrier performance of a factor one-to-three times lower than the barrier layers under investigation.

## Results and discussion

### A. Single layer comparison

Figure 1 shows the comparison between the FT-IR absorption spectra of the i-CVD poly( $V_3D_3$ ) and the PE-CVD  $SiO_xC_yH_z$  layers, normalized by their thickness, together with the liquid  $V_3D_3$  monomer spectrum<sup>37</sup> and the PE-CVD  $SiO_2$ -like barrier layer.

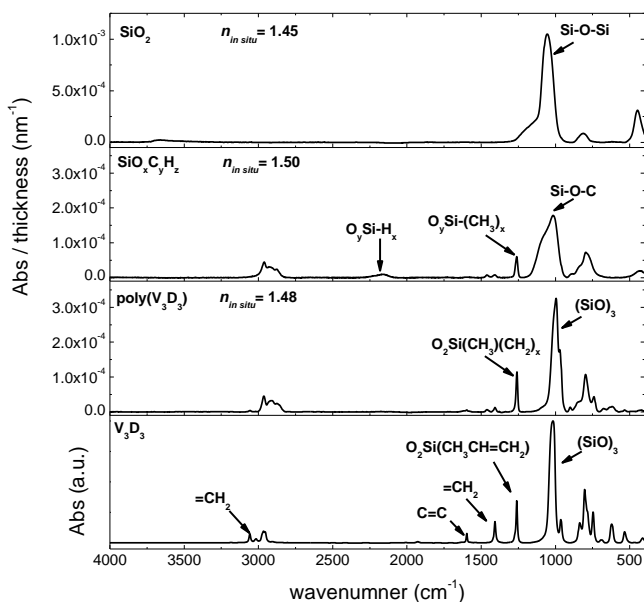


**Figure 1:** FT-IR spectra, normalized by the layer thickness, of the i-CVD poly( $V_3D_3$ ), PE-CVD  $SiO_xC_yH_z$  and PE-CVD  $SiO_2$ -like layers. The spectrum of the liquid phase  $V_3D_3$  monomer is added for comparison<sup>37</sup>. Also in the graph the in situ values of the layer refractive index are reported.

The monomer functional groups (namely the methyl group bonded to Si, Si-CH<sub>3</sub> bending signal at 1260 cm<sup>-1</sup><sup>41, 42</sup>, and the cyclotrisiloxane ring, Si-O-Si asymmetric stretching signal at 995 cm<sup>-1</sup><sup>37, 43</sup>) are fully retained in the poly( $V_3D_3$ ) structure, being the vinyl groups responsible for the polymerization process<sup>37, 41, 44, 45</sup>. On the contrary, the opening of the cyclotrisiloxane ring into the  $SiO_xC_yH_z$  layer spectrum, is witnessed by the broadening of the Si-O-Si asymmetric stretching signal centered

at  $1020\text{ cm}^{-1}$  showing a higher wavenumber ( $1080\text{ cm}^{-1}$ ) shoulder associated to short linear siloxane chains<sup>41, 46, 47</sup> and furthermore highlighted by presence of the Si-H<sub>x</sub> stretching in the O<sub>y</sub>Si-H<sub>x</sub> group at  $2100\text{ cm}^{-1}$ <sup>42, 47</sup>. The broadening and decrease in intensity of the Si-(CH<sub>3</sub>)<sub>x</sub> related signal, at  $1260\text{ cm}^{-1}$ , points out to a shift towards a O<sub>x</sub>Si-(CH<sub>3</sub>)<sub>y</sub> chemistry<sup>47-49</sup>, due to the fragmentation occurring in the plasma phase.

## B. Barrier Performances

The barrier performances of the above-mentioned multilayers deposited on PEN substrates have been tested and the extrinsic WVTR values are reported in Figure 2a.

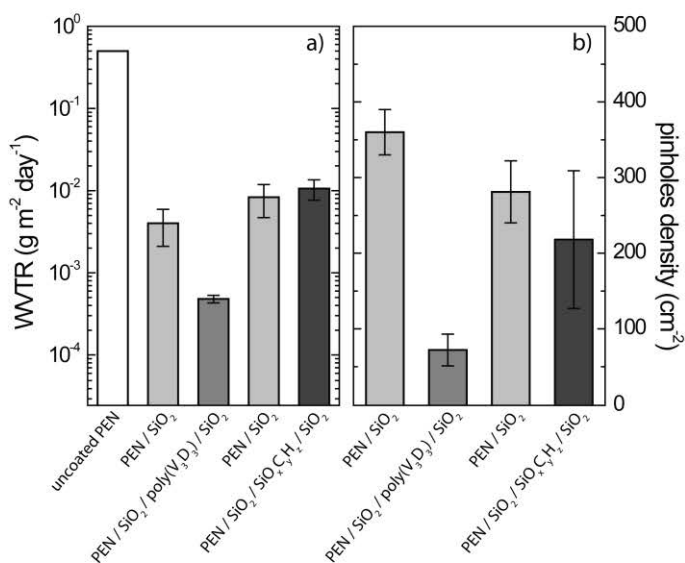


**Figure 2:** a) Extrinsic WVTR values and b) defect density of the single SiO<sub>2</sub>-like layer and the i-CVD/PE-CVD and PE-CVD multi-layers.

For each system a single SiO<sub>2</sub>-like layer has been deposited as reference. The 100 nm thick SiO<sub>2</sub>-like layer shows already very good extrinsic barrier properties with an average barrier improvement factor (BIF) of 80 with respect to the pristine PEN substrate, superior to other values reported in literature for PE-CVD deposited SiO<sub>2</sub>-like layers<sup>13, 16, 50</sup>. When two 100 nm thick SiO<sub>2</sub>-like layers are coupled with a 200

nm thick, poly(V<sub>3</sub>D<sub>3</sub>) layer, the barrier properties of the multilayer further decrease by almost an order of magnitude with a total BIF respect to the uncoated PEN of 1000. When the SiO<sub>2</sub>-like layers, are coupled with a 200 nm thick SiO<sub>x</sub>C<sub>y</sub>H<sub>z</sub> organic interlayer, no barrier improvement with respect to the single SiO<sub>2</sub>-like layer is observed.

On the basis of the considerations earlier outlined with respect to the role of the organic interlayer, we now evaluate the i-CVD and PE-CVD organic interlayers in terms of smoothening/decoupling and filling/infiltration of the SiO<sub>2</sub>-like nano-defects. The first effect can be inferred by comparing the defect density<sup>1</sup> evolution, derived from the detected white spots during the Ca test<sup>2</sup>, as shown in Figure 2b. The defects density is reduced by a factor 5 compared to the single SiO<sub>2</sub>-like layer, in the presence of the poly(V<sub>3</sub>D<sub>3</sub>) interlayer, while in the case of the SiO<sub>x</sub>C<sub>y</sub>H<sub>z</sub> interlayer, no decrease in defect density is reported. This suggests a smoothening/decoupling effect of the poly(V<sub>3</sub>D<sub>3</sub>) interlayer with respect to the SiO<sub>x</sub>C<sub>y</sub>H<sub>z</sub>, due to the higher conformality of the i-CVD layer<sup>51, 52</sup>, therefore capable of better coverage of the particles/defects<sup>16</sup>.

The second effect (i.e. the infiltration/filling of the organic interlayer into the nano-defects/porosity of the underlying inorganic barrier) can be investigated by comparing the poly(V<sub>3</sub>D<sub>3</sub>) and SiO<sub>x</sub>C<sub>y</sub>H<sub>z</sub> initial growth on the barrier layer, as shown in Figure 3.

---

<sup>1</sup> The defects present on the surface of the PEN substrate find their origin either in dust particles, antistatic particles, slurries or in the contamination due to the lab environment prior to the deposition process. The defect density can be rather scattered, as shown in Figure 2b. Therefore, each set of multi-layers has its own single SiO<sub>2</sub>-like barrier layer reference.

<sup>2</sup> i.e. the white spot development is due to the fast oxidation of Ca associated to the water permeating through a macro-defect or pinhole.

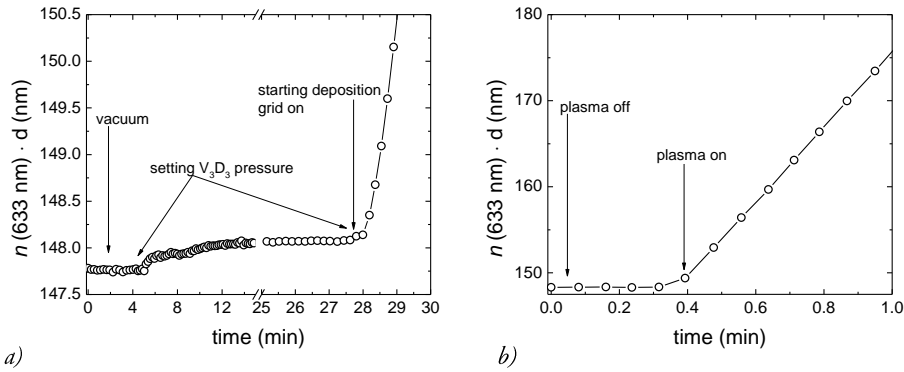


Figure 3: Initial growth of a) poly( $V_3D_3$ ) and b)  $SiO_xC_yH_z$  layers on the  $SiO_2$ -like barrier film.

For sake of comparison, the optical thickness of the layer is considered. In Figure 3a, the i-CVD process is monitored: during the setting of the deposition conditions (i.e. the setting of the pressure) an uptake of the optical thickness is observed due to the monomer adsorption in the open nano-scale porosity of the  $SiO_2$ -like layer, as we have already reported in [29]. After the pressure is set to the deposition conditions, the grid is heated up and the growth of the i-CVD layer proceeds linearly. In the case of the PE-CVD process, there is no change in optical thickness prior to the ignition of the plasma, indicating no monomer adsorption in the open porosity of the barrier layer. This difference can be easily interpreted in terms of the  $P_M/P_{sat}$  parameter, i.e. the ratio between the monomer partial pressure and its saturation pressure at a given temperature<sup>21</sup>, which controls the monomer surface adsorption. In the case of the poly( $V_3D_3$ ) layer,  $P_M/P_{sat} = 0.113$  at 333 K while in the case of the  $SiO_xC_yH_z$  this is of  $P_M/P_{sat} = 10^{-4}$ . Therefore, it can be expected that only in the case of the i-CVD/PE-CVD multilayer, the filling of the nano-defects by the poly( $V_3D_3$ ) may play a role in affecting the multi-layer barrier performance.

In order to investigate the role of the organic interlayer in affecting the barrier performance of the multilayer, the calcium test has been carried out as outlined in the Experimental part. The evaluation of the intrinsic WVTR values, i.e. in the Ca regions not affected by the local pinhole/defect density, allows highlighting the potentially beneficial effect of the filling of the nano-pores by the i-CVD monomer.

### C. Nano-pore infiltration of the SiO<sub>2</sub>-like layer by the poly(V<sub>3</sub>D<sub>3</sub>): effect on the intrinsic barrier performances.

The intrinsic barrier properties of several SiO<sub>2</sub>-like layers, with a WVTR in the range between  $2 \cdot 10^{-5} - 3 \cdot 10^{-3} \text{ g m}^{-2} \text{ day}^{-1}$ , have been compared with those of SiO<sub>2</sub>-like layers upon deposition of a 20 nm-thick poly(V<sub>3</sub>D<sub>3</sub>) layer, as shown in Figure 4.

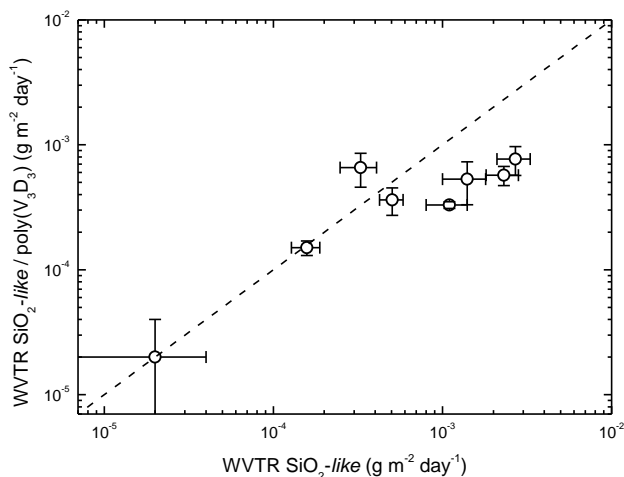


**Figure 4:** Intrinsic WVTR values of the SiO<sub>2</sub>-like/poly(V<sub>3</sub>D<sub>3</sub>) layer as function of the intrinsic WVTR of the SiO<sub>2</sub>-like layer. The determination of the intrinsic barrier properties for the layer exhibiting a WVTR as low as  $2 \cdot 10^{-5} \text{ g m}^{-2} \text{ day}^{-1}$  is characterized by a large error bar, because the Ca test has been stopped after 25 (SiO<sub>2</sub>-like) and 42 (SiO<sub>2</sub>-like /poly(V<sub>3</sub>D<sub>3</sub>)) days, respectively. The measurement was terminated because the white spots grew until covering the Ca area used to determine the intrinsic barrier properties. However, in both cases the minimum oxidation of 1 nm of Ca to CaO was not reached. Therefore, only upper limits values of WVTR have been reported in the graph. These values are  $(2 \pm 2) \cdot 10^{-5} \text{ g m}^{-2} \text{ day}^{-1}$  for both the SiO<sub>2</sub>-like and SiO<sub>2</sub>-like/poly(V<sub>3</sub>D<sub>3</sub>).

For WVTR values of the SiO<sub>2</sub>-like layer below  $3 \cdot 10^{-4} \text{ g m}^{-2} \text{ day}^{-1}$ , no intrinsic barrier improvement is observed upon infiltration of the V<sub>3</sub>D<sub>3</sub> monomer in the nanoporosity of the barrier layer. For a WVTR of the pristine SiO<sub>2</sub>-like layer above  $3 \cdot 10^{-4} \text{ g m}^{-2} \text{ day}^{-1}$ , an improvement in barrier properties is observed upon deposition of the 20 nm thick poly(V<sub>3</sub>D<sub>3</sub>). Under these conditions, however, the BIF is limited to a value of 4. The observed BIF values cannot be attributed to the poly(V<sub>3</sub>D<sub>3</sub>) intrinsic barrier performance by applying the ideal laminate theory series<sup>24</sup>, since they have



estimated to be in the same order of the PEN substrate barrier level, therefore negligible with respect to the pristine SiO<sub>2</sub>-like layers barrier performance.

In order to further investigate the dependence of the BIF from the SiO<sub>2</sub>-like intrinsic WVTR values, ellipsometric porosimetry measurements have been performed on the two extremes of the series, shown in Figure 4.

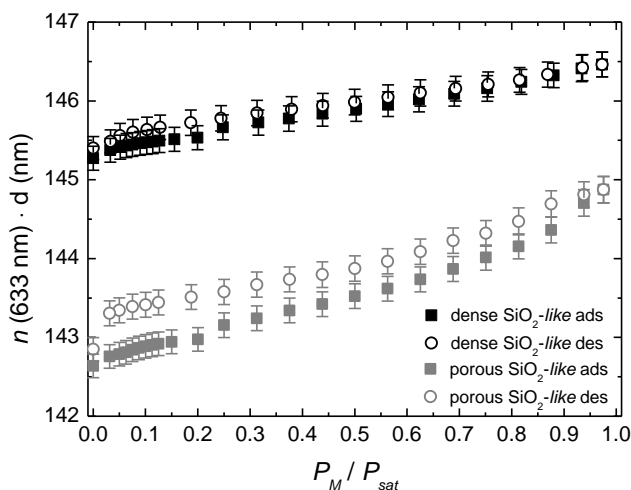


Figure 5: V<sub>3</sub>D<sub>3</sub> adsorption/desorption isotherms performed on dense ( $n_{m\ situ} = 1.447$ ) and porous ( $n_{m\ situ} = 1.422$ ) SiO<sub>2</sub>-like layers.

The data reported in Figure 5 show that a hybrid type I-II isotherm describes the deposited layers. According to the IUPAC classification<sup>35, 36</sup>, a type I corresponds to a nano-porous layer (pore size < 2 nm), while a type II corresponds to a non-(macro-)porous<sup>3</sup> layer. Indeed, during the adsorption path, an initial optical thickness uptake in the range of  $0 < P_M/P_{sat} < 0.2$  due to nano-pore filling develops, followed by monomer multilayer adsorption for  $P_M/P_{sat} > 0.2$ . Furthermore, while the isotherm associated to the denser SiO<sub>2</sub>-like layer shows reversibility, a hysteresis loop develops in the case of the porous SiO<sub>2</sub>-like layer extending to the lower  $P_M/P_{sat}$  range, and

<sup>3</sup> According to the IUPAC pore size classification, a macro-pore corresponds to a size > 50 nm, associated to a type II isotherm<sup>35,36</sup>.

most certainly related to chemisorption phenomena occurring between the silanol groups present in the porous SiO<sub>2</sub>-like layer and the oxygen of the cyclotrisiloxane ring of the V<sub>3</sub>D<sub>3</sub> via H bonding<sup>29</sup>. The difference in nano-pore density between the two layers can be inferred by considering the difference in nanoporosity<sup>4</sup> between the two layers at  $P_M/P_{sat} = 0.2$  (i.e. when the nano-pore filling is complete<sup>36</sup>), being 0.5 % and 0.7 % for the denser and porous SiO<sub>2</sub>-like layer, respectively. Although the difference in residual open porosity between the two layers is small, it is interesting to report that the correlation between the residual open porosity and the intrinsic WVTR appears to hold also for layers deposited by other methods. In Table III we report the comparison between the PE-CVD SiO<sub>2</sub>-like layers and a 30 nm thick plasma-assisted (PA-ALD) SiO<sub>2</sub>-like layer.

**Table III**

Nanoporosity (at  $P_M/P_{sat} = 0.2$ ) values, as determined by EP measurements, and WVTR values of the different SiO<sub>2</sub>-like layers deposited by PE-CVD and by PA-ALD. The in situ values of the layers refractive index are also reported.

layer	$n_{in\ situ}(633\text{ nm})$	nanoporosity (%)	WVTR ( $\text{g m}^{-2}\text{ day}^{-1}$ )
PE-CVD SiO <sub>2</sub> -like	1.447	0.5	$2 \cdot 10^{-5}$
	1.422	0.7	$3 \cdot 10^{-3}$
PA-ALD SiO <sub>2</sub> -like	1.420	1.1	$\geq 10^{-2}$

This latter is characterized by a residual porosity of 1.1%, corresponding to an increase in WVTR to  $\geq 10^{-2}\text{ g m}^{-2}\text{ day}^{-1}$ . Although the full characterization of the open porosity will be the subject of a next paper, it can be argued that the residual porosity controls the intrinsic WVTR of the inorganic layer. We should, however, note that the open porosity values here reported are related to pores with a size accessible for the V<sub>3</sub>D<sub>3</sub> molecule. The effective open porosity of a layer may be larger

<sup>4</sup> The layer porosity, P is calculated on the basis of the Lorentz-Lorenz Effective Medium Approximation by the following formula<sup>32</sup>:

$$P = \frac{\frac{n_{fill}^2(P_M/P_{sat}=0.2) - 1}{n_{fill}^2(P_M/P_{sat}=0.2) + 2} - \frac{n_0^2(P_M/P_{sat}=0) - 1}{n_0^2(P_M/P_{sat}=0) + 2}}{\frac{n^2(V_3D_3) - 1}{n^2(V_3D_3) + 2}}$$

where  $n_{fill}$  is the SiO<sub>2</sub>-like/V<sub>3</sub>D<sub>3</sub> refractive index at  $P_M/P_{sat} = 0.2$ ;  $n_0$  is the SiO<sub>2</sub>-like layer refractive index at  $P_M/P_{sat} = 0$  and  $n(V_3D_3)$  is the monomer refractive index.

due to the presence of pores with size below 1 nm, inaccessible to  $V_3D_3$ <sup>29,37</sup>, yet representing a permeation path for  $H_2O$  molecule. In this respect, it can be expected that by detecting the open porosity characterized by a size smaller than 1 nm, larger differences in pore content between the layers under investigation may be observed.

#### D. Contribution of the smoothening/decoupling effect with respect to the filling/infiltration effect on the overall barrier performances.

On the basis of the discussion earlier reported, it can be concluded that the improvement of the barrier properties of the  $SiO_2$ -like/poly( $V_3D_3$ )/ $SiO_2$ -like system on PEN (Figure 2), is attributed to the smoothening/decoupling effect of the poly( $V_3D_3$ ) layer. The filling of the  $SiO_2$ -like layer nano-porosity by the poly( $V_3D_3$ ) layer is negligible, since the  $SiO_2$ -like layer here under investigation is characterized by an intrinsic WVTR of  $10^{-5} \text{ g m}^{-2} \text{ day}^{-1}$  (see Figure 4).

We now further expand our analysis to the multilayers described in literature. Coclite *et al.*<sup>16</sup>, for example, reported on the deposition of a  $SiO_2$ -like layer by means of PE-CVD approach which showed poor barrier properties on PEN (WVTR =  $1.15 \text{ g m}^{-2} \text{ day}^{-1}$ ). However, when two  $SiO_2$ -like layers were deposited in combination with a 400 nm thick i-CVD deposited poly(hexavinylsiloxane) layer, a BIF equal to 10 was reported (WVTR  $\sim 0.1 \text{ g m}^{-2} \text{ day}^{-1}$ )<sup>16</sup>. The authors attributed the multilayer barrier improvement to the smoothening effect and the decoupling of the defects between the two  $SiO_2$ -like layers by the i-CVD deposited poly(HVDSO) layer. Due to the poor barrier properties of the single inorganic layer shown by Coclite *et al.*, the filling/infiltration of the  $SiO_2$ -like barrier layer nanopores by the poly(HVDSO) could still play a role in affecting the barrier performances. By assuming the ideal laminate theory (Equation 5) and by applying the relationship between the WVTR and the permeability of a barrier system at the steady-state (i.e. the difference in water partial pressure upstream the system  $p_0^5$  is much larger than the water partial pressure downstream  $p_f$ , i.e:  $p_0 \gg p_f$ )<sup>24</sup>:

$$\frac{d_{tot}}{P_{tot}} = \sum_i \frac{d_i}{P_i} \quad (5)$$

<sup>5</sup> As the conditions for the WVTR were of 298 K and 98 % of R.H. <sup>9</sup> a water partial pressure in the upstream can be calculated to be  $p_0 = 0.030 \text{ atm}$ .

$$WVTR \approx P \cdot \frac{P_0}{d_{tot}} \quad (6)$$

where  $d_{tot}$  and  $P_{tot}$  are the multilayer thickness and permeability and  $d_i$  and  $P_i$  are the substrate and single layer thickness and permeability. The permeability and the WVTR of the single SiO<sub>2</sub>-like layer can be derived from the data of Coclite *et al.*<sup>16</sup> (See Table IV)

**Table IV**  
Data related to the work of Coclite *et al.*<sup>16</sup>

	thickness	WVTR (g m <sup>-2</sup> day <sup>-1</sup> )
PEN	125 μm	1.16
(PEN)/SiO <sub>2</sub> -like	100 nm	1.15
(PEN)/SiO <sub>2</sub> -like/poly(HVDSO)/SiO <sub>2</sub> -like	600 nm	~ 0.1

By considering a BIF equal to 4, in agreement with our results, of the single SiO<sub>2</sub>-like layer due to the filling of the layer nano-pores during the i-CVD process, the permeability of the second SiO<sub>2</sub>-like layer, affected by the smoothening of the i-CVD layer underneath, can be derived from Equation 7<sup>6</sup>:

$$\frac{d_{PEN/SiO_2/i-CVD/SiO_2}}{P_{PEN/SiO_2/i-CVD/SiO_2}} = \frac{d_{PEN(i-CVD)}}{P_{PEN(i-CVD)}} + \frac{d_{SiO_2\ filling}}{P_{SiO_2\ filling}} + \frac{d_{SiO_2\ smoothening}}{P_{SiO_2\ smoothening}} \quad (7)$$

This leads to a  $P_{SiO_2\ like\ smoothening} = 4.5 \cdot 10^{-7} \text{ m}^2 \text{ day}^{-1} \text{ g m}^{-3} \text{ atm}^{-1}$  and to a WVTR of the second SiO<sub>2</sub>-like layer of 0.134 g m<sup>-2</sup> day<sup>-1</sup>, corresponding to a BIF approximately equal to 250 calculated with respect to the pristine SiO<sub>2</sub>-like layer. This result, compared with the BIF of 4, related to the filling effect of the barrier nanopores by the i-CVD layer, confirms our results and the conclusions by Coclite *et al.*<sup>16</sup>: the i-CVD layer quantitatively contributes to the smoothening of the barrier layer underneath and decoupling of macro-defects.

<sup>6</sup> The thickness of the i-CVD layer (400 nm) has been included into the thickness of PEN since the i-CVD permeability,  $P_{i-CVD}$ , has been assumed to be the same as of PEN.

## **Conclusions and Outlook**

In this work, the impact of the filling of residual nano-porosity in SiO<sub>2</sub>-like barrier layers by means of the i-CVD poly(V<sub>3</sub>D<sub>3</sub>) has been investigated with respect to the smoothening/decoupling effect of the SiO<sub>2</sub>-like layer macro-defects. Ca test measurements allowed discerning between the water permeation through the macro-defects/pinholes and the permeation through the matrix. The impact of the filling of the nano-pores has been found to be effective only for SiO<sub>2</sub>-like barriers characterized by an intrinsic WVTR value > 10<sup>-3</sup> g m<sup>-2</sup> day<sup>-1</sup> with a maximum BIF of 4. The BIF measured for the several SiO<sub>2</sub>-like layers has been correlated with their residual open porosity as detected by means of ellipsometric porosimetry. When the effect of the filling of the nanopores is compared with the impact of the poly(V<sub>3</sub>D<sub>3</sub>) in terms of control on the macro-defect density, it is concluded that the main contribution of the i-CVD layer is the smoothening/decoupling of the macro-defects. Considering the limited BIF values here reported, it can be argued that an infiltration into smaller size pores (i.e. < 1 nm) can provide better moisture permeation barrier levels, as these pores are still accessible to water vapor. Furthermore, a proper control on the chemistry of the organic interlayer in terms of water solubility and diffusivity, as suggested in the study of Graff<sup>26</sup>, can represent a valid approach towards higher intrinsic BIF values.

## **Acknowledgments**

The authors would like to thank J. J. A. Zeebregts, M. J. F. van de Sande, J. J. L. M. Meulendijks, H. M. M. de Jong, and W. Keuning for their skillful technical assistance. T. van Mol, J. J. Michels, S. Unnikrishnan, F. J. H. van Assche (Holst Centre, High Tech Campus, Eindhoven, The Netherlands), and P. van de Weijer (Philips Research, High Tech Campus, Eindhoven, The Netherlands), are acknowledged for the fruitful discussion of the data. P. van der Weijer, F. J. H. van Assche and P. Klaassen (Philips Research, High Tech Campus, Eindhoven) are kindly acknowledged for the WVTR measurements and the data discussion. This work forms part of the research programme of the *Dutch Polymer Institute* (DPI), project number 663 of the Large Area Thin Film Electronics (LATFE).

## References

- [1] P.E. Burrows, G. L. Graff, M. E. Gross, P.M. Martin, M. K. Shi, M. Hall, E. Mast, C. Bonham, W. Bennet, M. B. Sullivan, *Displays*, 22, 65-69, **2001**
- [2] G. Nisato, M. Kuiler, P. Bouten, L. Moro, O. Philips, N. Rutherford, *Proceedings Society for Information Display*, 550 – 553, **2003**
- [3] J.S. Lewis and M. S. Weaver, *IEEE Journal of Selected Topics in Quantum Electronics*, Vol. 10, No 1, 45-57, **2004**
- [4] F.J.H. van Assche, R.T. Vangheluwe, J.W.C. Maes, W.S. Mischke, M.D. Bijker, F.C. Dings, M.F.J. Evers, W.M.M. Kessels, M.C.M. van de Sanden, *Proceedings Society for Information Display*, 695 – 697, **2004**
- [5] S.P. Subbarao, M.E. Bahlke, and I. Kymissis, *IEEE Transactions on Electron Devices*, 57, 1, 153 – 156, **2010**
- [6] P. van de Weijer and T. van Mol, “White paper on the characterization of thin-film barrier layers for protection of organic Light-Emitting Diodes” Editor: M. Kilitziraki, **2009**
- [7] W. Keuning, P. van de Weijer, H. Lifka, W.M.M. Kessels, M. Creatore, *Journal of Vacuum Science and Technology A*, 31, 01A131-1 - 01A131-6, **2012**
- [8] K. Vaško, K. Noller, M. Mikula, S. Amberg-Schwab, U. Weber, *Central European Journal of Physics*, 7, 371 - 378, **2009**
- [9] Y. C. Lee, *Proceedings SPIE*, 7928, 792802, **2011**
- [10] A.A. Dameron, D. Seghete, B.B. Burton, S. D. Davidson, A.S. Cavanagh, J. A. Bertrand, S. M. George, *Chemistry of Materials*, 20, 3315 - 3326, **2008**
- [11] S.M. George, B. Yoon and A.A. Dameron, *Accounts of Chemical Research*, 42, 498 – 508, **2009**
- [12] T.W. Kim, M. Yan, A. G. Erlat, P. A. McConnelee, M. Pellow, J. Deluca, T.P. Feist, A.R. Duggal, M. Schaepekens, *Journal of Vacuum Science and Technology A*, 23, 4, **2005**
- [13] A. Francescangeli, F. Palumbo, R. d’Agostino, *Plasma Processes and Polymers*, 5, 708–717, **2008**
- [14] G. Dennler, C. Lungenschmied, H. Neugebauer, N.S. Sariciftci, M. Latreche, G. Czeremuszkin, M.R. Wertheimer, *Thin Solid Films*, 511 – 512, 349 – 353, **2006**

- [15] J. Fahlteich, M. Fahland, W. Schönberger, N. Schiller, *Thin Solid Films*, 517, 3075–3080, **2009**
- [16] A.M. Coclite, G. Ozaydin-Ince, F. Palumbo, A. Milella, K.K. Gleason, *Plasma Processes and Polymers*, 7, 561–570, **2010**
- [17] M.E. Alf, A. Asatekin, M.C. Barr, S.H. Baxamusa, H. Chelawat, G. Ozaydin-Ince, C.D. Petruczok, S. Sreenivasan, W.E. Tenhaeff, N.J. Trujillo, S. Vaddiraju, J. Xu, and K.K. Gleason, *Advanced Materials*, 22, 1993–2027, **2010**
- [18] A. Asatekin, M.C. Barr, S.H. Baxamusa, K.K.S. Lau, W. Tenhaeff, J. Xu, and K.K. Gleason, *Materials Today*, Vol. 13 N. 5, 26-33, **2010**
- [19] G. Ozaydin-Ince, A.M. Coclite and K.K. Gleason, *Reports on Progress in Physics*, 75, 016501, **2012**
- [20] K.K.S. Lau and K.K. Gleason, *Macromolecules*, 39, 3695-3703, **2006**
- [21] K.K.S. Lau and K.K. Gleason, *Macromolecules*, 39, 3688-3694, **2006**
- [22] A.P. Roberts, B.M. Henry, A.P. Sutton, C.R.M. Grovenor, G.A.D. Briggs, T. Miyamoto, M. Kano, Y. Tsukahara, M. Yanaka, *Journal of Membrane Science*, 208, 75–88, **2002**
- [23] A.S. da Silva Sobrinho, M. Latreche, G. Czeremuszkina, J. E. Klemberg-Sapieha, and M.R. Wertheimer, *Journal of Vacuum Science and Technology A*, 16, 6, 3190-3198, **1998**
- [24] J. Affinito, D. Hilliard, *47<sup>th</sup> Society of Vacuum Coaters Annual Technical Conference Proceedings*, 563-593, **2004**
- [25] D.G. Shaw and M.G. Langlois, *Proceedings 7th International Conference on Vacuum Web Coating*, 1993, pp. 268–276, **1993**
- [26] G.L. Graff, R.E. Williford, P.E. Burrows, *Journal of Applied Physics*, Vol. 96 No. 4, 1840-1849, **2004**
- [27] Y.G. Tropsha and N.G. Harvey, *Journal of Physical Chemistry B*, 101, 2259-2266, **1997**
- [28] A.G. Erlat, B.C. Wang, R.J. Spontak, Y. Tropsha, K.D. Mar, D.B. Montgomery, and E.A. Vogler, *Journal of Materials Research*, Vol. 15, No. 3, 704 – 717, **2000**
- [29] G. Aresta, J. Palmans, M.C.M. van de Sanden, M. Creatore, *Microporous and Mesoporous Materials*, 151, 434–439, **2012**



- [30] G. Nisato, P.C.P. Bouten, P.J. Slikkerveer, W.D. Bennet, G.L. Graff, N. Rutherford, L.Wiese, *21<sup>st</sup> Annual Asia Display, 8<sup>th</sup> International Display Workshop*, 1435 – 1438, **2001**
- [31] S. Elsave, F. Iacopi, M.R. Baklanov, C.E.A. Kirschhock, K. Maens, J.A. Martens, *Journal of the American Chemical Society*, 129, 9288 – 9289, **2007**
- [32] C. Licitra, R. Bouyssou, T. Chevolleau, F. Bertin, *Thin Solid Films* 518, 5140-5145, **2010**
- [33] K.S.W. Sing, D.H. Everett, R.A. W. Haul, L. Moscou, R.A. Pierotti, J. Rouquerol, T. Siemieniewska, *Pure Applied Chemistry*, Vol. 57 No. , 603 – 619, **1985**
- [34] K.S.W. Sing, *Colloids and Surface A*, 241, 3–7, **2004**
- [35] S.J. Gregg and K.S.W. Sing, “*Adsorption, Surface Area and porosity*”, (Academic Press Inc. Ltd, London, England), **1982**
- [36] F. Rouquerol, J. Rouquerol, K. Sing, “*Adsorption by powders & porous solids. Principles, methodology and applications*”, (Academic Press, London, England), **1999**
- [37] G. Aresta, J. Palmans, M.C.M. van de Sanden, M. Creatore, accepted for publication on *Journal of Vacuum Science and Technology A*, **2012**
- [38] [www.scifinder.cas.org](http://www.scifinder.cas.org)
- [39] H. Ahmed, C.F. Poole, G.E. Kozerski, *J. Chromatogr A*, 1169 179–192, **2007**
- [40] A.M.B. van Mol, P. van de Weijer, and C. Tanase, *Proceedings SPIE*, 6999, 46, **2008**
- [41] W.S. O’Shaughnessy, M. Gao, and K.K. Gleason, *Langmuir*, 22, 7021-7026, **2006**
- [42] C. Rau, W. Kulisch, *Thin Solid Films*, 249, 28- 37, **1994**
- [43] A. Lee Smith “*Analysis of Silicones*” John Wiley & Sons, Inc., **1974**
- [44] A.K.H. Achyuta, A.J. White, H.G. Pryce Lewis, and S.K. Murthy, *Macromolecules*, 42, 1970-1978, **2009**
- [45] W.S. O’Shaughnessy, S.K. Murthy, D.J. Edell, and K.K. Gleason, *Biomacromolecules*, 8, 2564-2570, **2008**
- [46] A. Grill and D.A. Neumayer, *Journal of Applied Physics*, Vol 94, N. 10, **2003**
- [47] T.B. Casserly, K.K. Gleason, *Plasma Processes and Polymers*, 2, 679–687, **2005**

- [48] D.D. Burkey, K.K. Gleason *Journal of Vacuum Science and Technology A*, 22, 1, 2004
- [49] D.D. Burkey and K.K. Gleason, , *Journal of Applied Physics.*, Vol. 93, No. 9, 2003
- [50] A. Francescangeli, F. Palumbo, R. d'Agostino, C. Defranoux, *Plasma Processes and Polymers*, 6, 132–138, 2009
- [51] S.H. Baxamusa and K.K. Gleason, *Chemical Vapor Deposition*, 14, 313–318, 2008
- [52] M. Gupta, V. Kapur, N.M. Pinkerton, and K.K. Gleason, *Chemistry of Materials*, 20, 1646–1651, 2008



## Chapter 5

### *Optical characterization of plasma-deposited SiO<sub>2</sub>-like layers on anisotropic polymeric substrates\**

#### Abstract

In this paper, the characterization of the optical anisotropy of poly(ethylene 2,6-naphthalate) (PEN) by means of Transmission Generalized Ellipsometry coupled with reflection multi-angle Spectroscopic Ellipsometric (SE) measurements, is presented. This study is functional to the determination of the refractive index of atmospheric pressure plasma-deposited SiO<sub>2</sub>-like layers deposited on PEN. The effect of the plasma duty cycle (DC) on the film properties is investigated. From the analysis of the optical properties, complemented with chemical and morphological studies, it is concluded that the increase in DC is responsible for the layer densification process, eventually causing an improvement in the PEN/SiO<sub>2</sub>-like system barrier properties.

---

\* Published as: G. Aresta, P. Antony Premkumar, S.A. Starostin, H. de Vries, M.C.M. van de Sanden, M. Creatore, *Plasma Processes and Polymers*, 7, 766, 2010

## Introduction

The determination of the optical properties of thin films is nowadays acknowledged as fundamental in thin film characterization. Spectroscopic ellipsometry (SE) measurements, usually performed in reflection mode at one or more angles of incidence, are widely carried out in applications ranging from optical and tribological to electrical and moisture/oxygen diffusion barrier coatings<sup>1-9</sup>. Among these, polymer characterization has received much attention and an example are the works of Drevillon *et al.*<sup>10-11</sup> and Martinu *et al.*<sup>12-13</sup> focusing on the study of plasma-induced polymer surface modification and of the adhesion of plasma-deposited thin films on polymer substrates (i.e. polycarbonate and polypropylene) by means of IR<sup>10</sup> and UV-Vis<sup>11</sup> Spectroscopic Ellipsometry measurements, also performed *in situ*<sup>12</sup>. Also worth of note is the study of the polymer substrate/thin film interphase development during the deposition process<sup>13</sup>. However, thin film and polymer (surface) characterization by means of SE may be challenged by the presence of optical anisotropy in the polymer. Polymer anisotropy generally occurs because of the extrusion and stretching processes which polymer webs undergo with the purpose of achieving the necessary thickness and specific mechanical properties. After the stretching process, the polymer macromolecular chains are preferentially oriented towards the stretching direction, generating optical anisotropy. Beside this, the induced crystallization results in an enhancement of polymers properties such as melting temperature (which increases), thermal stability and mechanical properties (e.g. Young modulus and the tensile strength), making these materials good candidates for many applications, i.e. flexible electronics, amongst others<sup>14</sup>.

An anisotropic material may be either uniaxial, i.e. having two different refractive indices<sup>1</sup>:  $n_a = n_b \neq n_c$ , or biaxial, i.e. having three different refractive indices:  $n_a \neq n_b \neq n_c$ . Here,  $n_a$ ,  $n_b$  and  $n_c$  are the principal refractive indices of the index ellipsoid of the material<sup>15</sup>, representing the interaction between polarized light and the material itself. Mathematically, the interaction of the polarized light with the (isotropic or anisotropic) sample is described by a  $2 \times 2$  matrix, also known as the Jones matrix<sup>15</sup>. While an isotropic material is defined by a diagonal Jones matrix (in which the diagonal elements are the coefficients for the reflected or transmitted *p*- and *s*-polarized light), an anisotropic material is described by a four elements Jones matrix

---

<sup>1</sup> For simplicity, the anisotropy is here investigated only in the range of transparency of the substrate. Therefore, the complex refractive index ( $n - ik$ ) is replaced by the real part  $n$ .

in which the off-diagonal elements are the reflection or transmission Fresnel coefficients related to the cross polarization effect due to the anisotropy of the material<sup>15</sup>.

For specific cases (i.e. the optical axis of a uniaxial material is placed parallel or perpendicular to the plane of incidence), the four element Jones matrix becomes a diagonal matrix and the material can be treated as isotropic. This approach has been described in the works of Logothetidis *et al.* reporting a detailed study of the optical properties of polymers such as PET<sup>16</sup>, PEN<sup>17</sup> in the UV-Vis and IR regions. These studies can be extended to anisotropic polymers deposited on isotropic substrates, as reported by Losurdo *et al.*<sup>18,19</sup>, who characterized the optical properties of different conjugated poly(arylenphenylene) uniaxial polymer films deposited by spin-on technique on glass. In all other cases, the determination of all elements of the anisotropic Jones matrix is carried out by a series of measurements known as Generalized Ellipsometry (GE) approach<sup>20</sup>. The advantage of this approach is that no specific orientation of the sample with respect to the plane of incidence is required<sup>20</sup>. Generalized Ellipsometry measurements allow obtaining the elements of the normalized Jones anisotropic matrix reported in Equation 1 - 3:

$$AnEt \{ \text{or } AnE \} = \frac{t_{pp}}{t_{ss}} \left\{ \text{or } \frac{r_{pp}}{r_{ss}} \right\} = \tan(\Psi) e^{i\Delta} \quad (1)$$

$$Apst \{ \text{or } Aps \} = \frac{t_{ps}}{t_{pp}} \left\{ \text{or } \frac{r_{ps}}{r_{pp}} \right\} = \tan(\Psi_{ps}) e^{i\Delta_{ps}} \quad (2)$$

$$Aspt \{ \text{or } Asp \} = \frac{t_{sp}}{t_{ss}} \left\{ \text{or } \frac{r_{sp}}{r_{ss}} \right\} = \tan(\Psi_{sp}) e^{i\Delta_{sp}} \quad (3)$$

in which *AnEt* (or *AnE*) is the experimental parameter related to the diagonal elements of the anisotropic Jones matrix, and *Apst* and *Aspt* (or *Aps* and *Asp*) are the experimental parameters related to the off diagonal elements of the Jones matrix<sup>21, 22</sup>. With this approach, the optical characterization of an anisotropic substrate (especially a transparent one) can be carried out by means of transmission generalized ellipsometric (TGE) measurements. By acquiring TGE spectra at several angles of incidence, including the normal, different sets of experimental data are obtained which allow to determine the presence of (in-plane and out-of-plane) anisotropy, as

well as the orientation of the material index ellipsoid with respect to the laboratory coordinate system, defined by Euler angles ( $\Phi_E$ ,  $\Theta_E$ ,  $\Psi_E$ ). However, reflection measurements are still needed to obtain the absolute value of the refractive indices. Examples of this approach are the work of Elman<sup>21</sup> and of Sassella<sup>22</sup> studying the optical anisotropy of a biaxially stretched PET foil and of a crystal of potassium acid phthalate, respectively.

If a high depolarizing effect induced by the sample is present (i.e. high surface roughness, thickness non uniformity, backside reflection)<sup>15</sup>, then the Jones matrix formalism cannot be used any longer and the Muller matrix (4x4 matrix) needs to be determined. In the Muller matrix formalism, the state of the light is described by the Stokes vectors<sup>15</sup> by which also the depolarized light can be characterized: the work of Hilfiker on several liquid crystal systems<sup>23, 24</sup>, of Logothetidis<sup>25</sup> on uniaxial inorganic films of SnSe and biaxial polymers and of Sassella and Wagner<sup>26</sup> on uniaxial PET crystals are valid examples of this approach.

In this paper we report the characterization of the optical anisotropy of the poly(2,6-ethylenenaphthalate), (PEN) in its transparent region, by using Transmission Generalized Ellipsometry (TGE) and reflection multi-angle spectroscopic ellipsometric (SE) measurements. While TGE measurements allow determining the in-plane and out-of-plane anisotropy and orientation of the material index ellipsoid, the determination of the optical dispersion of the polymer along the  $x$ ,  $y$ ,  $z$  axes (i.e. our laboratory frame) is achieved by means of reflection multi-angle SE measurements. Moreover, based on the results obtained from this analysis, a strategy for the determination of the optical properties of plasma-deposited SiO<sub>2</sub>-like layers on the anisotropic polymer has been developed. Furthermore, the optical properties of the SiO<sub>2</sub>-like layers have been correlated with the morphological, chemical and oxygen diffusion barrier properties.

This paper is organized as follows: in the Experimental Part section, an extensive description of the strategy used to determine the PEN optical anisotropy is given along with the deposition process of the SiO<sub>2</sub>-like layers on PEN and the other diagnostic tools. The results obtained from the PEN and the SiO<sub>2</sub>-like layers/PEN optical characterization are discussed in the Results and Discussion section and correlated with the outcome obtained from the analysis of the chemical, morphological and oxygen barrier properties. Finally, conclusions drawn from this study are provided.

## Experimental Part

### Characterization of the optical anisotropy of PEN

The studied polymer web is an industrially- supplied Advanced Photo System (APS)-PEN (also known as “optical grade PEN”) 100 μm thick and 18 cm wide. SE and TGE measurements are performed by using a rotating compensator ellipsometer J.A. Woollam Co. M-2000D<sup>®</sup> instrument, allowing the measurements of phase shifts,  $\Delta$ , in the full 0° - 360° range. The instrument is equipped with an automatized multi-angle stage, allowing spectra acquisition at different angles of incidence in reflection and transmission. The processing of the ellipsometric data is carried out by means of the J.A. Woollam Co. WVASE 32 (version 3.668) software and the mean squared error between the experimental data and the model is minimized by adjusting the fit parameters using the Levenberg-Marquardt algorithm. The spectra are acquired between 190 and 1000 nm with a resolution of 1.6 nm. In order to define the orientation of the polymer index ellipsoid with respect to the laboratory coordinate frame, a reference for the orientation of the PEN sample with respect to the plane of incidence is chosen. In Figure 1 the orientations of the polymer sample and plane of incidence are shown with respect to the laboratory frame (i.e. the  $x,y,z$  coordinate system). The sample may be placed either parallel to the unwinding direction of the web or at an arbitrary angle  $\alpha$ , measured with respect to the  $x$ -axis. Figure 1 shows also the Euler angles, representing the in-plane ( $\Phi_E$ ) and the out-of-plane rotation ( $\Theta_E$ ) of the material index ellipsoid with respect to the laboratory frame, where  $n_a$ ,  $n_b$  and  $n_c$  are the principal refractive indices of the material index ellipsoid.

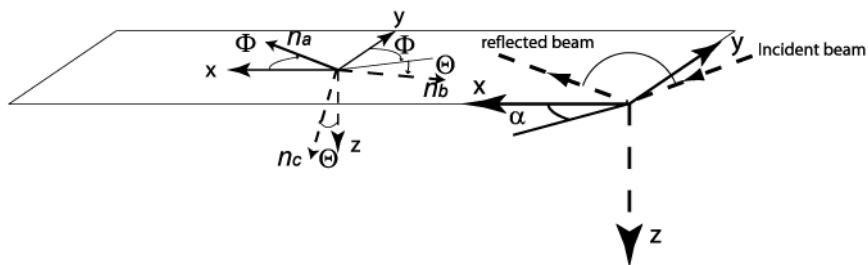


**Figure 1:** Polymer and plane of incidence orientation with respect to the laboratory frame. Also shown are the angle  $\alpha$  representing the sample orientation with respect to the  $x$ -axis and the Euler angles  $\Phi_E$  and  $\Theta_E$  describing the material index ellipsoid in plane orientation, and the out of plane orientation. In the picture the sample is placed with the unwinding direction parallel to the  $x$ -axis.



The ellipsometric measurements consist of three steps. TGE measurements taken at normal incidence are acquired to investigate the presence of the in-plane anisotropy: the in-plane anisotropy  $\Delta n_{xy}$  and the in-plane angle  $\Phi_E$  (Figure 1) with respect to the  $x$ -axis are the fit parameters. As a second step, TGE measurements, performed at different wavelengths and over a range of angles of incidence (from  $-40^\circ$  to  $+20^\circ$  by a step of  $0.5^\circ$  with a wavelength step of 25.5 nm) are recorded to check for the presence of the out-of-plane anisotropy. The fit parameters are the out-of-plane anisotropy  $\Delta n_{xz}$  and the out-of-plane angle  $\Theta_E$  (Figure 1), with respect to the  $z$ -axis. In this step  $\Delta n_{xy}$  and  $\Phi_E$  are kept constant at the values obtained in the 1<sup>st</sup> step. Finally, reflection measurements at different angles (from  $65^\circ$  to  $75^\circ$  by steps of  $5^\circ$ ) are acquired to determine the optical dispersion along the three axes, with the sample being roughened at the backside to avoid multiple light reflections. In this last step  $\Delta n_{xy}$ ,  $\Delta n_{xz}$  and the in-plane and out-of-plane orientations,  $\Phi_E$  and  $\Theta_E$  respectively, are kept fixed. The fit procedure of the last two steps is iterated. The optical properties of PEN are determined in its transparent region, i.e. 400-1000 nm. The chosen dispersion relation describing the optical behavior of the PEN in its transparency range is the Cauchy relation, defined according to Equation 4:

$$n(\lambda) = A + \frac{B}{\lambda^2} + \frac{C}{\lambda^4} \quad ; \quad k(\lambda) \approx 0 \quad (4)$$

where  $A$ ,  $B$ ,  $C$  are fitting parameters and  $n(\lambda)$  and  $k(\lambda)$  are the refractive index and the extinction coefficient, respectively. The optical model includes also a Bruggeman Effective Medium Approximation (BEMA) layer (50% polymer biaxial model, 50% voids) to take into account the polymer surface roughness.

### SiO<sub>2</sub>-like layers deposition and characterization

SiO<sub>2</sub>-like layers are deposited at room temperature by means of a roll-to-roll Atmospheric Pressure Glow Discharge (APGD)<sup>28-31</sup> in a dielectric barrier discharge configuration (DBD), from argon / nitrogen / oxygen + hexamethyldisiloxane mixtures, 11 / 2 / 0.2 l/min + 400 mg/hr. The DBD is open to ambient air and ignited between two plane parallel stainless steel electrodes (top electrode area: 40x150 mm<sup>2</sup>, bottom electrode area: 120x190 mm<sup>2</sup>) placed in the horizontal direction with a discharge gap of 0.6 mm corresponding to a discharge volume of 3.6 cm<sup>3</sup>. The edges of the top electrode are rounded ( $R = 2$  mm) in order to avoid parasitic breakdowns. The PEN polymer foil acts as dielectric barrier and substrate

for the deposition of the SiO<sub>2</sub>-like layers. Both electrodes are equipped with an independent precise foil transport and tension control system. The speed of the foil along the top and bottom electrode is 10 mm/min. The DBD is powered by a SEREN -5 AC sine-wave generator. Stabilization network and matching elements allow a uniform discharge avoiding filaments formation<sup>31-34</sup>. The current-voltage characteristics were monitored using a Tektronix TDS 3034B oscilloscope. In order to avoid thermal damage to the polymeric substrate, due to the discharge power, the high voltage is applied in a pulsed mode with pulse duration of 200 μs. The control of the discharge power is achieved by varying the duty cycle (DC) of the pulse period from 2 to 20 % resulting in an averaged discharge power of 0.2 to 1.9 W cm<sup>-2</sup>. Our previous work has shown that by pulsing the APGD discharge, stoichiometric and uniform SiO<sub>2</sub> films can be deposited on polymeric substrates, without dust formation involved during the deposition process<sup>30</sup>.

The SiO<sub>2</sub>-like layers have been stored in a vacuum desiccator cell within a few minutes after the deposition in order to limit the water uptake. Sample optical characterization has been performed within two days from the deposition. Spectroscopic ellipsometric spectra are acquired at an angle of incidence of 71° for each deposited sample first in ambient air, to monitor any water uptake in the sample, and, then, in a vacuum cell, with a base pressure of 10<sup>-4</sup> bar.

The SiO<sub>2</sub>-like layer optical properties and thickness are described by a Cauchy layer; the thickness values have been confirmed by means of SEM analysis of the deposited samples. The optical model is completed by a surface roughness layer, kept constant and equal to the surface roughness of the polymer substrate, since AFM<sup>27</sup> analysis has pointed out no surface roughness development during film deposition, as will be shown in the Results and Discussion part.

### **Complementary film characterization**

Atomic Force Microscopy (Digital Instruments Nanoscope IIIa Controller, Veeco Metrology) measurements are performed to determine the surface morphology of the PEN substrate and of the deposited layer, as well as the defect density. Measurements up to an area of 30×30 μm<sup>2</sup> are scanned in open air in tapping mode with a tip velocity of 12 μm/s. For each sample, 5 regions have been scanned. Silicon tips of radius of 10 nm are used for this analysis. Large area scans are applied to check the uniformity of the layers as well possible surface irregularity (i.e. pinholes

and foreign particles). The dimensions of the defects are obtained by the line scan analysis.

The chemistry of the layers is investigated by means of X-ray Photoelectron Spectroscopy (Quantera Q1), using a monochromatic X-ray beam source (Al K $\alpha$ -radiation, 1486.6 eV) with a scanned area of 1400  $\times$  500  $\mu\text{m}^2$ . The background pressure in the spectrometer during the analysis is  $2 \times 10^{-6}$  Pa. The measurements have been recorded at a take-off angle of 45°. Prior to the analysis, the surface of the samples is cleaned with argon ion sputtering (4 kV) for 15 seconds to remove surface contamination.

Finally, the oxygen transmission rate (OTR) measurements have been carried out by means of an OX-TRAN<sup>®</sup> 2/21 (MOCON<sup>®</sup>) at a constant temperature of 23°C and 0% of relative humidity (RH).

## Results and Discussion

### Characterization of the PEN optical anisotropy

As mentioned in the Introduction, GE measurements can be performed at an arbitrary orientation of the sample with respect to the laboratory coordinate frame. However, preliminary measurements at different angles  $\alpha$  are performed in order to highlight the in-plane anisotropy and in-plane orientation of the material index ellipsoid with respect to the  $x$ -axis. As an example, the  $\Psi_{ps}$  and  $\Psi_{sp}$  TGE spectra, acquired at  $0^\circ$  angle of incidence and  $\alpha \approx 0, 30^\circ$  and  $45^\circ$ , are shown in Figure 2: at each orientations, the off-diagonal elements in the  $\Psi$  spectra are larger than zero, pointing out the polymer in-plane anisotropy.

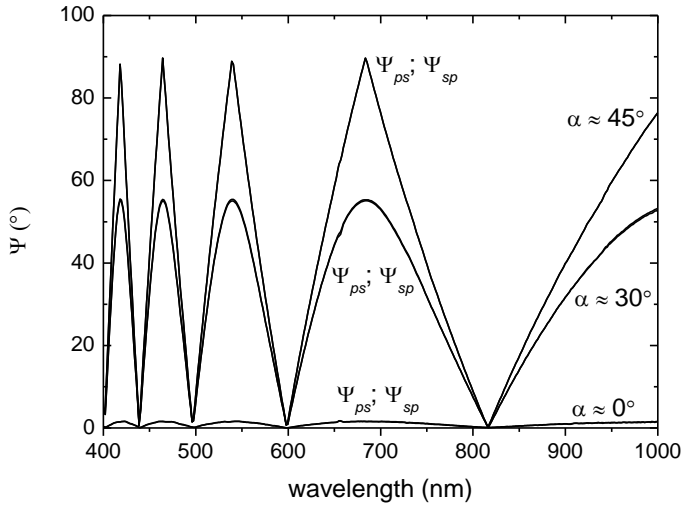


**Figure 2:** TGE anisotropic spectra (only  $\Psi_{ps}$  and  $\Psi_{sp}$  are shown) acquired at  $0^\circ$  angle of incidence of a PEN sample placed at  $\alpha \approx 45^\circ, 30^\circ$  and  $0^\circ$ .

However, by changing the orientation of the sample, the amplitude of  $\Psi_{ps}$  and  $\Psi_{sp}$  changes: at  $\alpha \approx 0^\circ$  the sample index ellipsoid is almost aligned with the laboratory frame coordinate system, instead, at  $\alpha \approx 45^\circ$ , the largest amplitude of  $\Psi_{ps}$  and  $\Psi_{sp}$  is achieved, suggesting that the sample index ellipsoid is completely misaligned with respect to the  $x$ -axis. This preliminary analysis has been performed for each analyzed

PEN sample pointing out also that the material index ellipsoid can vary for each sample at the same  $\alpha$  and therefore, a mapping of the in-plane orientation of the material index ellipsoid is needed in order to define a proper PEN reference sample for the analysis of the SiO<sub>2</sub>-like layers, as reported later in this paper. As an example of the characterization of the PEN optical anisotropy, in Figure 3 TGE data acquired at 0° angle of incidence (for simplicity only two of the off-diagonal related parameters, i.e.  $\Psi_{ps}$  and  $\Delta_{ps}$  are shown together with  $\Psi$  and  $\Delta$ ) are shown together with the fit curves of a PEN sample placed at an angle  $\alpha$  close to 45°.

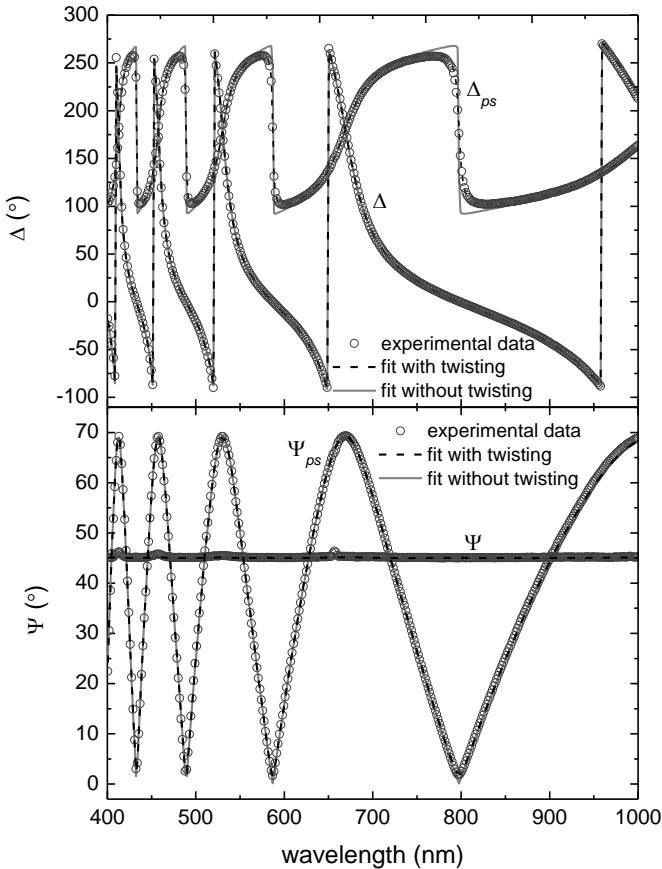


**Figure 3:** TGE anisotropic spectra ( $\Psi$ ;  $\Psi_{ps}$  and  $\Delta$ ;  $\Delta_{ps}$  are shown) acquired at 0° angle of incidence and relative fitting curves in the absence and in the presence of twisting of the optical constants along the polymer thickness.

The fit is already good in the case of a uniform in plane anisotropy through the whole polymer thickness, providing a value of  $\Phi_E = -34^\circ$ . However, when also a twisting in the in-plane orientation  $\Phi_E$  across the thickness is considered, the fit is further improved (see Figure 3,  $\Delta$  plot). Such step is included in the optical model by slicing the PEN foil in 10 layers with a graded function describing the Euler angle  $\Phi_E$ : the result is a twist of about  $1.5^\circ$  from the bottom to the surface of the polymer sample ( $-34.0^\circ$  at the bottom,  $-35.5^\circ$  at the top). The twisting of  $\Phi_E$  along the thickness could be attributed to a non uniform strain of the foil during the stretching in the production process. On the contrary, no change in the in plane anisotropy  $\Delta n_{xy}$  is observed, i.e.  $\Delta n_{xy}(633 \text{ nm}) = 0.017$  through the whole polymer thickness.

In Figure 4 the  $\Psi$  and  $\Psi_{ps}$  TGE spectra at three selected wavelengths (451 nm, 604 nm and 706 nm) as function of the angle of incidence from  $-40^\circ$  to  $+20^\circ$  are shown together with their relative fit. Also in this case the off-diagonal elements are larger than zero, pointing out the polymer out-of-plane anisotropy.

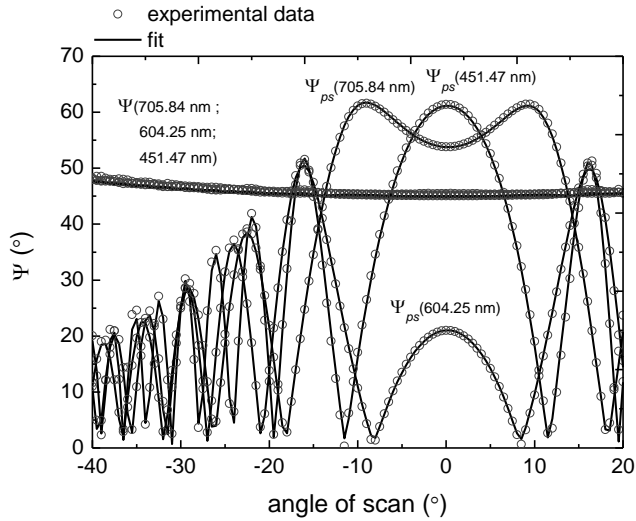


**Figure 4:** TGE angle scan anisotropic spectra and relative fitting curves at three selected wavelengths ( $\Psi$ ;  $\Psi_{ps}$  at 451 nm, 604 nm, 706 nm) as function of the angle of incidence.

The symmetry of the data with respect to 0° points out the fact that the out-of-plane deviation of the index ellipsoid from the lab frame is limited, in fact the fit of these data provides a value of  $\Theta = 0.05^\circ$ .

In Figure 5 the optical dispersion differences  $\Delta n_{xy}$  and  $\Delta n_{xz}$  into the  $x$ - $y$  and  $x$ - $z$  planes respectively, are shown.

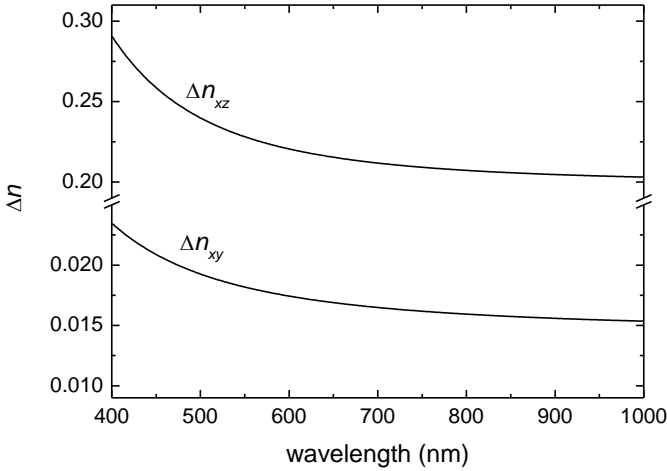


**Figure 5:** Optical dispersion differences  $\Delta n_{xy}$  and  $\Delta n_{xz}$  as function of the wavelength.

Finally, the outcome of the reflection measurements at 65°, 70° and 75° angle of incidence is shown in Figure 6 together with the relative fits. The polymer surface roughness, as obtained from the ellipsometric fit, is  $6 \pm 2$  nm, and it is larger than the value obtained from the AFM analysis of  $1.50 \pm 0.05$  nm. The difference in the values obtained by the two techniques can be explained considering the different nature of the techniques: the SE roughness layer is a mixture of materials and voids, while the AFM roughness measures the average height of features on top of the polymer foil. The exact relationship between them is not known, being still under debate<sup>35-39</sup>.

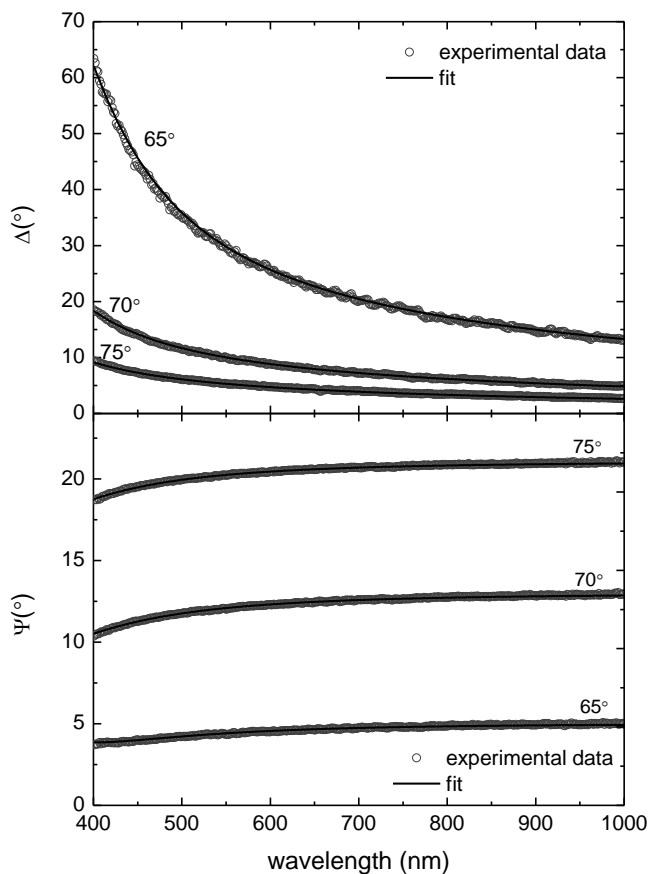


**Figure 6:** SE reflection measurements and relative fitting curves at 65°, 70° and 75° angles of incidence.

The absolute values of the refractive index along the three axes, as obtained from the modeling of the reflection ellipsometric data, are reported in Figure 7.



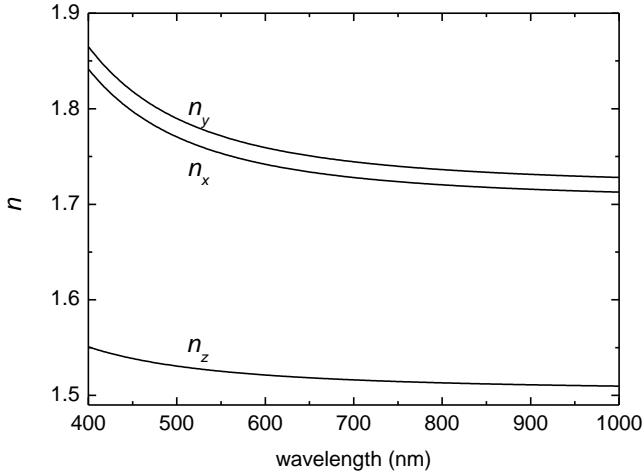
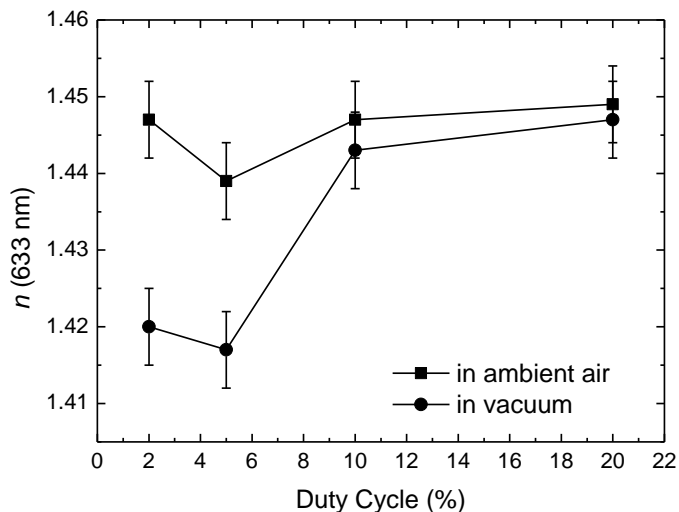


Figure 7: PEN optical dispersion in the spectral range between 400 nm and 1000 nm along the  $x$ ,  $y$ ,  $z$  axes.

### SiO<sub>2</sub>-like layer characterization

The optical properties of SiO<sub>2</sub>-like layers deposited on anisotropic PEN substrates by means of atmospheric plasma glow discharges in Ar/N<sub>2</sub>/O<sub>2</sub>/HMDSO mixtures have been determined as function of the DC. For each SiO<sub>2</sub>-like layer sample, a PEN reference sample has been analyzed to provide the proper substrate for the optical model. The choice has fallen on a reference PEN sample placed along the  $x$ -axis and in line with the analyzed SiO<sub>2</sub>-like layer. This is based on a previous extensive mapping of an A4 PEN foil showing that the variation of the in-plane orientation of the PEN index ellipsoid  $\Phi_E$  is within 2° along the  $x$ -axis, while it extends to a 10° variation along polymer width/  $y$ -axis. The above mentioned choice, therefore, decreases the error in the determination of the SiO<sub>2</sub>-like layer refractive index, as determined to be  $5 \cdot 10^{-3}$ . The SE fit provided a layer thickness in the range of 120-222 nm for the different DC values.

Figure 8 reports the layer refractive index at  $\lambda = 633$  nm as function of the DC measured in ambient air ( $n_{amb}$ ) and in vacuum ( $n_{vac}$ ): both series show an increase as function of the DC, which could be ascribed to an increase in layer density (the refractive index of thermally grown SiO<sub>2</sub> is 1.465). In order to confirm such hypothesis, the chemistry of the layers has been also investigated by means of XPS analysis, which has pointed out a negligible carbon content (< 3%) for all layers, except for the one deposited at DC = 2% (see Table I).



**Figure 8:** Ambient air and in vacuum refractive index values for the deposited SiO<sub>2</sub>-like layers as function of the Duty Cycle.

Furthermore, all layers are characterized by an O-to-Si ratio slightly higher than 2, which can be attributed to the residual hydrogen presence as OH groups<sup>40, 41</sup>. The hypothesis on the increase in layer density is supported by the comparison of the  $n_{amb}$  with the  $n_{vac}$  values as function of the DC: the  $n_{amb}$  are always higher than the  $n_{vac}$  values, due to water absorption in the open pores of the layer ( $n_{H_2O} = 1.33$ ), but, as the DC increases, less water uptake occurs due to the ongoing film densification process and the difference between the two series becomes negligible.

**Table I**

*Chemical composition of the analyzed SiO<sub>2</sub>-like layers deposited at different duty cycle values.*

Duty Cycle (%)	% C	% O	% Si
2	7.3 ± 0.2	64.3 ± 0.2	28.4 ± 0.1
5	2.4 ± 0.2	66.0 ± 0.2	31.6 ± 0.1
10	1.9 ± 0.2	66.2 ± 0.2	31.9 ± 0.1
20	2.7 ± 0.1	67.5 ± 0.4	29.8 ± 0.1

Note that the refractive index value of the layer deposited at a DC of 2%: carbon-containing SiO<sub>2</sub>-like layers are known to be characterized by a higher refractive index than carbon-free SiO<sub>2</sub>-like layers, as extensively investigated in ref<sup>5</sup>. The decrease in refractive index from a DC of 2% to a DC of 5%, therefore, is due to the quantitative decrease (approx. a factor three) of the carbon content, followed by the increase in refractive index trend, due to the gradual removal of porosity in the SiO<sub>2</sub>-like layers with the DC.

**Table II**

*In vacuum refractive indices of SiO<sub>2</sub>-like layers as determined by including/excluding the polymer anisotropy in the optical model.*

Duty Cycle (%)	$n$ (633 nm) SiO <sub>2</sub> -like (PEN anisotropic substrate)	$n$ (633 nm) SiO <sub>2</sub> -like (PEN isotropic substrate)
2	1.420 ± 0.005	1.452 ± 0.002
5	1.417 ± 0.005	1.450 ± 0.002
10	1.443 ± 0.005	1.470 ± 0.002
20	1.447 ± 0.005	1.475 ± 0.002

The importance of the determination of the optical anisotropy of the polymer substrate can be quantitatively appreciated by comparing the in vacuum refractive indices of the deposited layers in the case an isotropic (i.e. the PEN substrate is modeled by means of a Cauchy isotropic layer) and an anisotropic layer modeling (i.e. the biaxial model) for the PEN substrate are applied, as reported in Table II. If polymer anisotropy is not taken into account, the SiO<sub>2</sub>-like layers are found to have considerably higher refractive index values than in the case of polymer anisotropy. This overestimation of the refractive index can lead to erroneous conclusions regarding the quality of the deposited layers.

Further layer characterization has been carried out by means of AFM to study the morphology and defect presence (pinholes, dust particles) of the deposited layers and the results are shown in Figure 9.

The pristine PEN and the inorganic layers defect density, derived from large area AFM studies, are reported. The trend of surface roughness suggests the growth of a conformal layer on top of the polymer substrate with a limited roughness development. Furthermore, no development of dust particles during plasma deposition occurs, as the surface defect density as well as the particle size is the same

as in the case of the pristine polymer surface (i.e.  $< 2 \times 10^{-2} \mu\text{m}^{-2}$  and in the range of 50-100 nm, respectively).

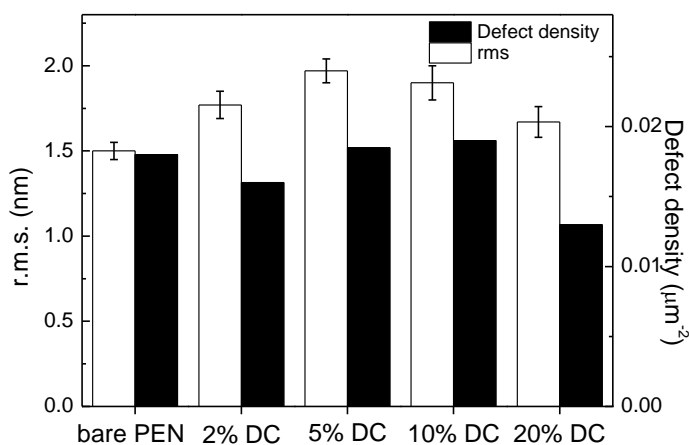


**Figure 9:** AFM surface roughness ( $2.2 \mu\text{m}^2$  area) and defect density ( $30.30 \mu\text{m}^2$  area) values of the pristine PEN and SiO<sub>2</sub>-like layers, deposited at different DC settings.

Finally, the OTR values of the PEN/SiO<sub>2</sub> system for different DC settings have been measured and a barrier improvement factor (BIF), i.e.  $\text{OTR}_{\text{PEN}}/\text{OTR}_{\text{PEN+SiO}_2}$ , of 42 has been recorded in the case of the SiO<sub>2</sub> film deposited at 20% DC. A comparison with literature data is challenging to perform as too many parameters play a role on the final barrier performance, i.e. the polymer chemistry, thickness and its surface status and possible pre-treatment, the inorganic layer thickness and its quality. Chatham has provided in 1996<sup>42</sup> a nice review for BIF values, which, in the case of PET/SiO<sub>2</sub> layers range from 10 up to 100. In the most recent years, values in the same range have been reported<sup>9, 43, 44</sup>, and as high as 1000<sup>45</sup>. Our barriers on PEN, although falling within the rather spread range of data of Chatham<sup>42</sup>, cannot be considered excellent and a possible explanation for this is reported here below.

Generally, the gas/moisture permeation barrier property of a thin film is dependent on intrinsic factors, such as the layer chemistry, density and surface morphology, as well as external factors, such as the polymer surface status, i.e. presence of defects, and the possible development of dust during film growth. In the case of dense inorganic layers, i.e. when impurities such as carbon and residual porosity are

quantitatively removed, the ultimate barrier performance is dependent on the defect level and it is found to be characterized by the presence of a critical thickness<sup>42,45,46</sup>, i.e. a layer thickness at which the transmission rate has experienced a consistent decrease and above which the permeation barely changes any further, therefore, indicative of a residual defect- driven permeation mechanism. Under the experimental conditions here investigated, the deposited layers are characterized by the same chemistry, morphology and defect status, as the extensive film characterization has pointed out. Therefore, it is plausible to conclude that the O<sub>2</sub> diffusion barrier performance is governed by the residual porosity in the layer, on the basis of the trend of the layer refractive index earlier reported in Figure 8. Since the film thickness is variable for the different DC values, the OTR values of 3.8, 0.6 and 0.1 cm<sup>3</sup> m<sup>-2</sup> day<sup>-1</sup> have been normalized by the film thickness, i.e. 120, 190 and 160 nm, for the DC values of 2, 10 and 20%, respectively (Figure 10).

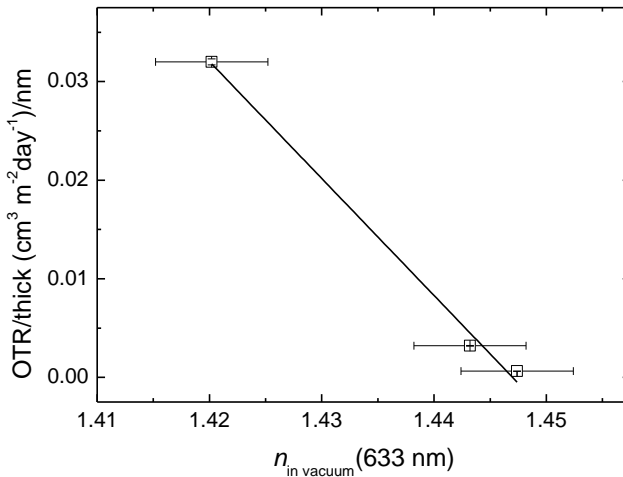


**Figure 10:** Oxygen transmission rates normalized by the film thickness as function of the refractive index values of the SiO<sub>2</sub>-like layers deposited at different DC (2%, 10%, and 20%). The Oxygen transmission rate of the pristine PEN substrate is 4.2 cm<sup>3</sup> m<sup>-2</sup> day<sup>-1</sup>.

## Conclusion

In this work, the characterization of the PEN optical anisotropy has been presented by modeling the TGE measurements acquired at normal incidence and at different angles of incidence to determine the in-plane and out-of-plane anisotropy as well as the in-plane and out-of-plane orientations of the material index ellipsoid with respect to the laboratory frame. Reflection multi-angle SE measurements have allowed the determination of the PEN optical dispersions along the  $x$ ,  $y$ ,  $z$  axes. A larger out-of-plane anisotropy than in-plane anisotropy has been found in the PEN substrate, quantified in terms of  $\Delta n_{xz}$  (633 nm) = 0.217 vs.  $\Delta n_{xy}$  (633 nm) = 0.017. Furthermore, the polymer index ellipsoid has been found almost aligned with the  $z$  axis (i.e.  $\Theta = 0.05^\circ$ ), while the in-plane orientation is found to change in the  $x$ - $y$  plane, pointing out the necessity of selecting a proper reference PEN substrate for the optical modeling of layers deposited on the polymer. The values of the refractive index determined at 633 nm are  $n_x = 1.74$ ,  $n_y = 1.75$  and  $n_z = 1.52$ . This extensive optical characterization of the PEN is functional to the correct determination of the refractive index of thin SiO<sub>2</sub>-like layers deposited by means of roll-to-roll APG discharges on PEN substrates. The effect of the plasma duty cycle on the deposited layers has been investigated: an increase in the refractive index with the DC has been reported together with a decrease of the water uptake upon exposure to the ambient air, pointing out a layer density increase with DC. The increase in layer density is found responsible for the improvement in oxygen permeation barrier properties of the PEN/SiO<sub>2</sub>-like layer system, with a final barrier improvement factor of 42, for a DC value of 20%.

The extensive optical characterization of the polymer anisotropy reported in this work paves the way towards in situ real time studies of thin film growth on polymers, aimed to unravel the interphase development and its mechanism, without the use of destructive or post-deposition (ex situ) characterization techniques.

## **Acknowledgements**

The author would like to thank Dr. T. Wagner (LOT-Oriel GmbH & Co) for the fruitful discussions on the characterization of the polymer optical anisotropy. The group of Photonic and Semiconductor Nanophysics (Applied Physics department, TU/Eindhoven) is acknowledged for the AFM measurements. This work forms part of the research programme of the Dutch Polymer Institute (DPI), project number 663 of the Large Area Thin Film Electronics (LATFE). P.A.P and S.A.S. carried out this research under the project number MC3.06279 in the framework of the Research Program of the Materials innovation institute M2i ([www.m2i.nl](http://www.m2i.nl)), the former Netherlands Institute for Metals Research.

## References

- [1] A. Amassian, R. Vernhes, J.E. Klemberg-Sapieha, P. Desjardins, L. Martinu, *Thin Solid Films*, 469-470 47-53, **2004**
- [2] J. Čížek, J. Vlček, Š. Potocký, J. Houška, Z. Soukup, J. Kalaš, P. Jedrzejowski, J.E. Klemberg-Sapieha, L. Martinu, *Thin Solid Films*, 516, 7286–7293, **2008**
- [3] T. Schwarz-Selinger, A. von Keudell, and W. Jacob, *Journal of Applied Physics*, Vol. 87, No. 7, **1999**
- [4] M. Creatore, J.-C. Cigal, G.M.W. Kroesen, M.C.M. van de Sanden, *Thin Solid Films*, 484, 104–111, **2005**
- [5] M. Creatore, S.M. Rieter, Y. Barrell, M.C.M. van de Sanden, R. Vernhes, L. Martinu, *Thin Solid Films*, 516, 8547-8553, **2008**
- [6] V. Nguyen Van, A. Brunet-Bruneau, S. Fisson, J.M. Frigerio, G. Vuye, Y. Wang, F. Abeles, J. Rivory, M. Berger, and P. Chaton, *Applied Optics*, Vol.35, No. 28, **1996**
- [7] X. Tan, J. Woojick, and P. Mascher, *Journal of Vacuum Science and Technology*, A 22 (4), **2004**
- [8] A. Francescangeli, F. Palumbo, R. D’Agostino, C. Defranoux, *Plasma Processes and Polymers*,6, 132-138, **2009**
- [9] J. Fahlreich, M. Fahland, W. Schönberger, N. Schiller, *Thin Solid Films*, 517, 3075-3080, **2009**
- [10] S. Vallon and B. Drevillon, J. C. Rostaing *Thin Solid Films*, 233, 256-259, **1993**
- [11] S. Vallon, B. Drevillon, F. Poncin-Epaillard, *Applied Surface Science*, 108, 177-185, **1997**
- [12] S. Vallon and B. Drevillon, F. Poncin-Epaillard, J.E. Klemberg-Sapieha and L. Martinu, *Journal of Vacuum Science and Technology*, A 14, (6), **1996**
- [13] A. Bergeron, J. E. Klemberg-Sapieha, and L. Martinu, *Journal of Vacuum Science and Technology A* 16 (06), **1998**
- [14] W.A. MacDonald, *Journal of Materials Chemistry*, 14, 4-10, **2004**
- [15] “*Spectroscopic Ellipsometry Principles and Applications*”, H. Fujiwara, John Wiley & Sons Ltd, **2007**
- [16] A. Laskarakis, M. Gioti, E. Pavlopoulou, N. Polulakis, S. Logothetidis, *Macromolecules Symposium*, 205, 95-104, **2004**
- [17] A. Laskarakis and S. Logothetidis, *Journal of Applied Physics*, 101, (053503), **2007**



- [18] M. Losurdo, G. Bruno, E.A. Irene, *Journal of Applied Physics*, Vol 94, No 8, **2003**
- [19] M. Losurdo, M.M. Giangregorio, Pio Capezzuto, G. Bruno, F. Babudri, D. Colangiuli, G. M. Farinola, and F. Naso, *Macromolecules*, 36, 4492-4497, **2003**
- [20] M. Schubert, *Thin Solid Films*, 313-314, 323-332, **1998**
- [21] J.F. Elman, J. Greener, C.M. Herzinger, B. Johs, *Thin Solid Films*, 313-314, 814-818, **1998**
- [22] A. Sassella and A. Borghesi, Th. Wagner, J.Hilfiker, *Journal of Applied Physic*, **90**, 8, **2007**
- [23] J.N. Hilfiker, C.M. Herzinger, T. Wagner, A.Marino, G. Delgais, G. Abbate, *Thin Solid Films*, 455 -456, 591-595, **2004**
- [24] J.N. Hilfiker, B. Johs, C.M. Herzinger, J.F. Elman, E. Montbach, D. Bryant, P.J. Bos, *Thin Solid Films*, 455 -456, 596-600, **2004**
- [25] A. Laskarakis, S. Logothetidis, E. Pavlopoulou, M. Gioti, *Thin Solid Films*, 455-456, 43-49, **2004**
- [26] A. Sassella, Th. Wagner, C. Herzinger, Genbo Su, Youping He, Chenjia, Chen *Thin Solid Films*, 455 -456, 576-580, **2004**
- [27] P.A. Premkumar, S.A. Starostin, H. de Vries, R. M. J. Paffen, M. Creatore, T. Eijkemans, P. M. Koenraad, M. C. M. van de Sanden, *Plasma Processes and Polymers.*, 6, 693-702, **2009**
- [28] S.A. Starostin, P.A. Premkumar, M. Creatore, E.M. van Veldhuizen, H. de Vries, R.M.J. Paffen, M.C.M. van de Sanden *Plasma Sources Science and Technology*, **18**, 045021, **2009**
- [29] S. Starostine, E. Aldea, H. de Vries, M. Creatore, M.C.M. van de Sanden, *Plasma Processes and Polymers*, 4, S440-S444, **2007**
- [30] S.A. Starostin, M.A. M. El Sabbagh, E. Aldea, H. de Vries, M. Creatore, and M.C.M. van de Sanden, *IEEE transactions on Plasma Science*, 36, 4, **2008**
- [31] US 6774569, EP 1381257, Fuji Photo Film B.V., invs.: H. de Vries, F. Mori, E. Aldea, M.C.M. van de Sanden., **2004**
- [32] EP 1548795 A1, Fuji Photo Film B.V., invs.: J. Bouwstra, E. Aldea, M.C.M. van de Sanden, H. de Vries., **2005**
- [33] EP 1626613 A1, Fuji Photo Film B.V., invs.: H. de Vries, J. Bouwstra, E. Aldea, M.C.M. van de Sanden, P. Peeters., **2006**
- [34] D. Turnec, A. Brablec, J. Buchta, *Journal of Physics D: Applied Physics*, 34, 1697, **2001**
- [35] H. Fujiwara, M. Kondo, and A. Matsuda, *Physical Review B*, 63, 115306, **2001**

- [36] I.Y. Kim, S.H. Hong, A. Consoli, J. Benedikt, and A. von Keudell, *Journal of Applied Physics*, 100, 053302, 2006
- [37] J. Koh, Y. Lu, C.R. Wronski, Y. Kuang, R. Collins, T.T. Tsong, Y.E. Strausser, *Applied Physics Letters*, 69, 9, 1996
- [38] A.A.E. Stevens and H.C.W. Beijerinck, *Journal of Vacuum Science and Technology A*, 23 (1), 2005
- [39] P. Petrik, L.P. Biro, M. Fried, T. Lohner, R. Berger, C. Schneider, J. Gyulai, H. Ryssel, *Thin Solid Films*, 315, 186-191, 1998,
- [40] F. Massines, N. Gherardi, A. Fornelli, S. Martin, *Surface Coatings and Technology*, 200, 1855, 2005
- [41] F. Fracassi, R. d'Agostino, P. Favia, *Journal of the Electrochemical Society*, 1992, 139, 2636.
- [42] H. Chatham, *Surface Coatings and Technology*, 78, 1, 1996
- [43] R. Lamendola, R. d'Agostino, *Pure Applied Chemistry*, 70(6), 1203, 1998
- [44] M. Deilmann, S. Theiß, P. Awakowicz, *Surface Coatings and Technology*, 202, 1911, 2008
- [45] A.S. da Silva Sobrinho, M. Latreche, G. Czeremuszkina, J.E. Klemberg-Sapieha, M.R. Wertheimer, *Journal of Vacuum Science and Technology A*, 16, 3190, 1998
- [46] A.S. da Silva Sobrinho, G. Czeremuszkina, M. Latreche, M.R. Wertheimer, *Journal of Vacuum Science and Technology A*, 18(1), 149, 2000



*Summary*

# Summary

## Chemical vapor deposition of (in)organic layers:

*in situ* film growth studies, nano-porosity and moisture permeation barrier properties

Although polymers represent the substrate of choice for flexible devices such as solar cells and OLEDs because they are lightweight, flexible, transparent, inexpensive, and compatible with roll-to-roll processing, they have the drawback to be highly permeable to moisture and oxygen. This poses severe limitations to the performance of the flexible device. This drawback is presently addressed by depositing inorganic ( $\text{Al}_2\text{O}_3$ ,  $\text{SiO}_2$ ,  $\text{Si}_3\text{N}_4$ ) thin film barrier layers on the polymer substrate. Despite their impermeable bulk counterpart, the (water vapor) permeation through single barrier layers is driven by several paths, which include nm-sized pores as well as substrate/process induced macro-defects. It is, therefore, of paramount importance to determine and control the density of the macro-defects, as well as to control the inorganic barrier layer microstructure, defined by its (open) nano-porosity. The state-of-the art in barrier layer technology applied to polymer substrates as well as to the direct encapsulation of the (flexible) device is a  $\mu\text{m}$ -thick multilayer consisting of inorganic barrier layers decoupled by organic interlayers. This encapsulation solution against water permeation into the device can virtually guarantee a device lifetime of ten years. Although several approaches have been followed in engineering the multilayer, there is still a debate on the effective role of the organic interlayer in affecting the multilayer barrier properties. It is generally considered that the organic interlayer acts as smoothening layer allowing the decoupling between macro-defects either present on the polymer substrate or in the inorganic barrier layer. It is also hypothesized that the organic interlayer infiltrates into the nano-pores present in the barrier layer, therefore affecting the barrier itself at microstructure level. However, this hypothesis has neither been followed by any experimental evidence, nor it has been investigated in the case of organic interlayer deposition methods other than polymerization from its liquid phase.

This thesis work aimed to gain insight into the role of the organic interlayer in affecting the multilayer barrier properties. A model system, based on a siloxane chemistry, has been adopted in which the multi-layer is developed by means of two vacuum deposition techniques, i.e. PECVD for the inorganic  $\text{SiO}_2$ -like barrier layer and initiated-chemical vapor deposition (i-CVD) for the poly( $\text{V}_3\text{D}_3$ ) organic interlayer. This latter allows the polymerization process to develop organic films with full retention of the monomer chemistry. A novel deposition setup has been, therefore, developed to implement both deposition processes in a vacuum chamber,

equipped with *in situ* real time diagnostic tools, such as spectroscopic ellipsometry (SE).

As first research step, the i-CVD polymer growth has been studied *in situ* by means of SE which allowed following all stages of the deposition process from the initial monomer adsorption to the linear film growth and to the thickness losses due to the presence of unreacted monomer units at the end of the deposition process. Moreover, *in situ* SE measurements allowed characterizing the thickness losses as bulk-related phenomenon and brought new information on the polymerization process which propagate not only at the surface of the growing layer but also in the bulk. Furthermore, a correlation has been made between specific process parameters (i.e. the monomer surface concentration) and the deposition of stable, highly cross-linked polymer layers (i.e. exhibiting no thickness loss upon evacuation). This has allowed to define a process parameter window, i.e.  $P_M/P_{sat}$ , followed *in situ* by SE, which controls the deposition of high quality poly(V<sub>3</sub>D<sub>3</sub>) layers.

The follow-up studies of the i-CVD polymer growth on SiO<sub>2</sub>-like moisture permeation barrier layers, performed by means i-CVD monomer (V<sub>3</sub>D<sub>3</sub>) adsorption/desorption isothermal studies, have highlighted the filling/infiltration of the i-CVD monomer into the open nano-defects/porosity of the SiO<sub>2</sub>-like layer underneath. This result has, therefore, provided support to the above-mentioned hypothesis on the infiltration of the organic interlayer into the nano-porosity of the SiO<sub>2</sub>-like barrier layer underneath.

Finally, the contribution to the improvement of the barrier performance of the PE-CVD/i-CVD deposited multilayer due the filling of the PE-CVD deposited SiO<sub>2</sub>-like layer nano-pores has been studied with respect to the smoothening/decoupling effect of the SiO<sub>2</sub>-like layers macro-defects. Ca test measurements allowed discerning between the water permeation through the macro-defects/pinholes and the permeation through the matrix. The effect of the filling/infiltration of the SiO<sub>2</sub>-like layer nano-defects has been studied as function of intrinsic porosity of the SiO<sub>2</sub>-like layer (i.e. as function of the intrinsic WVTR values). It is concluded that the effect of the SiO<sub>2</sub>-like nano-defect filling by the poly(V<sub>3</sub>D<sub>3</sub>) is effective only for SiO<sub>2</sub>-like layers initially exhibiting an intrinsic WVTR value > 10<sup>-3</sup> g m<sup>-2</sup> day<sup>-1</sup>. The above-mentioned results, in combination with an evaluation of the local macro-defects prior and upon deposition of the organic interlayer, and a comparison with parallel studies reported in literature, allow to conclude that the main contribution of the i-CVD layer in improving the multilayer barrier properties is given by the smoothening/decoupling of the macro-defects.

The SiO<sub>2</sub>-like layer microstructure characterization has been carried out on layers deposited on a silicon substrate by means of ellipsometric porosimetry measurements

## *Summary*

which allowed discerning between the different residual open porosity of the deposited SiO<sub>2</sub>-like layers. The same characterization in terms of refractive index and residual open porosity, however, should be also carried out in case of polymers as substrates, for example for barrier-on-foil applications. However, polymeric substrates often show optical anisotropy and the proper determination of the barrier layer optical constants can be achieved only by a proper optical characterization of the substrate. In order to perform the microstructure characterization of barrier layers deposited on polymers, the polymer (poly(ethylenenaphthalate), PEN) anisotropy has been characterized by means of the Generalized and Spectroscopic Ellipsometry combined approach. This approach has allowed defining the optical constants of a SiO<sub>2</sub>-like barrier layer deposited on PEN.

## List of Publications:

[1] G. Aresta, J. Palmans, M.C.M. van de Sanden, M. Creatore, *Journal of Vacuum Science and Technology A*, **Accepted for publication, 2012**

[2] G. Aresta, J. Palmans, M.C.M. van de Sanden, M. Creatore, *Microporous and Mesoporous Materials*, 151, 434 - 439, **2012**

[3] G. Aresta, P.A. Premkumar, S.A. Starostin, H. de Vries, M.C.M. van de Sanden, M. Creatore, *Plasma Processes and Polymers*, 7, 766–774, **2010**





# Acknowledgements

## *Acknowledgements*

The PhD work presented here is the outcome not only of my efforts but also of those of many other people I would like to thank.

First of all I would like to thank **Richard** for possibility he gave me to do this PhD, and for his support during all the research period. Thanks for your enthusiasm, for sharing your knowledge with me and for saying always the right words at the time I needed them. Next to Richard, I would like to thank **Adriana**, grazie per avermi insegnato come si fa Ricerca, per avermi guidato e incoraggiato sempre lungo tutto questo periodo di Dottorato. Se oggi ho raggiunto il traguardo di questa tesi, lo devo soprattutto a te e ai tuoi preziosi consigli.

Moreover, I would like to thank the Dutch Polymer Institute (DPI) for having founded this research project and the involved industrial partners. Many thanks to **Ton van Mol** (Holst Centre), **Jasper Michels** (Holst Centre), **Sandeep Unnikrishnan** (Holst Centre) and **Ferdie van Assche** (Holst Centre) for the fruitful discussion of the data during our meetings and the given support during this PhD period. Special thanks to **Peter van der Weijer** (Philips Research laboratories) for WVTR measurements, the fruitful, pleasant and endless discussions of the data, the suggestions and the support during the whole PhD period.

Starting a PhD from an idea which implies the project and engineering of setup and getting also a PhD thesis out of it is possible only if you have the best technical staff ever. Fortunately, we do have the best technical staff you could ever get! **Janneke**, grazie per aver trasformato l'idea in un setup. Il tuo enorme lavoro ha permesso di ottenere preziosi risultati che sono presenti in questa tesi. Close to Janneke, are **Ries** and **Joris**, they did a terrific job in mounting, fixing, thinking of all the possible solutions to the requests I was asking them (almost daily...). **Ries**, someone should make a statue of you! Thanks for all the help you gave me at any moment. **Joris**, same thing applies to you, thanks and "... beren in het bos?". Many thanks also to **Herman** for all the work he did with my RF system. Many thanks also to **Paul Aendenroomer** (GTD) for the technical assistance during the testing of the setup. **Ad** and **Wim Kemper** are acknowledged for the engineering of the grid system and all the assistance given during this work. **Wytze**, I really appreciated your help in starting the work with *in situ* SE and the ongoing work on the barrier layers. **Bernardette**, grazie per la tua squisita gentilezza ed il tuo interesse per me ed il mio lavoro. Thanks also to **Ana Barros**, for the help she gave me during the initial test of the setup.

## *Acknowledgements*

P&MP is first of all a research group, but it is mainly a group and also a special one. This means people always willing to help, listen, discuss, support you in any moment you need it. I should thank all the > 50 people composing it during these > 4 years of my staying in P&MP. First of all I want to thank my “fun room” mates **Noemi**, **Jan-Willem** and **Nick**. Thanks, most of all, for having accepted me, as I really am, in the family of the “fun room” and for supporting me during all the ups and downs of this PhD. Anyone else who will take my place will be a lucky guy. Then the “brothers in arms”, my PhD colleagues, **Aafke**, **Mikhail**, **Kashish**, **Anu**, **Jie**, thanks for all you did for me and the pleasant time we spent together at P&MP. I would like to thank our group secretaries Lianne and Jeanne for the assistance and the help in all the documentations. A special thank to my first Master student **Jurgen**, with whom we setup all the i-CVD work. Thanks for your help, patience and your thoughtful silences ending in: “couldn’t be that...” which started endless discussions. Next to Jurgen I would like to thank **Erik** my second Master student who contributed to the final part of this work. I would also like to thank the “old school” P&MP members **Erik Langereis**, **Cristina**, **Anitha**, **Annalisa**, **Paul**, **Joost**, **Onno**, **Vikram**, **Terje**, **Teo** and **Pavel** for the pleasant time spent together at P&MP. Still P&MP but the Italian side, many thanks to **Andrea**, grazie per essermi stato vicino nel periodo iniziale, quando eravamo entrambi soli, e per aver opposto al mio anarchismo la tua mentalità “milanese-catto-calvinista”. A special thank to **Patty** and **Salvatore**, i miei due “angeli custodi”, grazie per essere stati vicino sempre a me ed a Marianna in questo “periodo olandese”, chissà cosa faremo dopo, ma resteremo sempre amici. Then I would like to thank the women of my life, **Lucia** (my grandmother), **Rosa** (my Mother), **Eliana** (my sister), **Nunzia** (my aunt), for having, always, supported me unconditionally in many ways and “forms”. Last, but not least, I would like to thank **Marianna** (The Woman of my life) for all she has done for me during this PhD and for having supported/understood me in all the ups and (many) downs of it “...non so dirti come e quando, ma un bel giorno cambierà...” ☺.

Gianfranco Aresta

Eindhoven, April 2012

*Acknowledgements*

# Curriculum Vitae

**16<sup>th</sup> October 1977**

Born in Bari, Italy

**July 1996**

Scientific Lyceum Diploma

*Liceo Scientifico Statale "E. Fermi", Bari, Italy*

**March 2007**

Master of Science (M.Sc.) degree in Chemistry

*Università degli Studi di Bari "Aldo Moro", Bari, Italy*

**July 2007 – September 2007**

Process Engineer

*Università degli Studi di Bari "Aldo Moro", Bari, Italy*

**November 2007 – March 2012**

Ph.D. candidate in the group Plasma & Materials Processing, Department of  
Applied Physics

*Eindhoven University of Technology, Eindhoven, the Netherlands*

